# PREDICTION OF BURST PRESSURE ON STEEL PIPES USING GURSON-TVERGAARD-NEEDLEMAN (GTN) MODEL

CHONG KIM SUNG

Report submitted in partial fulfillment of the requirements for the award of the degree of Bachelor of Mechanical Engineering

Faculty of Mechanical Engineering
UNIVERSITI MALAYSIA PAHANG

JUNE 2013

**UNIVERSITY MALAYSIA PAHANG**

**FACULTY OF MECHNICAL ENGINEERING**

I certify that the project entitled "Prediction of Burst Pressure On Steel Pipe Using Gurson-Tvergaard-Needleman (GTN) Model" is written by Chong Kim Sung. I have examined the final copy of this project and in my opinion; it is fully adequate in terms of language standard, and report formatting requirement for the award of the degree of Bachelor of Engineering. I herewith recommend that it be accepted in partial fulfillment of the requirements for the degree of Bachelor of Mechanical Engineering.

(Ms Nur Azhani Abd Razak)
Examiner Signature

## SUPERVISOR'S DECLARATION

I hereby declare that I have checked this project report and in my opinion this project is satisfactory in terms of scope and quality for the award of the degree of Bachelor of Mechanical Engineering.

Signature :
Name of Supervisor: DR.AHMAD SYAHRIZAN BIN SULAIMAN
Position : LECTURER
Date :

## STUDENT DECLARATION

I hereby declare that the work in this report is my own except for quotations and summaries which have been duly acknowledged. The report has not been accepted for any degree and is not concurrently submitted for award of other degree.

Signature:

Name: CHONG KIM SUNG

ID Number: MA09105

Date: 26 June 2013

**Specially dedicated to**

**My beloved family and those who guided and inspired me**

**Throughout my journey of learning**

## ACKNOWLEDGEMENTS

First and foremost I would like to express my sincere appreciation to my supervisor, Dr. Ahmand Syahrizan bin Sulaiman for his continuous guidance, ideas and support to help in completing this project. It is a great gratitude to have his knowledge to be shared with me and this indeed has helps me to be able to see the bigger picture and understand wider scope of this project. Besides, I am grateful for the constant weekly discussion time he spent on me to continue guide me on my project problems. Also, I want to thank him for correcting and comment the mistakes in my project and this can help in my future report writing skills.

My sincere appreciation also goes to Mr Nasrul bin Alang, who is so willing to help and guide me even though I am not his PSM student. He has open my mind on how to relate and compare the different method used in research on the pipe burst pressure and stress and strain development. With his help, I can understand well the methods I am using for my project. Also, thanks for the time spent on figuring the problems encounters during my Patran analysis and comments on simulations even after office hours.

Moreover, I would like to express my gratitude to Puan Norhaida, for her ideas in helping me during my initial learning process using Patran software. Also, for her continuous concern and support on my project.

Lastly, I would like to thank my loving parents for their continuous support and concern throughout my study at University Malaysia Pahang.

## ABSTRACT

A micromechanical model of ductile fracture is applied for API X65 steel to predict ductile failure of a full-scale API X65 pipes with simulated corrosion and defects under internal pressure. The micromechanical model is the Gurson model, incorporating void nucleation, growth and coalescence where the burst pressure is predicted based on the critical void volume fraction. The present study involves experimental comparison and numerical studies of the burst pressure of pipe under ductile fracture. The main objective of the present study is to determine the burst pressure of steel pipe using GursonTevaagard model. For the experimental, the results are from the previous research journal. For the finite element analysis, the pipe model is modeled as a 3 dimensional, quarter-model in MSC.PATRAN with MSC.MARC as nonlinear implicit solver. Results with proposed ductile fracture model indicates that predicted failure pressure attain maximum load for all cases, and are in good agreement with experimental data. It also showed that the burst pressure is decreasing for increasing defect depth and length. For the characters of void volume fraction, f, it can be seen that once the void reach void growth, it soon come to void coalescence, where the burst pressures are predicted at critical void and then fracture. The results from gouge defect varies in length is analyze based on the equivalent plastic strain, $\varepsilon_p$ and the stress triaxially, $T = \frac{\sigma_m}{\sigma_e}$ where void growth dependent on this two key quantities. Void volume fraction are examined based on the equivalent plastic strain and stress triaxiality on the normalize distance along the defect length and depth. It is found that distribution of equivalent plastic strain agreed well with the void volume fraction and the critical point occur at the defect tip along the defect depth and length.

# ABSTRAK

Satu model micromechanical patah mulur dipohon API X65 keluli untuk meramalkan kegagalan mulur daripada skala penuh API X65 paip dengan kakisan simulasi dan kecacatan di bawah tekanan dalaman. Model micromechanical adalah model Gurson, menggabungkan sah penukleusan, pertumbuhan dan tautan di mana tekanan pecah diramalkan berdasarkan kekosongan kritikal jumlah kecil. Kajian ini melibatkan perbandingan eksperimen dan kajian berangka tekanan pecah paip bawah patahmulur.Objektif utama kajian ini adalah untuk menentukan tekanan pecahpaip keluli menggunakan Gurson model Tevaagard. Bagi eksperimen, keputusan adalah dari jurnal penyelidikan sebelumnya. Untuk analisis unsur terhingga, model paip dimodelkan sebagai satu dimensi, suku model 3 dalam MSC.PATRAN dengan MSC.MARC sebagai penyelesai tersirat linear. Keputusan dengan cadangan model patahmulur menunjukkan bahawa tekanan kegagalan meramalkan mencapai beban maksimum bagi semua kes, dan berada dalam perjanjian yang baik dengan data eksperimen.Ia juga menunjukkan bahawa tekanan pecah semakin berkurangan untuk meningkatkan kedalaman kecacatan dan panjang. Untuk watak-watak tidak sah jumlah pecahan, f, ia boleh dilihat bahawa apabila tidak sah mencapai pertumbuhan tidak sah, ia tidak lama lagi dating untuk membatalkan tautan, di mana tekanan pecah diramalkan di sah kritikal dan kemudian patah.Hasil daripada menipu kecacatan berbeza panjang adalah menganalisis berdasarkan tekanan bersamaan plastik, $\varepsilon_p$ dan tekanan triaxially, $T = \frac{\sigma_m}{\sigma_e}$ di mana pertumbuhan tidak sah ini bergantung kepada dua kuantiti utama. Tidak sah jumlah kecil diperiksa berdasarkan tekanan bersamaan plastic dan triaxiality tekanan pada jarak normal sepanjang kecacatan dan mendalam. Ia didapati bahawa taburan terikan plastic bersamaan juga bersetuju dengan jumlah kecil tidaksah dan titik kritikal berlaku pada hujung kecacatan sepanjang kedalaman kecacatan dan panjang.

# TABLE OF CONTENTS

**CHAPTER 3 METHODOLOGY**



**CHAPTER 4 RESULTS AND ANALYSIS**



**CHAPTER 5 CONCLUSION**

**APPENDICES**

# LIST OF TABLES

# LIST OF FIGURES

# LIST OF SYMBOLS

| | |
|---|---|
| $P_y$ | Internal pressure on the onset of yield |
| $P_u$ | Ultimate pressure |
| $\sigma_{Vonmises}$ | Von Mises yield criteria |
| $\sigma_1$ | Ratio of the applied tensile force F to the metal area A |
| $\varepsilon_i$ | Strain at onset of instability |
| n | Strain coefficient |
| D | Pipe outer diameter |
| t | Pipe wall thickness |
| k | Strength coefficient |
| c | Defect width |
| L | Pipe length |
| $l$ | Defect length |
| d | Defect depth |
| $P_{\exp}$ | Experimental pressure |
| $V_{Void}$ | Volume of voids |
| $V_{Matrix}$ | Volume of matrix |
| $f$ | Void volume fraction |
| $\sigma_y$ | Yield stress |
| $\phi$ | Non-dilatational strain energy |
| $\sigma_0$ | Von Mises effective stress |

| | |
|---|---|
| $q_1$ | Tvergaard coefficients describing the plastic properties of the material |
| $f^*$ | Actual void volume fraction |
| $\sigma_m$ | Hydrostatic pressure (mean stress) |
| $\sigma_{eq}$ | Von Mises effective stress |
| $f_C$ | Critical void volume fraction |
| $f_F$ | Void volume fraction corresponding to the loss of material strength |
| $\dot{\varepsilon}_{ii}^{*P}$ | Plastic part of the strain rate tensor |
| $(R/R_0)_c$ | Critical void growth ratio |
| $d\varepsilon_{eq}^{P}$ | Equivalent plastic strain increment |
| $\alpha$ | Material constant |
| $\varepsilon_f$ | Fracture strain |
| T | Stress triaxiality |
| $\varepsilon_{eq}$ | Strain equivalent |

# LIST OF ABBREVIATIONS

| | |
|---|---|
| FE | Finite Element |
| SMCS | Stress modified fracture criteria |
| ASME | American Society for Mechanical Engineer |
| Eq. | Equation |
| UTS | Ultimate Tensile Strength |
| GTN | GursonTevargaard model |
| VGM | Void Growth model |
| API | American Petroleum Institute |

# Chapter 1

# INTRODUCTION

## 1.1 BACKGROUND OF STUDY

Pipelines are one of the major means of transporting hydrocarbons (oil and natural gas) from one point to the other point, which may be routed within onshore or offshore locations. There is a great risk that defects will occur during the service life of these pipelines. Corrosion, either internal or external is one of the common defects observed in many instants. With the passage of time the corrosion that occurs either at a localized point or onto a large area cause the metal loss and hence the strength or in other words load bearing capacity of the pipeline is reduced. Corrosion induced micromechanical ductile fracture in pipe body due to the growth of void and coalescence in the materials which will lead to plastic deformation that cause bursting of pipe. The prediction of burst pressure is based on the ultimate pressure, $P_u > P_y$ yield pressure (Antaki, G.A., 2003). Also, identification of different types of corrosion can help in applying the suitable analysis method and solution. Hence, predictive measurement on defect assessment for high pressure piping is important aimed at quantifying the impacts of the defects and for safety precautions procedure.

An initiative has been taken by the European gas transmission system operators on the frequencies and probabilities study that cause incidents in pipelines. ($8^{th}$ Report of EGIG, Dec 2011). It is divided into two groups, first, the primary failure frequency which is by the external interference, corrosion material defect, ground movement and others. The other is secondary failure frequencies which consider the influence of design parameters (pressure, diameter, wall thickness, etc.) The external interference the activity having caused the incident such as digging, piling, and equipment involved in incident. Next, corrosion includes the location either internal or external, and the

corrosion type. Then the material failure, which is the type of defect, next is ground movement like erosion, flood and others. The installation of the annual length of pipelines was equal to 129,719 km in 2007 and increase to 135,211 km in 2010. Also, the incidents were reported of total 1,249 cases over the period 1970-2010 with primary failure frequency per 1000km-yr is 0.372. Whereas for an interval of 5 years between 2006-2010, the number of incidents occurs are 106 cases and the primary failure frequency per 1000km-yr is 0.162. In fact, external interference is highest incidents causes with contribution 0f 48.4% followed by material failure and corrosion with 16.7% and 16.1% respectively. From the statistics, except for the external interference incident causes, from the view of internal, that is the material failure and corrosion, it have given a big impact on the incident occur in pipelines. Hence, a careful study and analysis need to be carried out to ensure the integrity of pipeline service in this oil and gas field.

In fact, numerous experiments on the material failure and corrosion which is the impact of defects and analytical researches has been done especially on the burst pressure predictions of pipelines but this entire are still not enough to ensure its integrity. This is due to the lack of experimental and analytical researches ability in performing tests reflecting complex geometries and loading condition. As it is known that pipeline which lying on the seabed and is subjected to the physical environmental aspects must be taken care of in order to ensure its integrity. The loading conditions are referring to the physical environmental aspect which includes the oceans depth and distances, hydrostatic pressure, temperature, seawater and sea-air interface chemistry, and crude oil composition. Hence, in order to study the incidents consequence of the material failure and corrosion, the application of micromechanical model using finite element method is important to study more detail of the internal failure mechanism and sensitivity analysis can help improve the study.

## 1.2 PROBLEM STATEMENT

Experimental and analytical study on the material failure of steel pipe is not enough to ensure its integrity due to the lack of experimental and analytical researches ability in performing tests reflecting complex geometries and variable loading condition. Hence, Gurson model which is the micromechanical model transfer better detection of the defect analysis in studying the ductile fracture of pipeline by predicting its burst pressure. This Gurson model will be based on finite element method to study the material fracture in terms of void where the variable factors that cause pipeline fracture can be analyzed.

## 1.3 OBJECTIVES

The aim of this research is about the study and application of micromechanical model, GTN model in predicting pipe burst pressure. Hence, the objectives of this study are:

i. To predict the burst pressure of steel pipe using Gurson-Tvergaard-Needleman (GTN) model.

ii. To determine the effect of depth and length of the defect towards the failure pressure of the pipe.

## 1.4 SCOPE OF PROJECT

i. The material used in this project is steel with API X65.

ii. The outer diameter of the pipe is fixed to 762 mm, thickness 17.5 mm and length 2300 mm and it is analyses with different defect depth and length.

iii. The defect depth of 25%, 50% and 75% and defect length of 100 mm, 200mm, 300 mm, 400 mm, and 600 mm are used in the present study.

iv. A quarter of a full pipe was modeled due to symmetry conditions.

v. A finite element analysis using three-dimensional elastic-plastic damage analyses were performed to simulate the pipe burst tests using Marc Patran.

vi. The failure assessment has been compared with limit load analysis (ASME B31G, modified ASME B31G,and PCORRC)

## 1.5 SIGNIFICANCE OF PROJECT

In the present study, different types of defects which variant in defect depth and length is carried out to test more cases and this contributed more data which expand the scope of analysis. Besides, the prediction of burst pressure will be based on the character of void volume fraction using failure criterion approach in FEA. Unlike the previous research (Chang, S.O., 2011) where, even the Gurson model is simulated for ductile damage and failure, but the prediction of burst pressure of pipe is based on the empirical-based burst pressure equation for axial cracked pipe and also using stress modified fracture strain model. The usage of void volume fraction makes the prediction simpler as it is based on the critical void volume fraction whether it exceed or not.

# CHAPTER 2

# LITERATURE REVIEW

## 2.1 INTRODUCTION

There will be two main parts discussed in this chapter. The first part is on the material and corrosion of steel pipe. The second part will be on the method of predicting failure in pipeline of this project. For the first part, it include the von Mises yield criteria of burst pressure, where $P_u \geq P_y$. It is followed by some steel pipe standard categories. Burst pressure occurs as result of wall thinning due to corrosion. In fact, there are few categories of pipe crack, for instance, longitudinal crack, circumference crack, and spiral crack.

In the second part of the prediction of failure of structures, there are the global approaches and the local approach. (Clotilde, B., et.al. 2004). The global approach was first proposed more than 50 years ago, in the framework of linear fracture mechanics, and then extended to plasticity and viscoplasticity through nonlinear fracture mechanics about 30 years ago. Although this global approach are extremely useful, frequently used and still improving, they have been proved to suffer from several limitations; where industrial need new methodologies tools to be analyzed realistically and mastered practically. This need for new methods, combined with the development of physically-based models of mechanical behavior and micromechanical treatments, has proposed by McClintock (McMlintock, 1963) in the early 80's to the so-called “local approach to fracture”. Unlike the “global” treatment, which makes the fracture resistance of a component mainly depend on a single global parameter, whatever the damage and deformation mechanisms of the specific material under study, the “local” approach emphasizes these material specificities: it combines a detailed experimental analysis of the considered materials and of their specific damage mechanisms, a realistic modeling

of these mechanisms and the implementation of these models into a numerical simulation of the response of the structural components under investigation.

Under the local approach of fracture, depending on the model employed for simulating damage, it divided into damage based on volume which is micromechanical model and damage based on surface which is phenomenological model. Micromechanical model is divided into strain based (include uncoupled and coupled) and stress based (the design codes).The uncoupled modeling are SMCS and VGM whereas the coupled modeling is GTN. The stresses based are ASME B31G, Modified ASME B31Gand PCORRC. The micromechanical model is incorporating void nucleation, growth and coalescence, for instance, the Gurson–Tvergaard–Needleman model (Tvergaard, V., 1981, 1982). The damage based on surface is using a phenomenological model for ductile fracture, which is the cohesive zone model (Chen CR, 2003). All these methods will be summarizing in the Figure 2.1.

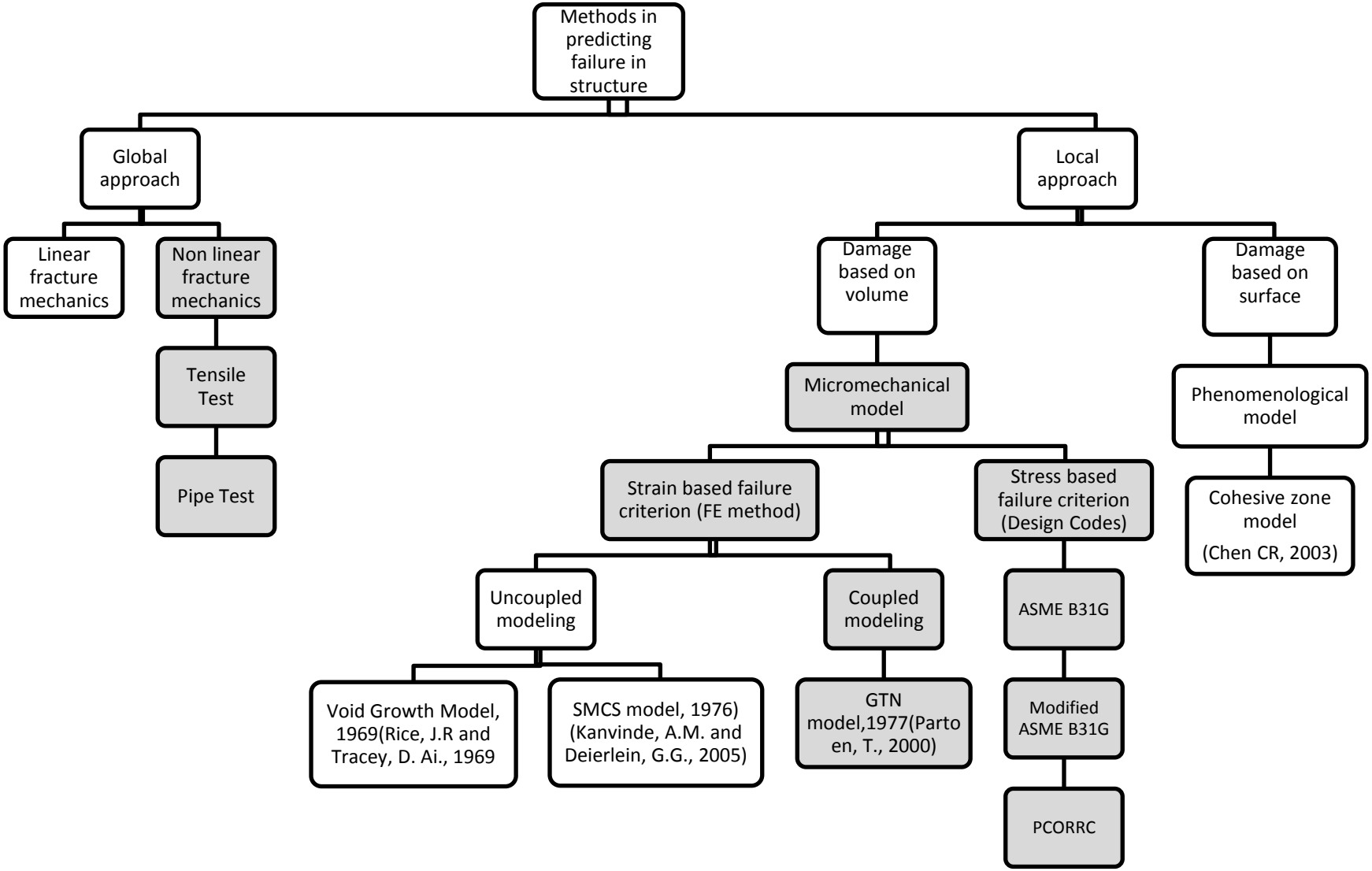


**Figure 2.1:** This highlight box will be the methods used in present study. The methods used in present study are the nonlinear method (pipe test), strain based method (GTN model) and stress based method (design codes) as to validate each other's.

For the present study, the methods used are those highlighted which are the non-finite element method (experimental method), finite element (FE) analysis (GTN model), and closed form method (the design codes). These three methods are important in predicting burst pressure of steel pipe as they all acts together to give verification and comparison between each other. Finite element method is important as it can greatly enhance the overall result by checking against deformation, stress or vibration specifications. Most importantly, FE analysis results identify critical areas which carry most of the load, as well as areas where material may be saved. The burst pressure from FE was then compared with values calculated using design codes for pipelines containing defects.

## 2.2 BURST PRESSURE

Burst pressure of steel pipe occur when corrosion induce wall thinning on the pipe and hence result in metal loss which is the failure. In fact, burst pressure occurs when $P_u \geq P_y$, where $P_u$ is the ultimate pressure and $P_y$ is the internal pressure at onset of yield.

### 2.2.1 von Mises Yield Criteria

Based on the von Mises criterion, the yielding of the pipe wall will take place when the distortion energy reaches a certain limit value $\sigma_{vonMises}$. (Antaki, G.A., 2003). This can be shown as in Eq. (2.1).

$$(\sigma_h - \sigma_1)^2 + (\sigma_1 - \sigma_r)^2 + (\sigma_r - \sigma_h)^2 = \sigma_{vonmises} \tag{2.1}$$

The value $\sigma_{Vonmises}$ is obtained from the tensile test. In the case, $\sigma_h = \sigma_r = 0$ and $\sigma_1$=F/A is the ratio of the applied tensile force F to the metal area A. In fact, yielding will take place when $\sigma_1 = S_y$, where the von Mises criterion can be written as in Eq. (2.2):

$$(0 - S_y)^2 + (S_y - 0)^2 + (0 - 0)^2 = \sigma_{Vonmises} = 2S_y{}^2 \tag{2.2}$$

By substitution, the internal pressure at which the pipe wall yields is as shown in Eq. (2.3). (Antaki, G.A., 2003).

$$Py = \frac{Sy}{\sqrt{\frac{3}{4}\left(\frac{D}{2t}\right)^2 + \frac{3}{2}\left(\frac{D}{2t}\right) + 1}} \tag{2.3}$$

$P_y$ =internal pressure at onset of yield, psi

For large diameter to thickness ratio (D/t>>1) we obtain the internal pressure at the onset of yield as in Eq. (2.4).

$$Py = \frac{4tSy}{D\sqrt{3}} \tag{2.4}$$

As the internal pressure continues to increase beyond the yield pressure, $P_y$ the pipe wall will bulge outward and reach a point of instability. Actually, in reality the material is not perfectly uniform and this bulging does not take place exactly uniformly around the circumference but preferentially on the side of the pipe wall. The hoop strain at which instability occurs is as shown in Eq. (2.5).

$$\varepsilon_i = n/2 \tag{2.5}$$

$\varepsilon_i$ = strain at onset of instability

n= strain coefficient

After the instability, which is the outward bulge in pipe wall, the pipe ruptures. The pressure at ruptures is the ultimate pressure $P_u$ given as in Eq.(2.6):

$$P_u = (2kt/D)e^{-n}\{n/[2(3/4)^{(1+n)/n}]\}^n \tag{2.6}$$

Where $\sigma_u$ = ultimate pressure at burst, psi

t= pipe wall thickness, in

k= strength coefficient, psi

D=pipe outer diameter, in

### 2.2.2 Steel Pipe

Steel pipe is the most common pipe that has been use in global industries. This is because the material properties of the steel pipe itself. Steel is among the best material in aspect of durability and long live lasting compare to the other material. This kind of pipe normally used in many industries to transfer fluid such as oil, gas, water, chemical, smoke and others. In steel pipe itself, there are certain level or grades for differentiate the steel pipe durability. There are various grades of steel, but the common used by industries is X65, X80 and X100 steels. The higher grades mean the higher durability of the steel. Table 2.1 shows the mechanical properties for the pipelines steel.

**Table 2.1:** Mechanical properties of various grades of pipelines steel (Cheng, LY.2012)

| Mechanical properties (steel) | X65 | X80 | X100 | X42 |
|---|---|---|---|---|
| Young's modulus (MPa) | 207000 | 207000 | 207000 | 207000 |
| Poisson's ratio | 0.3 | 0.3 | 0.3 | 0.3 |
| Yield Strength (MPa) | 456 | 646 | 802 | 290 |
| Tensile Strength (MPa) | 570 | 760 | 891 | 420 |

## 2.3 MAJOR CORROSIONS IN PIPELINES CARRYING GAS AND CRUDE OIL

Corrosion is one of the leading that cause failure in onshore and offshore transmission pipelines. As these oil and gas pipelines play a critical role in delivering energy resources needed to power communities around the world, its causes of corrosion leading to failure are need to be identified. There are two areas of corrosion occur in pipelines: corrosion from medium carried inside the pipes (internal corrosion); also corrosion attack upon the outside of the pipes (external corrosion).

Corrosion, either internal or external is an electrochemical, time dependent mechanism process that causes metal loss. It is referring to the loss extending over a significant area of the pipe resulting in wall thickness decrease. Wall thinning on pipe occur when the load (pressure) of the pipe increases. This local wall thinning could continue, leading to necking of the wall and failure due to void nucleation, growth and coalescence in a manner comparable to that of a tensile test specimen.

Corrosion mechanism causes an irregularity of local surface which is due to presence of micro-stress raisers which lead to crack through a process of void nucleation and growth. The behavior after the initiation of a crack would depend on the toughness of the material. In a high toughness material, initiation would be delayed to a higher load and further stable ductile tearing would be slower, or a growing crack could blunt; wall thinning would continue and the failure load would tend to that of plastic collapse. However, in a lower toughness material, once initiated, the crack would extend by stable ductile tearing, reducing the remaining wall thickness and hence reducing the degree of wall thinning that occurs before failure. The load at failure would be less than that predicted by the plastic collapse limit state because of the stable ductile tearing. Figure 2.2 below shows the reducing in thickness of pipe thickness due to wall thinning.

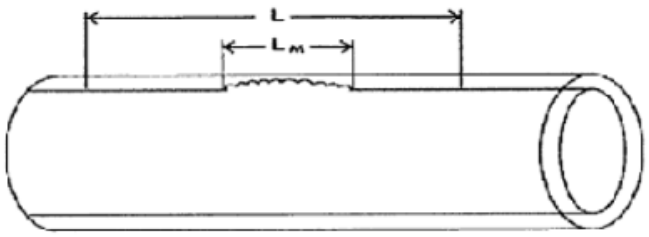


**Figure 2.2:** Reducing in thickness of pipe thickness due to wall thinning.

Source: Piping and pipeline engineering (Antaki, G.A., 2003).

### 2.3.1 Factors that contribute to external corrosion in pipelines

i. Soil conditions

Buried pipelines are exposed to the soil structure and conditions where the factors like the soil type, drainage, temperature, $CO_2$ concentration and electrical conductivity may contribute to the creation of a corrosive environment. This is underground corrosion and an electrolytic process occur where the moisture content of the soil act as an electrolyte, and the ions required to conduct the current are supplied by water-soluble salts (chlorides, sulfates, etc.)

ii. Temperature

The temperature of the soil as well as the temperature of the pipe may create favorable conditions for attack on pipeline materials. Liquid and gas lines have slightly different operating temperature characteristics but both are still susceptible.

iii. Pipe pressure

Pipeline placed on the seabed is subjected to high pressure. Corrosion, in particular cracking, is related to the pressures exerted on the pipe. As the pressures within the pipe are increased, the growth rates for cracks also increase. The circumferential stress (hoop stress) generated by the pipeline operating pressure is usually the highest stress component that exists.

iv. Corrosion resulting from passing through soils of different material content

The potential along the pipe line depends to some extent on the soluble salt content of the soil. It is found the sections of a pipe passing through soil of high salt content are anodic to sections about which the salt content of the soil is lower as shown in Figure 2.3.

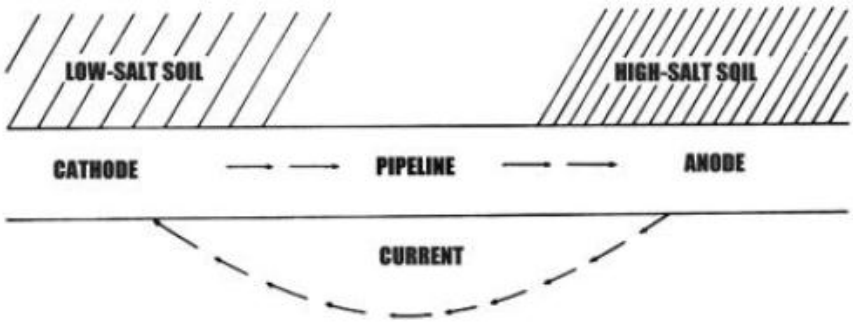


**Figure 2.3**: Pipeline corrosion in different soils

v. Marine Organisms

Marine organisms effect upon pipeline structure when the increase of drag due to the obstruction of the free flow of water past the surface of the structure. This is the 'fouling' of the pipe surface. Fouling increases the size of the member and more importantly increase the surface roughness. Mussels, barnacles and algae increase the diameter of the steel pipe besides, barnacles and algae urchins secrete an acid which pits and erodes steel.

vi. Marine bacteria

Anaerobic sulphur-based are often trapped in the ancient sediments of the oil reservoir. Upon release to the saltwater, they convert to sulphates and upon subsequent contact with air they produce sulphides ( $H_2S$ ). These bacteria and sulphides produced, will attack weak and permeable concrete and cause pitting corrosion in steel.

### 2.3.2 Factor that contribute to internal corrosion in pipelines

Factors that contribute to internal corrosion in pipelines are influenced by temperature, $CO_2$ and $H_2S$ content, water chemistry, flow velocity, oil or water wetting and composition and surface condition of the steel.

(i) Water chemistry

Crude oil, being a non-conducting electrolyte, does not support corrosion. However, if the crude oil contains water, then corrosion may take place in those locations where water drops out of crude oil and comes in contact with the metallic surface. The bulk crude oil may indirectly affect the corrosion but when the pipelines travel over distances, which is considered unlikely at one location can become significant when summed over a pipeline infrastructure. Hence, the water (an electrolyte) also the sediments are the components of the corrosion cell. Without it, corrosion will not occur at appreciable rates within the transmission pipeline.

### 2.3.3 Corrosion Mechanism on pipeline

Corrosion encountered in pipeline industry involves several mechanisms. These have been grouped into electrochemical corrosion, chemical corrosion, and mechanical corrosion.

#### 2.3.3.1 Electrochemical corrosion

i. Crevice corrosion

This type of corrosion often starts at drill pipe joints or the tubing collar of the pipe. The gap in the joint becomes devoid of oxygen and anodic. In salty water the corrosion is promoted by the migration of negatively charged chloride ions to the crevice. These not only counteract the buildup of positive charges around the crevice, but also act as a catalyst accelerating the dissolution of metal. This on-going process leads to deep pits.

ii. Pitting Corrosion

Pitting corrosion is the localized corrosion of a metal surface confined to a point or small area that takes the form of cavities due to the sulfides produce

from anaerobic sulfur-based bacteria for the case of offshore pipeline. Pitting corrosion is usually due to two affecting factors, which are the environmental (chemistry) and the material (metallurgy). The environment may set up a differential aeration cell (a water droplet on the surface of a steel, for example) and pitting can initiate at the anodic site (centre of the water droplet). Also, pitting factor is the ratio of the depth of the deepest pit resulting from corrosion divided by the average penetration as calculated from weight loss.

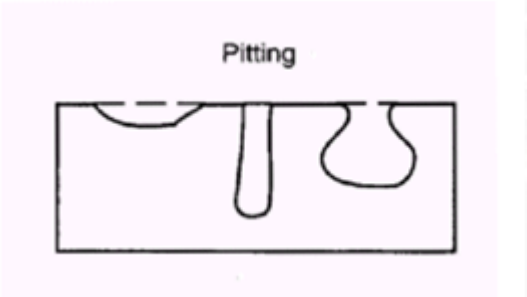


**Figure 2.4:** Pitting corrosion

Source: WebCorr Corrosion Consulting Services.1995-2013. Different types of Corrosion-Pitting Corrosion (online).

### 2.3.3.2 Chemical corrosion

(i) Hydrogen Sulfide

Hydrogen Sulfide ($H_2S$) when dissolved in water, is a weak acid and is a source of hydrogen ions and it is corrosive. The corrosion products are iron sulphides and hydrogen. Iron sulphides form a scale that at low temperature can act as a barrier to slow corrosion. However, in seawater, the presence of chloride and oxygen has made the casing and galvanic corrosion starts.Especially the presence of chloride ions, the barnacle type corrosion occurs, which can be sustained under thick but porous iron sulphide deposits. The chloride forms a layer of iron chloride, which is acidic.

(ii) Carbon Dioxide

Like $H_2S$ , carbon dioxide is a weakly acidic gas and becomes corrosive when dissolved in water. However, carbon dioxide just hydrate to carbonic acid ( $H_2CO_3$), a relatively slow process before it becomes acidic.

(iii) Microbiologically-Influenced Corrosion (MIC)

MIC, also known as microbial corrosion or biological corrosion, is the deterioration of metals as a result of the metabolic activity of microorganisms which occurs in waters and soils with pH 4~9 and temperature 10 degree Celcius-50 degree Celcius. These bacteria can be broadly classified as aerobic (requires oxygen to become active) or anaerobic (oxygen is toxic to the bacteria). Sulphate reducing bacteria (SRB) is anaerobic and is responsible for most instances of accelerated corrosion damages to offshore steel structures. These anaerobic bacteria metabolize sulphate ions and produce hydrogen sulphide. Colonies of SRBs can form deposits that lead to crevice corrosion with produced $H_2S$ accelerating corrosion.

**2.3.3.3 Mechanical corrosion**

(i) Sulfide Stress Corrosion

Production of hydrogen results from sulphide stress cracking (SSC). SSC occurs when a susceptible metal is under tensile stress and exposed to water containing hydrogen sulphide. Corrosion cells generate FeS and atomic hydrogen. The amount of hydrogen into the metal is usually into impurities at the grain boundaries. Penetration of hydrogen into the body of metal reduces ductility and accumulation of hydrogen generates pressure. For high strength steel the combination of lack of ductility and internal stress superimposed on the tensile stress causes the metal to break and crack.

## 2.4 TYPES OF CRACKS

In case of evaluating internal burst pressure of a wall thinned straight pipe, the crack can be divided into three types of defect crack, the axial crack, longitudinal crack and circumference crack as shown in figure 2.5. In fact, the axial crack can be grouped in to planar flaw and non-planar flaw as shown in figure 2.6 below.

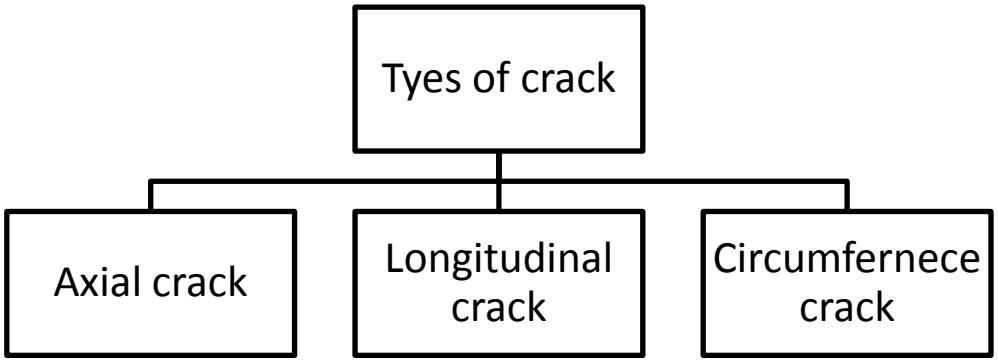


**Figure 2.5:** Classification of crack in pipeline

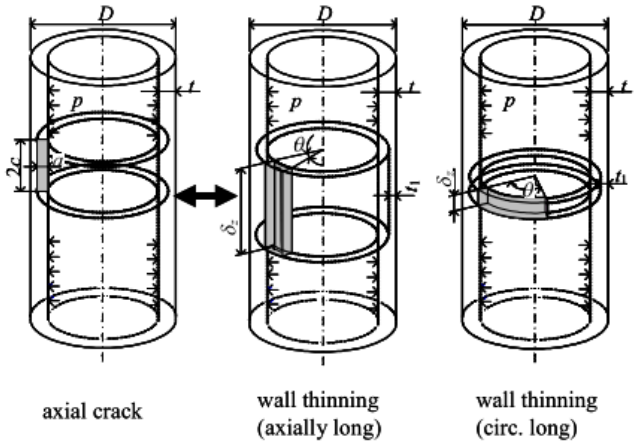


| | crack | wall thinning |
|---|---|---|
| flaw depth | $a$ | $t$-$t_1$ |
| axial length | $2c$ | $\delta_z$ |
| circ. length | | $\theta$ |

**Figure 2.6:** Axial planar flaw and non-planar flaws) in a pipe.

Source: Toshiyuki, M. (2010)

Longitudinal cracks are formed as a result of excessive soil and traffic loads or inadequate pipe bedding. In fact, visible longitudinal cracks observed at top and invert inside the pipe should be more severe than those on the outside because tensile stress occur at top and invert portion of the inside of the pipes. On the contrary, longitudinal cracks formed outside the pipe at the sides of concrete pipe should be more severe than those on the inside.

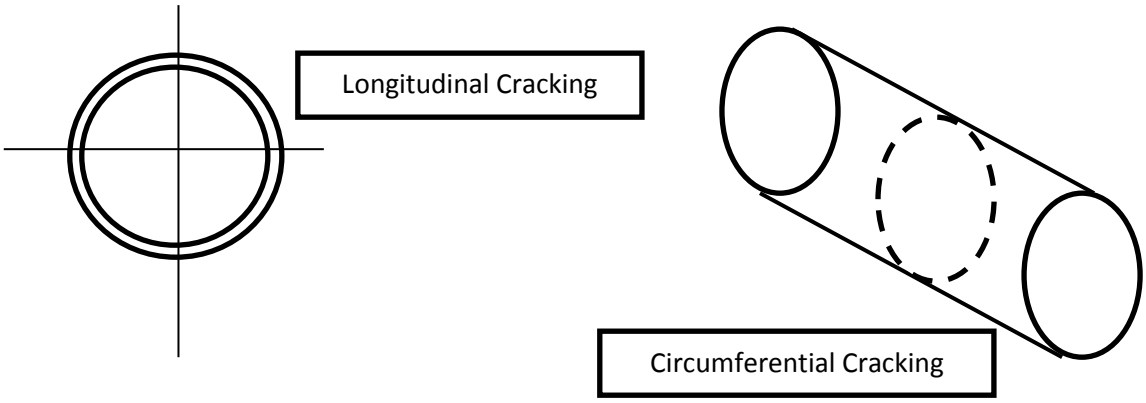


**Figure 2.7:** Longitudinal cracks circumferential cracking

Source: Hansen, B., Lee, D. and Demartini, C. The cracking of stormwater pipe and the significance of construction loads.

Also, longitudinal cracks wandered between 11 to 1 o'clock and 5 to 7 o'clock. These indicated an overload from a vertical load on a fully supported pipe. It can be assumed that corresponding cracks would be present on the outside of the pipe around the 3 and 9 o'clock positions.

For the circumferential cracks, it appeared at the midpoint of the pipe or at around the third points. The midpoint cracks indicate a bending overload with the pipe acting as a beam. The third point cracks suggest the pipe is acting as a cantilever.

## 2.5 STRAIN BASED FAILURE CRITERION (MICROMECHNICAL MODEL)

Strain based failure criterion can be grouped into micro-mechanical models. In fact, over the decade, micromechanical has been used to predict ductile fracture initiation of alloys by modeling void nucleation, growth and coalescence. Voids nucleate around secondary phase inclusions in the steel matrix, and grow under plastic strains in the presence of multiaxial stress fields to coalesce and form the macroscopic fracture surface. Analytical derivations by Rice and Tracey (1969) suggest that void growth is dependent on the evolution of two key quantities—the equivalent plastic strain $\varepsilon_p$, and the stress triaxiality. The stress triaxiality, $T = \sigma_m / \sigma_e$, is a ratio of the mean or hydrostatic stress $\sigma_m$, and the effective or von Mises stress $\sigma_e$. Although classical metal plasticity assumes yielding to be unaffected by mean stress at a macro level in a void-free continuum, the mean stress (and similarly triaxiality) is largely responsible for localized yielding around voids to cause void growth.

A lot of models has been developed which enable the application of ductile fracture analysis in a way that is to the largest extent in accordance with actual phenomena in a material. This is especially true for the corrosion in steel pipes as it is about the study of local stresses strains at the spots of structure highly exposed to external loading which induce to high stress concentration caused by change of geometrical form exists, is prerequisite for application of this micromechanical models. Also, micromechanical models often involve using of parameters and it is reliable on numerical tools in solving these problems. In fact the application of the finite element method (FEM) has become almost an unavoidable part of micromechanical analysis.

Micromechanical models for ductile fracture, incorporating void nucleation, growth and coalescence are Gurson-Tvergaard-Needleman (GTN) model (Tvergaard, V., 1981, 1982), void growth model (Rice, J.R and Tracey, D. Ai., 1969). However for Stress modified critical strain model (SMCS) (Kanvinde, A.M. and Deierlein, G.G., 2005) it is the phenomenological model for ductile fracture. As mentioned, GTN model will be used in this project, but the other two models will be discussed also, which are VGM model, based on research by Rice and Tracey (Rice, J.R and Tracey, D. Ai., 1969) and SMCS model, based on research by Hancock and Mackenzie (Hancock, J.W., et.al., 1977)

### 2.5.1 Ductile Fracture

Ductile fracture is one of the most common fracture mechanisms in metals, where ductile materials fail as a result of nucleation, growth and coalescence of micro voids. Figure 2.6 displays the whole ductile fracture process. The single steps are explained in the following subsections. Ductile crack initiation is affected by many processes including initial void distributions, anisotropy in the inclusion spacing and shape, void nucleation, evolution of void shapes, void-to-void interactions and the nucleation and growth of secondary voids near coalescence.

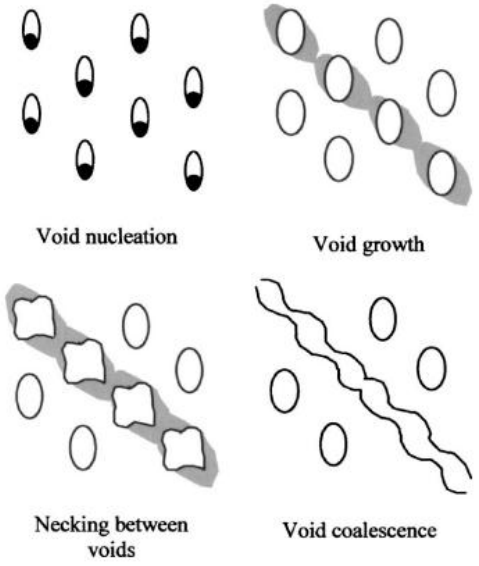


**Figure 2.8:** Ductile fracture process

Source: (Kanvinde, A.M. and Delerlein, G.G.2007)

#### 2.5.1.1 Void Nucleation

Voids nucleate at inclusions or second phase particles when enough stress is applied. Then the interfacial connection between particle and matrix is broken. The nucleation of the void is often the critical step and fracture happens soon after that. However, for materials, where the voids nucleate easily, the fracture behaviour is controlled by void growth and void coalescence.

### 2.5.1.2 Void Growth

Void growth is caused by increasing plastic strain and hydrostatic stress after void nucleation. For instance, for the growth of penny-shaped voids, it started with plastic deformation, it opened and become a more rounded voids (Lassance, D. et.al. 2006). The flat voids is due to the partial decohesion of particle. At some point, strong interactions take place between neighboring voids leading to the localization of the plastic flow within the ligament, which involve the onset of the void coalescence process.

For a relative low initial void volume fraction f, the void growth goes off independently. But after f becomes larger than a certain critical value fc neighboring voids will interact. Plastic strain is concentrated along several voids and local necking starts. This and continuing void growth finally lead to connection of the voids what is equal to separation of material.

### 2.5.1.3 Void Coalescence

Void coalescence is the final stage in the failure mode of ductile materials. It consists in the localization of plastic deformation at the microscale inside the intervoid ligament between neighboring voids, with material off the localization plane usually undergoing elastic unloading (Lassance, D. et.al. 2006). Localization can occur at any orientation relative to the principal straining axis, depending on the orientation of the ligament between the two coalescing voids: tensile (i.e. normal separations) or shear localizations are possible.

The tensile void coalescence mechanism means a transition to a uniaxial straining mode of the representative volume element and it happen such that in micro scale. There are some terms that have to be specified, the ‘void coalescence’ is for the void enlargement evolution after the transition to the uniaxial straining mode and the ‘void growth’ is for void enlargement before localization. Also, “shear” coalescence is for low stress triaxiality, low strain biaxiality and low strain-hardening. “Void sheet” is for when a second, smaller population of voids intervenes, the coalescence mechanism.

The void coalescence mechanism is a localization mechanism at the scale of the void size that must thus be distinguished from the localization in a band at the microscopic scale with a width typically of the order of one or more void spacing (e.g. Tvergaard, 1981). The confusion can arise because of the fact that when such a microscopic localized band develops, coalescence usually follows soon after leading to fracture with a small additional increase in remote displacements. Inside the band, the cavities grow very rapidly due to the large microscopic strain rates. Void coalescence, in the sense defined here, follows the onset of the macroscopic plastic localization when one occurs. For practical purposes, microscopic localization can be regarded as the onset of fracture, even though the distinct micro mechanism of coalescence will develop somewhat later within the band.

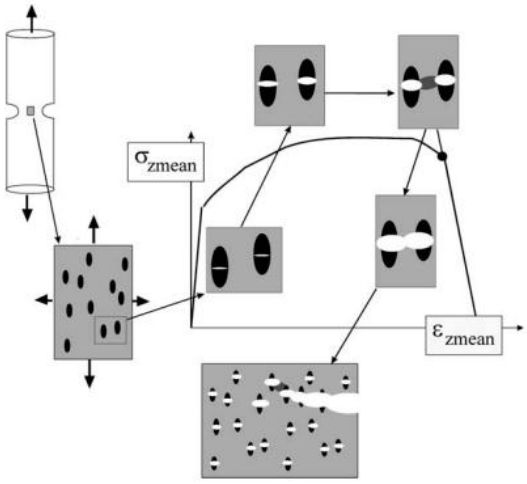


**Figure 2.9:** Sequence of damage mechanisms starting with particle fracture, followed by a stable void growth stage from an initially very flat void geometry, void coalescence, and crack propagation; the sequence is related to the overall stress strain curve associated to a representative volume of material.

Source: Lassance, D. et.al. (2006)

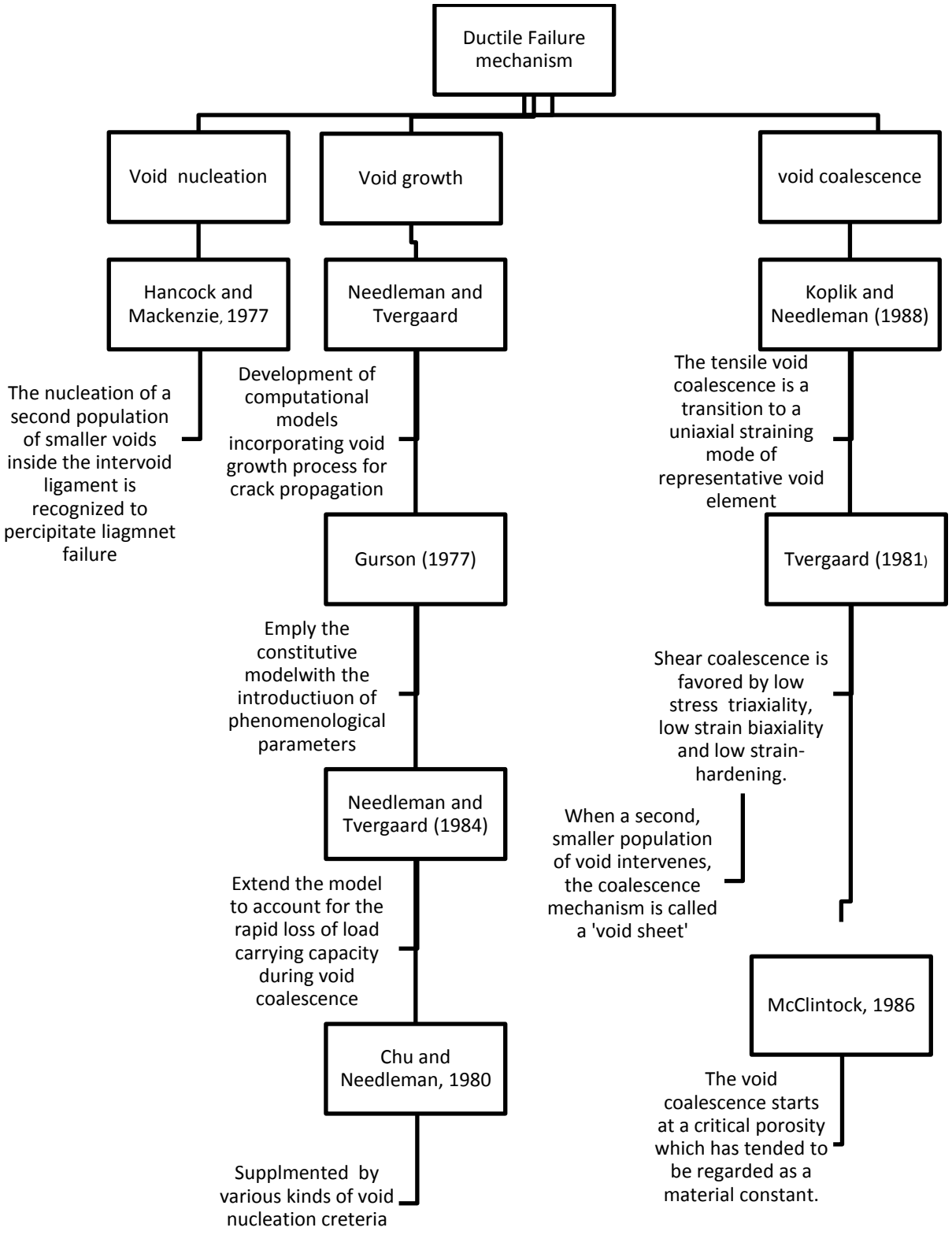


**Figure 2.10:** Ductile fracture mechanism on void following authors.

## 2.6 CLASSIFICATION OF MICROMECHNICAL MODEL

All the micromechanical models mentioned may be classified in two large groups: uncoupled micromechanical models and coupled micromechanical models (Rakina, M. et.al, 2004) According to the uncoupled micromechanical damage models; the damage parameter is calculated in the post-processing phase of the finite element (FE) analysis. Here the VGM and SMCS model will be applied here. The Rice–Tracey void growth model will be evaluating damage parameter–void growth ratio $R / R_0$ .

Whereas, for the coupled micromechanical models, one or more parameters are calculated to predict ductile fracture initiation and GTN model will be applied here. Thus, the FE analysis must include procedure for calculation of these parameters and optionally, fracture initiation criterion. The most frequently used damage parameter is the void volume fraction. Applied micromechanical model was incorporated into the Patran for calculation using FEM.

### 2.6.1 Coupled Micromechanical Modeling

For the coupled micromechanical modeling, the damage parameter has been "inserted into" numerical procedure and is estimated in the FE post processing evaluation. As mention earlier, the void growth depends on two key quantities: the equivalent strain, $\varepsilon_p$ and stress triaxality, T, where these two quantities influence cannot be avoided. The reason behind it is that coupled approach to the material damage and ductile fracture initiation considers alloy as a porous medium. that It allows us to predict the response of a material to certain micromechanical phenomena leading to failure, for instance void nucleation, coalescence and growth.

For GTN model, it was Gurson who found a mathematical function that partly describes part of the ductile material behaviour. He proposed a yield condition as a function of the void volume fraction f for a metal containing a dilute concentration of voids. In this condition the void volume fraction f is the ratio between the volume of voids $V_{void}$ and the volume of the whole matrix $V_{matrix}$ : Eq. (2.10)

$$f = \frac{V_{void}}{V_{matrix}} \tag{2.10}$$

In fact, the void volume fraction, f is introduced for plastic potential, as because the GTN model is based on the hypothesis that void nucleation and growth in metal may be macroscopically described by extending the Von Mises plasticity theory to cover the effect of porosity occurring in the material. Gurson's yield condition bases on the spherically symmetric deformation of a rigid-perfectly plastic body around a single spherical void and can be written in the following form, where q denotes the von-Mises effective stress, $\sigma_y$ represents the yield stress and p is the hydrostatic stress in Eq. (2.11)

$$\phi = \left(\frac{q}{\sigma_y}\right) + 2f\cosh\left\{-\frac{3}{2}\frac{p}{\sigma_y}\right\} - \left(1+f^2\right) = 0 \tag{2.11}$$

Later on, Tvergaard (1981, 1982) modified the model by introducing two parameters, $q_1$ and $q_2$, which are used to analyse the plastic behaviour of materials. Tvergaard found that the values that best fit the micromechanical cell model results correspond with $q_1$ = 1.5 and $q_2$ = 1.0, $q_3 = q_1^2$ =2.25. In the original Gurson model, $q_1 = q_2 = q_3 = 1$. For the two adjusting parameters introduced by Koplik and Needleman (1988) proposed the values of $q_1$ = 1.25 and $q_2$ = 1.0. These values provide improved agreement between GT model and the finite-element results of a voided cell.

For simplicity it is as in Eq. (2.12):

$$\phi = \left(\frac{\sigma_{eq}}{\sigma_0}\right)^2 + 2q_1 f^* \cosh\left(-q_2\frac{3\sigma_m}{2\sigma_0}\right) - \left(1+q_3 f^{*2}\right) = 0 \tag{2.12}$$

Where:

$\phi$- non-dilatational strain energy,

$\sigma_{eq}$ -von Mises effective stress

$\sigma_0$ - material strength resulting from the tensile strength curve (yield stress)

$\sigma_m$ -hydrostatic pressure (mean stress),

$f^*$-actual void volume fraction,

$q_1$-Tvergaard coefficients describing the plastic properties of the material

However, this modified Gurson model just describes void growth; thus a simulation of void coalescence was still missing. In 1984, Needleman and Tvergaard defined Equation 2.3 in order to simulate void coalescence, where f in Equation 2.2 must be replaced by $f^*$. Furthermore in the following equation, $f_c$ represents the critical void volume fraction and $f_F$ is the void volume fraction of final failure as in Eq. (2.13):

$$f^* = \begin{cases} f & f \le f_c \\ f_c + \dfrac{\bar{f}_F - f_c}{f_F - f_c}(f - f_c) & f_c < f < f_F \\ \bar{f}_F & f \ge f_F \end{cases} \qquad (2.13)$$

Where: $f_c$ - critical void volume fraction

$f_F$-void volume fraction corresponding to the loss of material strength

$$\bar{f}_F = \frac{q_1 + \sqrt{q_1^{\,2} - q_3}}{q_3}$$

This function implies that after void coalescence has started (f > $f_c$), the void volume fraction is amplified. Before void coalescence (f ≤ $f_c$) the void growth and the decrease of load carrying capacity follows the modified Gurson model according to Equation 2.13. Two phenomena contribute to increase the void volume fraction in FEM calculation with incorporated GTN yield criterion: One is the growth of the existing voids and the other is the nucleation of new voids during the external loading as in Eq. (2.4):

$$\dot{f}^* = \dot{f}^*_{nucleation} + \dot{f}^*_{growth} \qquad \text{Where, } \dot{f}^*_{nucleation} = A\dot{\varepsilon}^{*\,p}_{eq},\ \dot{f}^*_{growth} = (1-f)\dot{\varepsilon}^{*\,P}_{ii} \qquad (2.14)$$

$\dot{\varepsilon}_{ii}^{P}$ is the plastic part of the strain rate tensor. Nucleation of the secondary voids caused by strain increase has most frequently been tried to describe using two approaches.

### 2.6.2 Evolution of Gurson-Tvergaard-Needleman model

It is a known fact that the macroscopic parameter for ductile fracture, such as ductility and crack resistance curve cannot be directly transferred from one geometry to another. Thus, it can only be done by separating transferable parameters for ductile fracture from the parameters which describe geometry effect. As in most engineering alloys, ductile fracture often comes after the nucleation, growth and coalescence of micro voids. Hence, it is more reasonable to make contact ductile fracture to parameters that involve in micro-ductile fracture mechanisms rather than to macroscopic fracture parameters. The Gurson model is one of the widely used micromechanical models for ductile fracture. However, Gurson can only simulate the microvoid nucleation and growth and no ability to predict the void coalescence. This is due to Gurson only use homogenous deformation mode which is not sufficient. Hence, Tvergaard come out with the parameters, $q_1$ and $q_2$ to better capture the effects of the strain hardening and void shape evolution and finally extended by Needleman and Tvergaard (Needleman, A., Tvergaard, V., 1987).

Later this model is completed by two types of analytical void coalescence criteria, one for internal necking, Thomason (Thomason PF., 1990) and one for void sheet, McClintock (McClintock, F.A., 1968). Thomason proposed plastic limit load (Zhang, Z.L., 2000) where it says that localized deformation state of void coalescence is very different to the homogenous deformation state during void nucleation and growth. So the solution is, localized deformation and homogenous deformation should be considered together in ductile fracture modelling. So, a complete Gurson by Thomason can be obtained by neglecting the void shape effect and assume voids are always spherical. The extending of Gurson model by different authors and explanation is shown in Figure 2.11:

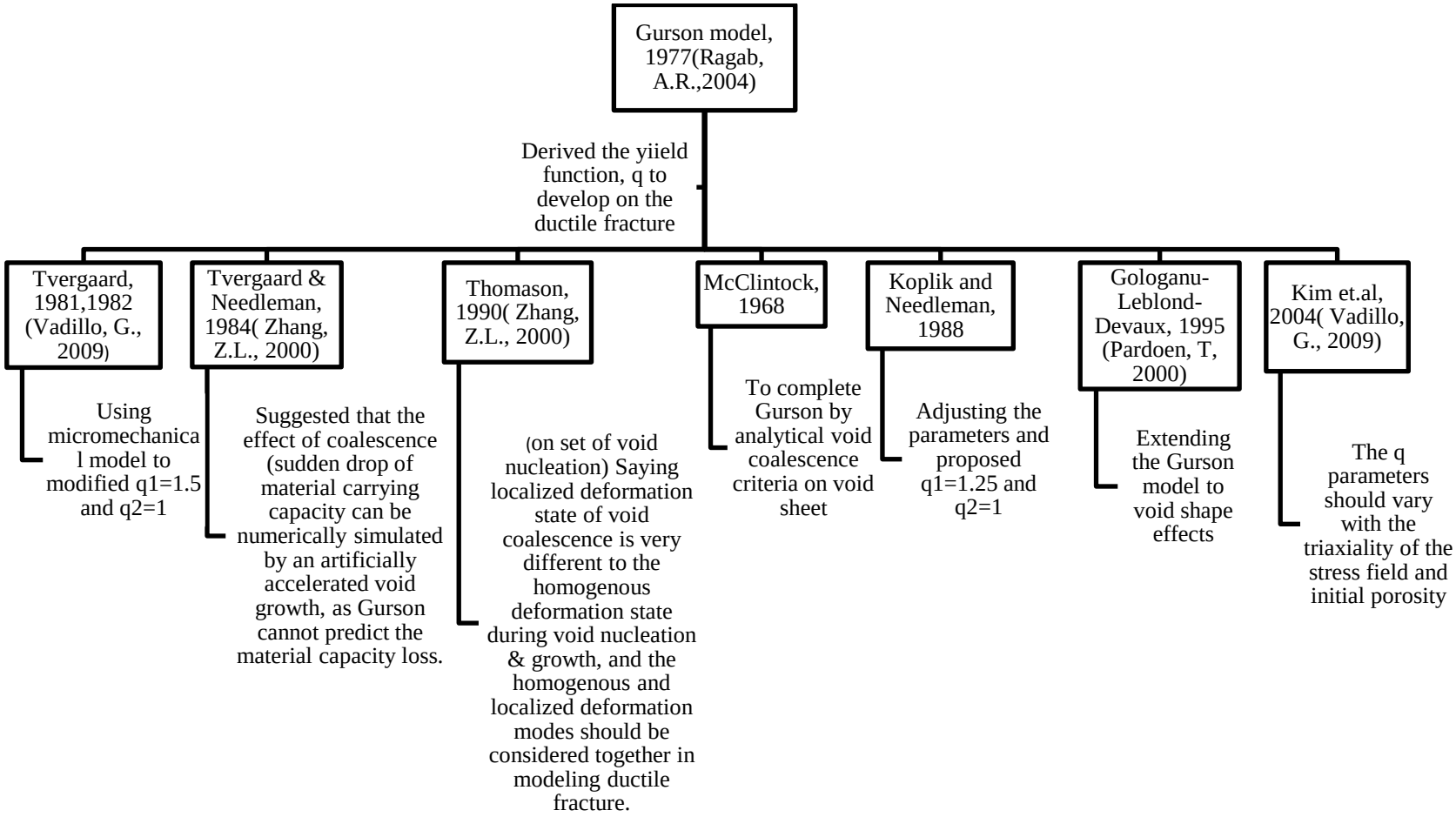


**Figure 2.11:** The authors and extending that involved in modifying Gurson model.

### 2.6.3 Uncoupled micromechanical modelling

There will be two models discussed here, VGM and SMCS models. The VGM involves an explicit integration of the stress and strain histories, whereas the SMCS is a simpler approach that is based only on the instantaneous values of the stress-strain quantities at fracture initiation. In fact, growth of nucleated voids is strongly dependent on stress and strain state. Also, there are experiments and analyses show an exponential increase with the stress triaxiality, defined as the ratio of the mean stress $\sigma_m$ and equivalent stress $\sigma_{eq}$. These describe the basis of uncoupled approach to the material damage in micromechanical analysis.

#### 2.6.3.1 Void Growth model (VGM)

In that case Von Mises criterion is most frequently used as a yield criterion. Rice and Tracey considered growth of isolated void in remote uniform Von Mises plastic field. Using the Rice–Tracey model (Rice, J.R. and Tracey, D.Ai., 1969) and taking into account material hardening proposed by Beremin (Beremin, FM., 1981), critical void growth ratio $\left(R/R_0\right)_c$ can be written as in Eq. (2.5):

$$In\left(\frac{R}{R_0}\right)_c = \int_{\varepsilon=0}^{\varepsilon_c} 0.283\exp\left(\frac{3\sigma_m}{2\sigma_{eq}}\right) d\varepsilon_{eq}{}^P \tag{2.15}$$

Where R stands for the actual mean void radius, $R_0$ is its initial value, $\sigma_M / \sigma_{eq}$ represents stress state triaxiality, and $d\varepsilon_{eq}{}^P$ is the equivalent plastic strain increment.

Besides, Expanding on the derivations of Rice and Tracey (1969), fracture is predicted to occur in the material when a quantity termed the void growth index (VGI) is equal to a critical value; $VGI_{critical}$. This corresponds to the voids growing large enough to exceed a critical void size to trigger necking instabilities between voids resulting in coalescence and macro crack formation. Mathematically, void growth is evaluated by the following expression that forms that basis of the VGM in Eq. (2.16):

$$VGI = \int_0^{\varepsilon_p^{critical}} \exp\left(-1.5\frac{\sigma_m}{\sigma_e}\right) d\varepsilon_p > VGI_{critical} \quad (2.16)$$

Where $\sigma_m$ and $\sigma_e$ =mean and the effective stress; $d\varepsilon_p$ =incremental equivalent plastic strain; and $VGI_{critical}$ =material parameter that quantifies the critical void ratio. The critical void growth index $VGI_{criticsl}$ increases with material toughness and indicates a more ductile material. As described later, $VGI_{critical}$ is determined by calibration to notch bar material tests. Further details on the VGM are described by Rice and Tracey (1969) and Kanvinde and Deierlein (2005). The value of 1.5 used in the equation above is based on theoretical derivations by Rice and Tracey (1969).

### 2.6.3.2 Stress Modified Critical Strain Model (SMCS)

Whereas the VGM model explicitly integrates the triaxiality and plastic strain history, in many realistic situations, the triaxiality remains relatively constant during the loading history. As recognized by Hancock and Mackenzie (1977), this enables direct calculation of critical plastic strain as a function of triaxiality, where higher triaxiality leads to a lower critical plastic strain and vice versa. This assumption underlies the SMCS criterion, where the critical plastic strain is determined by the following Eq.( 2.17):

$$\varepsilon_p^{critical} = \alpha \exp\left(-1.5\frac{\sigma_m}{\sigma_e}\right) \quad (2.17)$$

Where the toughness index α =material constant that is determined through material testing, similar to $V_{critical}$ in the VGM. The SMCS model is simpler to apply than VGM because it does not require integration of the plastic strain and triaxiality. Rather, it only requires an instantaneous check of plastic strain demand against $\varepsilon_p^{critical}$ which is a function of the corresponding triaxiality. SMCS is a simpler approach that is based only on the instantaneous values of the stress-strain quantities at fracture initiation. However, when triaxiality varies significantly during loading, the SMCS criterion may be less accurate than the VGM.

### 2.6.4 Criteria in developing ductile fracture prediction

Numbers criteria have been developed for ductile fracture prediction in metal plastic deformation. This is by creating diverse stress and strain states and fracture modes. In fact, the experimental and simulation shows the following. (i) A decrease of stress triaxiality leads to a reduction in the accuracy of DF prediction by the two DFC categories of DFCs, due to the interplay between the principal stress dominant fracture and the shear–stress dominant factor. (ii) For deformations with a higher - value, both categories of DFCs predict the fracture location reasonably well. For those with a lower or even negative g-value, the GTN provides relatively better predictions.

The applicability of the ductile fractures depends on the use of suitable damage evolution rules (void nucleation/growth/coalescence and shear band) and consideration of several influential factors, including pressure stress, stress triaxiality, the Lode parameter, and the equivalent plastic strain or shear stress. These parameters determine the deformation mode (shear dominant or maximum principal stress dominant deformation). For GTN, micromechanics-based criteria, the behavior of a void-containing solid is described by the pressure-sensitive plastic flow, and the damage value (the void volume fraction) is employed in the constitutive equation as imperfection and interacts with the other state variables.

In the uncoupled DFC category, damage accumulation is formulated empirically or semi-empirically. In terms of certain macroscopic variables such as the equivalent plastic strain, tensile stress and hydrostatic stress, that are most relevant to fracture initiation and propagation.Because ductility increases with an increase in hydrostatic stress. But most of the uncoupled criteria consider the effects of such stress. Despite its limitation in representing the deterioration of damaged materials, the uncoupled approach has been widely adopted due to its simple formulation and ease of calibration. In Gurson-like micromechanics-based criteria, the behavior of a void-containing solid is described by the pressure-sensitive plastic flow, and the damage value (the void volume fraction) is employed in the constitutive equation as imperfection and interacts with the other state variables. From the physical mechanism viewpoint, DF is seen as a

macroscopic phenomenon that involves the initiation and growth of microvoids (cavities) and microcracks that are induced and stimulated by a large degree of PD.

### 2.6.5 Determination of Gurson parameters

Gurson model with the improvement by Tvergaard in 1981 is used to predict the damage of ductile fracture with total 8 parameters can be classified into two principal families:

i. The constitutive parameters: $q_1$ and $q_2$.

ii. The material parameters, which are classified into two parts. Firstly, "the initial material and nucleation parameters", which are determined as the initial void volume fraction $f_0$ and void nucleation parameters $f_n$, $\varepsilon_n$ and $S_n$. Secondly, "the critical and final failure parameters", the critical void volume fraction $f_c$ and $f_F$.

In fact, a combination of numerical results and experimental data is necessary in order to determine some of the parameters. In order to describe the material ductile fracture, Tvergaard has suggested fixing the $q_1$ =1.5 and $q_2$ =1.0.

For the material parameters: $f_0, f_N, f_c, f_F, \varepsilon_N, S_N$ The values of the nucleation parameters $f_{N,}\varepsilon_N, S_N$ are fixed.Whereas, Initial void volume fraction, $f_0$ and volume fraction of void nucleating particles $f_F$ are evaluated by microscopically examination of the undamaged material which using the computational cell methodology, and the critical void volume fraction $f_c$ is obtained by fitting the numerical calculations with experimental results. According to (Zhang et al., 2000), $f_c$ is not a constant but decreases when the stress triaxiality ratio T increases. However, other authors note that $f_c$ can be taken as a constant only for small $f_0$ values. However, (Steglich et al., 1998) confirm that the $f_c$ value depends on stress triaxiality T: $f_c$ decreases with the increase of T. According to (Koplik and Needleman., 1988) the $f_c$ value, which signifies the onset of coalescence, seems tovary slowly with stress triaxiality ratio but depends strongly on the initial void volume fraction $f_0$ and is generally smaller than 0.15. Only

for small $f_0$, as a first approximation, can the value of fc be taken as a constant. Tvergaard and Needleman suggested that the value of fc can be taken as 0.15. For the failure void, (Zhang et al., 2000)have proposed an empirical expression for $f_F$ and $f_0$, which is written as a linear equation: $f_F = 0.15+2 \text{ x } f_0$. This signifies that $f_F$ can be fixed to first approximation at 0.15 for low $f_0$ values. As shown in Table 2.2, this parameter can take values between 0.15and0.44.

#### 2.6.5.1 Determination of $f_0$ and $f_F$ using computational cells

The computational cell methodology proposed by Xia and Shih provides a model for ductile crack growth that includes a realistic void growth mechanism, and a microstructural length-scale physically coupled to the size of the fracture process zone. As shown in Fig. 2.12(a). The diagram depicts a crack growing under Mode I conditionsin an idealize material which contains populations of large and small inclusions. The larger inclusions (e.g. MnS) provide sites for the formation of microstructural voids which grow, then coalesce with the current crack tip to create new crack surfaces. In the ductile growth process, the smaller inclusions (e.g. carbides) provide initiation sites for sharp micro cracks which may accelerate the final stages of coalescence. (Arne S. Gullerud. et at, 2000)

Most metals which fail by void growth and coalescence display a macroscopically planar process zone for fracture having a thickness of 1-2x the spacing of larger inclusions. This observation led X&S to idealize ductile fracture by limiting void growth and coalescence to a material thickness D ahead of the crack, where D is associated with the mean spacing of the layer, void initiating inclusions. Figure (b) illustrates this computational model. Each cell of dimensions (D x D) in this layer contains a ‘smeared’ cavity of initial volume fraction. This simplification implies that voids nucleate from inclusions of relative size $f_0$ immediately upon loading. Then in order to model the progressive damage macroscopic softening in cells, the computational cell methodology utilizes the Gurson- Tvergaard (GT) for dilatant plasticity. The GT constitutive model does not predict a realistic loss of macroscopic stress in a cell at large void fraction. When f in the cell incident on the current crack

front reaches a specified critical value, $f_F$ the computational procedures remove the cell thereby advancing the crack front in discrete increments of the cell size. Fig. 2.12(c) shows a typical, finite element representation of the computational cell model in a plane normal to the advancing crack front. The model has a single element per cell, where symmetry about the crack plane requires elements of size D/2.

(a)

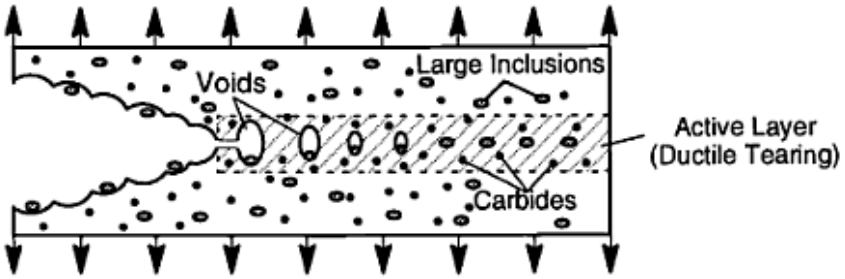


(b)

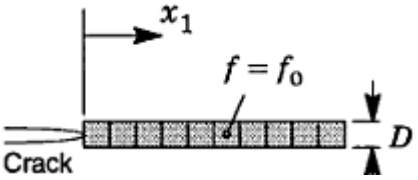


(c)

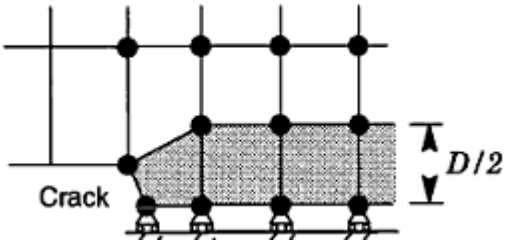


**Figure 2.12**: Modelling of ductile crack growth using computational cells. (a) Schmetic representation of a ductile crack extending through a material containing populations of large and small inclusions. (b) Computational cell model of ductile crack extension. (c) Finite element representation of computational cell model.

Source: (Arne S. Gullerud. et at, 2000)

Alternatively, metallurgical surveys of inclusion volume fractions and sizes may be used with various packing arrangements (e.g. nearest neighbor distance) to estimate D and/or $f_0$. Once determined in this manner, D and $f_0$ become ``material" parameters and remain fixed in analyses of all other specimen geometries for the same material. The calibration process typically requires a number of analyses with different $f_0$ values, thus the use of full 3D models for the entire calibration process becomes computationally expensive. To reduce the computational cost, preliminary plane strain analyses provide a good initial estimate for $f_0$: The final $f_0$ value calibrated using 3D analyses generally has a lower value than obtained with plane strain analyses.

### 2.6.5.2 Determination of Gurson model parameters for present study

For the API X65 steel, the authors have already calibrated parameters for GTN model. Chang, K.O., 2007. Three parameters which are $\varepsilon_N$ =0.3, $S_N$ =0.1 and $f_N$ =0.0008 were fixed to typical values. The parameter $f_0$ was determined from Frankiln's formula (based on the assumption of a spherical inclusion) Chang, K.O., 2007, which leads to $f_0$ =0.000125 for the API X65 steel. Resulting values of $f_c$ and $f_f$ were determined by calibrating smooth and notched tensile bar test results with simulated results using GTN model. The summary of the GTN parameters are shown in Table 2.2

**Table 2.2:** GTN parameters for API X65 steel

| GTN Parameters for API X65 steel | Symbols | value |
|---|---|---|
| First void volume multiplier | $q_1$ | 1.5 |
| Second void volume multiplier | $q_2$ | 1.0 |
| Initial void volume fracture | $f_0$ | 0.000125 |
| Volume fraction of void nucleating particles | $f_N$ | 0.0008 |
| Mean strain for nucleation | $\varepsilon_N$ | 0.3 |
| Standard deviation | $S_N$ | 0.1 |
| Critical void volume fraction | $f_c$ | 0.015 |
| Failure void volume | $f_f$ | 0.25 |

**Table 2.3:** GTN model parameter values from the literature

| Group | Ref. | $q_1$ | $f_0$ | $f_c$ | $f_F$ | K | $f_N$ | $\varepsilon_N$ | $S_N$ | Material | $\sigma_y(MPa)$ | Specimen |
|---|---|---|---|---|---|---|---|---|---|---|---|---|
| **Steel** | Bauvineau L. et al, (1996) | 1.5 | 0.002 | 0.004 | - | 2.3 | - | - | - | C-Mn steel (at $300^{\circ}C$) | - | SENT25 CT22.5 |
| | Decamp K. et al, 1997 | 1.5 | 0.0023 | 0.004 | - | 3 | - | - | - | C-Mn steel (at $300^{\circ}C$) | 190 | AE2,4 and 10 |
| | (N.Benseddiq, A. Imad., 2008) | 1.25 | 0.00033 | 0.026 | 0.15 | 6.24 | 0.006 | 0.3 | 0.1 | CMn steel | 360 | - |
| | Bauvineau L. et al, (1996) | 1.5 | 0.001 | 0.01 | 0.15 | - | 0.01 | 0.3 | 0.1 | Steel stE 690 | 690 | - |
| | Chang-KyunOha., et al | 1.5 | 0.00015 | 0.00074 | 0.18 | - | - | | | API X70 | - | - |
| | Chang-KyunOha .et al.(2007) | 1.5 | 0.000125 | 0.015 | 0.25 | - | 0.0008 | 0.3 | 0.1 | APIX65 | 464.5 | - |
| | Chang-KyunOha., et al | 1.5 | 0.008 | 0.0 | 0.2 | | | | | API X60 | - | - |
| | (N.Benseddiq, A. Imad., 2008) | 1.47 | 0.00016 | 0.0005 | - | 2.8 | - | - | - | A508 C13 A | 471 | AE2 |
| | (N.Benseddiq, A. Imad., 2008) | 1.47 | 0.0001 | 0.0003 | - | 4.3 | - | - | - | A508 C13 B | 470 | AE2 |
| | (N.Benseddiq, A. Imad., 2008) | 1.5 | 0.0015 | 0.035 | 0.15 | 5.49 | 0.00085 | 0.3 | 0.1 | E690 | 779 | AE2 SENB (B=25) |
| | | 1.5 | 0.0025 | 0.021 | - | 3.4 | 0.02 | 0.3 | 0.1 | E460 steel | - | - |
| | (N.Benseddiq, | 1.25 | 0.005 | - | 0.2 | - | 0.001 | 0.04 | 0.01 | A533B | - | - |

| | | | | | | | | | | | |
|---|---|---|---|---|---|---|---|---|---|---|---|
| | A. Imad., 2008) | | | | | | | | | | |
| | (N.Benseddiq, A. Imad., 2008) | 1.5 | 0 | 0.06 | 0.212 | 4 | 0.002 | 0.3 | 0.1 | steel | 440 | |
| | (N.Benseddiq, A. Imad., 2008) | 1.5 | 0 | 0.04 | 0.197 | 4 | 0.002 | 0.3 | 0.1 | | 620 | SEN B |
| | (N.Benseddiq, A. Imad., 2008) | 1.5 | 0 | 0.03 | 0.189 | 4 | 0.002 | 0.3 | 0.1 | | 320 | |
| | P.F.Liu. et al | 1.5 | 1E-8 | 0.15 | 0.25 | - | 0.04 | 0.3 | 0.1 | 34CrMo4 | 755 | - |
| **Aluminium** | Cheng Jin et.al | 1.5 | - | 0.043 | 0.045 | - | 0.03 | 0.3 | 0.01 | AL-6061 (T6) | - | - |
| | Cheng Jin et.al | 1.5 | 0.0001 | 0.016 | 0.05 | - | 0.006 | 0.007 | 0.023 | 5A06 AI alloy (BM) | - | - |
| | Majid Anvari.et al (2007) | 1.5 | 0.002 | 0.6 | - | 2 | - | - | - | AA6060-T6 | | |
| | Cheng Jin et.al | 1.5 | 0.0003 | 0.015 | 0.05 | - | 0.012 | 0.009 | 0.025 | 5A06 AI alloy (WM) | - | - |
| | Cheng Jin et.al | 1.5 | 0.0005 | 0.011 | 0.05 | - | 0.03 | 0.0021 | 0.01 | 5A06 AI alloy (HAZ) | - | - |
| | He R. et al (1998) | 1.5 | 0 | 0.02 | 0.34 | 2 | 0.04 | 0.5 | 2 | AI-AI3Ti | 54.7 | |
| **Composite** | He R. et al (1998) | 1.5 | 0.08 | 0.15 | 0.28 | 4 | 0 | 0 | 0 | Composite | - | - |
| **Cast Iron** | (N.Benseddiq, A. Imad., 2008) | 1.5 | 0.077 | 0.12 | 0.2 | 6.8 | - | - | - | GGG40 | 230 | CT25 AE4 |
| | (N.Benseddiq, A. Imad., 2008) | 1.1 | 0.114 | 0.3 | 0.44 | 4.35 | - | - | - | GGG40 | - | - |
| **Coppper** | (N.Benseddiq, A. Imad.,2008) | 1.47 | 0.002 | 0.028 | - | - | - | - | - | Cu | 312 | AEI 2 4 8 |

It is to note that the GTN parameters that input in FE analysis for this research is from Chang-KyunOha .et al.2007. Where parameter set 1 is preferred.

The conventional elastic-plastic mechanics cannot predict the crack initiation because of two reasons: The incompressibility of volume and the independence of plastic deformation on the hydrostatic pressure are invalid during the softening stage of materials. Hence, the understanding on the ductile fracture is important.

## 2.7 COMPARISON BETWEEN THREE PROPOSED MODELS

Kanvinde and Deierlein (2005) compares both VGM and SMCS models in predicting the ductile failure of structural steels. The results from Kanvinde and Deierlein conclude that both models can be applied accurately to the entire spectrum of structural steels in predicting ductile failure. However, the VGM requires tedious mathematical technique where the stress triaxiality and plastic strain history need to explicitly integrated. Mackenzie and Hancock (1977) first developed the SMCS and reported that the model is a direct approach since the critical plastic strain as a function of stress triaxiality can be directly calculated. Due to its simplicity and accuracy, SMCS model is preferred to predict the ductile failure of the materials.

For GTN model, tests conducted for structural steel and other alloys confirm that the Gurson-Tvergaard-Needleman (GTN) model offers a higher concordance of the theoretical results (numerical analysis) with the experimental data than the classical models and criterions. In fact, Gurson model is the best candidates chosen in micromechanical model analysis due to the facts as below:

i. Because it involves the modeling of void nucleation, growth and coalescence for the analysis and prediction of ductile fracture initiation of alloys.
ii. Applicable to the actual phenomena of material as a large number of models have been developed.
iii. Transferability of model parameters to different geometries.

**Table 2.4** The differences and similarities between GTN, VGM and SMCS.

| **Model** | | **GTN** | **VGM** | **SMCS** |
|---|---|---|---|---|
| **Similarities** | | All these criteria's integrate plastic strains and triaxial stresses to predict crack initiation associated with the mechanisms of void initiation, growth and coalescence. | | |
| **Differences** | Types of micromechanical modelling | Coupled | Uncoupled | Uncoupled |
| | Damage parameter | It is "built into" numerical procedure | It is already exist in the numerical procedure | It is already exist in the numerical procedure |
| | Integration of plastic strain and triaxiality | | The triaxialityand plastic strain history have to explicitly integrate. | SMCS is simpler to apply than VGM because it does not require integration of the plastic strain and triaxiality |
| | Consistency of triaxiality | | The triaxiality remains relatively constant during the loading history. this enables direct calculation of critical plastic strain as a function of triaxiality, where higher triaxiality leads to a lower critical plastic strain and vice versa. | When triaxiality varies significantly during loading, the SMCS criterion may be less accurate than the VGM. |
| | Parameters in FE analysis | Procedure for calculation of parameters must include in FE analysis | The parameters is calculated in post-processing phase of the FE analysis | |
| | Damage parameters used | Critical void volume fraction, $f_c$ | Critical void growth ratio, $\left(\frac{R}{R_0}\right)_c$ | Fracture strain, $\varepsilon_f$ |

## 2.8 EXPERIMENTAL INVESTIGATION

### 2.8.1 Tensile Test

Tensile testing is one of the most common ways of measuring material strength. It involves the linear stretching of a material until failure or some critical value is achieved. Tensile testing can be performed on most types of materials and gives information about yield strength, ultimate tensile strength, modulus of elasticity (stiffness), elongation, and other important properties.

Basically, in the tensile test, a mono-axial stress is generated in a steel sample. This stress is induced via external loading of the sample in a longitudinal direction via a tensile force. There is then an even distribution of direct stress in the test cross-section of the sample. In order to determine the strength of the material, loading of the sample is slowly and continuously increased until its fails.

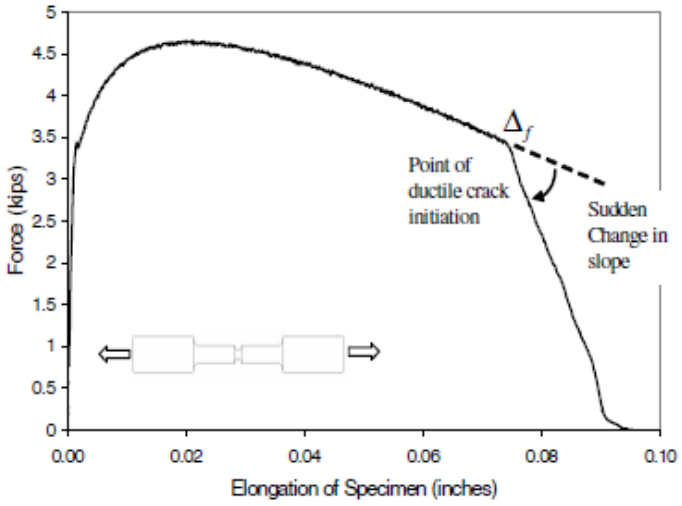


**Figure 2.13:** Specimen after tensile test and the graph of force with elongation of the specimen.

Source: Stress strain curves (Roylance, D.2001)

The maximum test force occurring is a measurement of the strength of the material. The so- called tensile strength, $\sigma$ calculated from the maximum test force, F and the initial cross-section, A of the sample:

$$\sigma=F/A$$

Example of experiments on the material stress strain relation are, including tensile stress-strain tests, notched round specimens, ASTM fracture tests, Charpy V-notch CVN impact tests, ASTM grain-size analyses, and spectrochemical analysis of chemical composition.

### 2.8.1.1 Stress-strain Diagram

The stress strain diagram characterizes the behavior of the material tested. It is most often plotted using engineering stress and strain measures, because the reference length and cross-sectional area are easily measured. Stress-strain curves generated from tensile test results help engineers gain insight into the constitutive relationship between stress and strain for a particular material. It provides quantitative information such as the elastic region, yielding, strain hardening, necking and failure. All these are shown in figure 2.11 below:

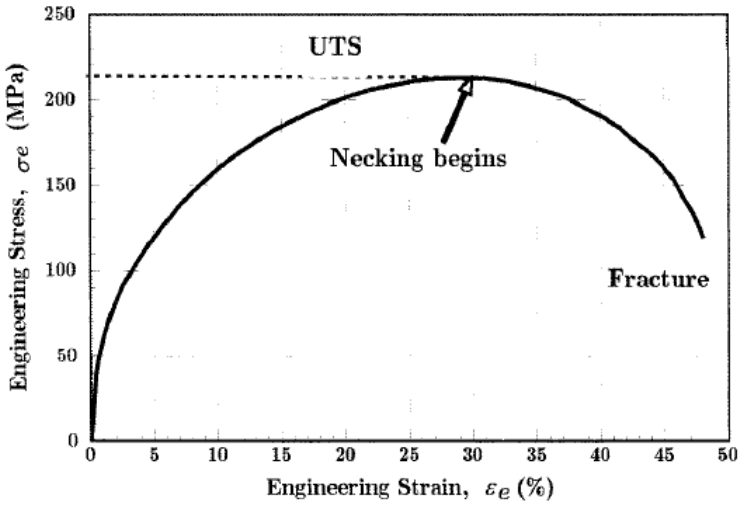


**Figure 2.15:** Full engineering stress strain curve.

Source: Stress strain curves (Roylance, D.2001)

### 2.8.2 Burst Test

Test pipe were prepared and both ends were capped by circumferential welding. The pipes were pressurized by water and burst pressures were experimentally determined at the point when the ligament failed.

#### 2.8.2.1 Full Scale Burst Tests of real and Artificial Corrosion Defects

Both full scales burst tests of real and artificial corrosion defects are normally orientated longitudinal and subject to internal pressure. Artificial defect are normally machined pits, grooves and patches, blunt, flat-bottomed defects with a uniform profile. Whereas for real corrosion defects, it has an irregular profile. The profile of a corroded area must be considered if an accurate prediction of the burst pressure is desired.

The AGA/PRCI Database of Corroded Pipe Tests (Vieth, PH. And Kiefner, JF.1994, 1995) is the most comprehensive source of publicly available burst tests of real and simulated corrosion in line pipe material. In fact, it has identified more than 300 tests on real and artificial corrosion defects, and has come out with the following information:

i. The longitudinal extent of a corroded area is the most important length parameter for the burst strength under internal pressure loading. The circumferential extent has a small influence on the burst strength, but the effect is sufficiently small to not need considering. However, the circumferential extent must be considered if external axial and/or bending loads are present.

ii. External loads reduce the burst pressure compared to the case of an end-capped pressure vessel (axial stress equal to half the hoop stress). The effect of tensile external loads is generally small, whilst compressive loads can cause a significant reduction in the burst pressure.

iii. No difference between the behaviour of internal and external corrosion has been noted in full scale tests or finite element analyses (but noting that pipelines are thin-walled geometries).

iv. Short defects (typically less than 3t in length) of any depth record high burst pressures, typically above the pressure required to yield the uncorroded pipe.
v. In modern, tough, line pipe steel the flow stress for smooth corrosion defects is the ultimate tensile strength of the material.

## 2.9 STRESS BASED FAILURE CRITERIA (CLOSED FORM METHOD)

The corrosion assessment codes is used to estimate the burst pressure of corroded pipeline. The selection of these assessment codes is concerned either with the longitudinal extent of the corroded area or circumferentially orientated. There are several methods for design codes method and also the other methods. For the purpose of this project, where it concerned about the longitudinal orientated and internal pressure, commercial codes, such as ASME B31G, Modified B31G, DNV RP-F-101 and PCORRC will be discussed in the preceding sections. Besides, all of these codes mentioned use assessment of non-interacting defects, except the DNV-RP- F101. Figure 2.17 below shows the methods for corrosion assessment.

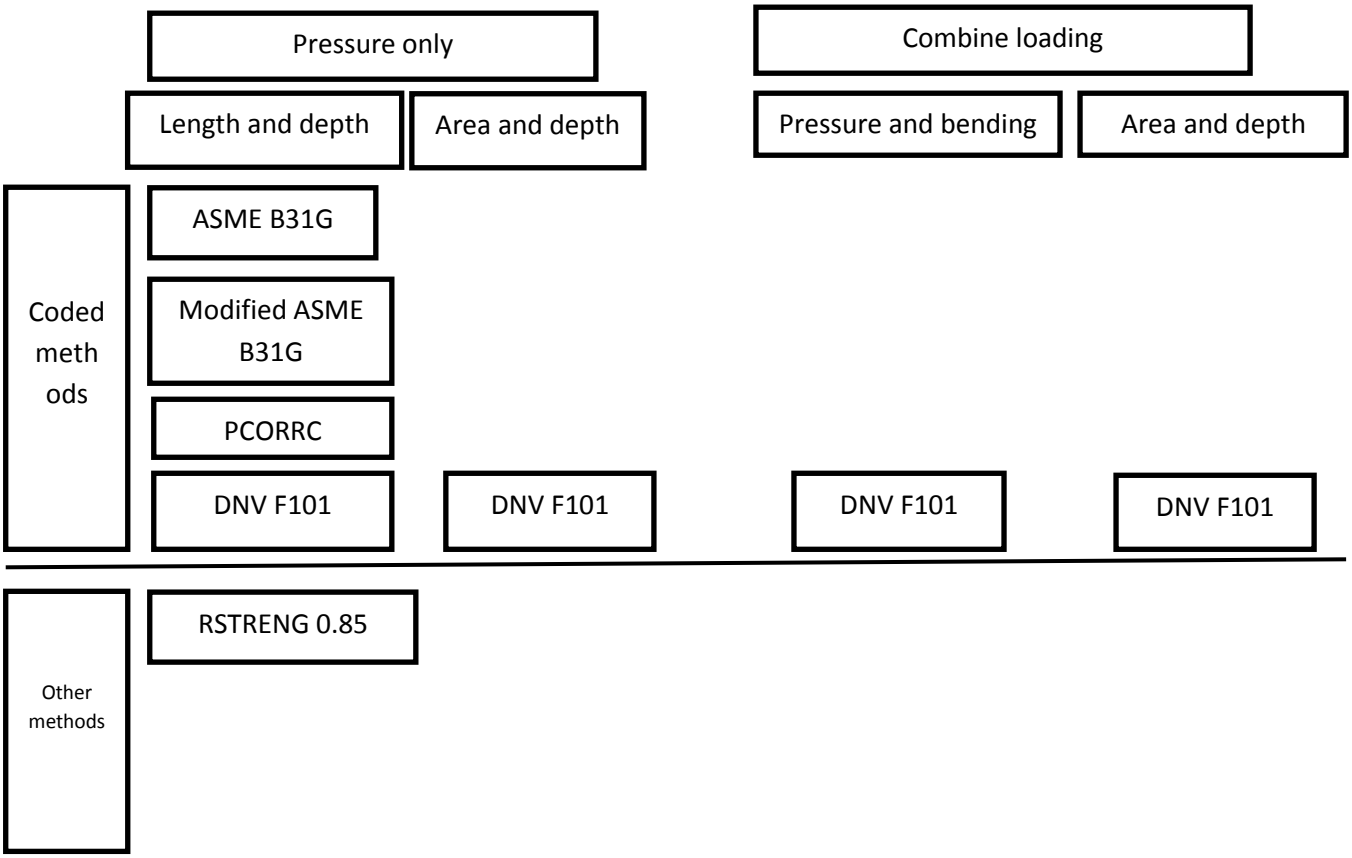


**Figure 2.17:** Methods for corrosion assessment including codified and other methods.

### 2.9.1 ASME B31G

The ASME B31G methodology is used for the determination of the remaining strength of externally corroded pipe subjected to internal pressure loading. It is used to modelize defects by their depth d and by their length L in the longitudinal direction. The defect width w is not considered explicitly in the calculation.
The capacity of pressurized intact pipeline can be calculated by Barlow equation. The assumption is based on allowable maximum hoop stress as in Eq. (2.19).

$$P_{b,\mathrm{int}act} = \frac{2t}{D-t}\sigma_u \tag{2.19}$$

The ASME B31G criterion is developed based on full scale tests of pressured to failure corroded pipes. It allows determination of the remaining strength of the corroded pipes and estimating of the maximum allowable operating pressure (MAOP). However, the B31G criterion contains some simplifications. Another shortage, is the possibility of only proving the pipe integrity under internal pressure, other stresses are not taken into account. There is also restriction in assessable defects, namely the corroded area depth cannot be greater than 80% of the wall thickness and not less.

This method is based on the measurement of the longitudinal extent of the corroded area as shown in Figure 2.18. It considers the depth and longitudinal extent of corrosion, but ignores its circumferential extent.

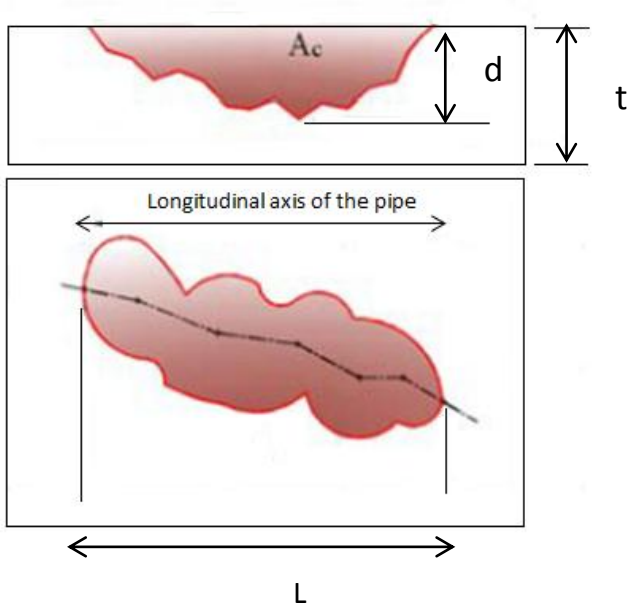


**Figure 2.18:** Longitudinal extent of the corrosion area

The corroded area is approximated depending on the defect length as parabolic or rectangular shape. Short longitudinal extent of corrosion areas are approximated by the parabolic shape and long longitudinal extent of corrosion areas are approximated by the rectangular shape, as shown in Figure 2.19 and Figure 2.20, respectively.

$$L \begin{cases} \leq \sqrt{20Dt} \Rightarrow A_c = \frac{2}{3}dL \\ > \sqrt{20Dt} \Rightarrow A_c = dL \end{cases} \qquad (2.20)$$

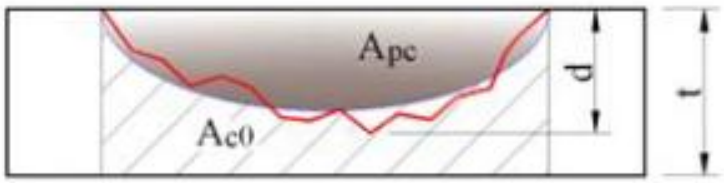


**Figure 2.19:** Assumed parabolic corroded area for relatively short corrosion defect

The predicted failure pressure can be estimated by Equation 2.21 and Equation 2.22 for short and long defect, respectively. However, the maximum allowable operating pressure (MAOP) can be limited to a multiple of the estimated failure pressure by the design factor, as in Eq.(2.21), Eq.(2.22) and Eq.(2.23).

$$P_f = SMYS \frac{2t}{D}\left(\frac{1-\frac{2}{3}\frac{d}{t}}{1-\frac{1}{M}\frac{2}{3}\frac{d}{t}}\right) \tag{2.21}$$

$$P_f = SMYS \frac{2t}{D}\left(1-\frac{d}{t}\right) \tag{2.22}$$

$$M = \sqrt{1+0.8\frac{L^2}{Dt}} \tag{2.23}$$

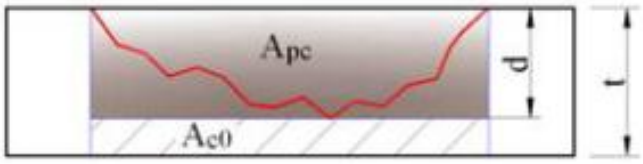


**Figure 2.20:** Assumed rectangular corroded area for longer corrosion defect

### 2.9.2 Modified B31G Criterion (0.85dL Area Method)

The B31G method was found to be too conservative and has been modified, the new method is called Modified B31G or 0.85-area Method. One of the most significant changes to the original B31G method is the defect geometry approximation. Corrosion area is defined by 0.85dL as illustrated in Figure 2.21.

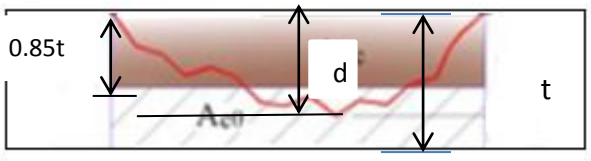


**Figure 2.21:** Assumed Ac =0.85dL method for corrosion defect

This method removes some conservation by changing the flow stress limit to SMYS+ 69MPa (10ksi), This is very close to the conventional fracture mechanism definition of the flow stress: the average of the yield and ultimate strength. This modification results in the change of the failure equation, which is also dependent on the limit on defect length. The equation to calculate the failure pressure is modified as in Eq.(2.24).

$$P_f = (SMYS + 69.1MPa)\frac{2t}{D}\left(\frac{1-0.85\frac{d}{t}}{1-0.85\frac{1}{M}\frac{d}{t}}\right) \tag{2.24}$$

For, $L \le \sqrt{50Dt}$ the Folias factor is given by:

$$M = \sqrt{1+0.6257\frac{L^2}{Dt}-0.003375\left(\frac{L^2}{Dt}\right)^2} \tag{2.25}$$

But if $L > \sqrt{50Dt}$ ,

$$M = 3.3+0.032\frac{L^2}{Dt} \tag{2.26}$$

### 2.9.3 DNV RP-F-101 Criterion

The DNV provides guidance on single and interacting defects under pressure only and combined loading. The RP-F101 provides two methods of analysis: a partial safety factor method and an allowable stress design method. The allowable corroded pipe pressure of a single metal loss defect subjected to internal pressure loading is given by the following acceptance Eq. (2.27).

$$P_f = \gamma_m SMTS \frac{2t}{D-t}\left(\frac{1-\gamma_d\left(\frac{d}{t}\right)^*}{1-\gamma_d \frac{1}{Q}\left(\frac{d}{t}\right)^*}\right) \tag{2.27}$$

Where the relative corrosion depth and the factor Q are given as in Eq.(2.28) and Eq.(2.29):

$$\left(\frac{d}{t}\right)^* = \left(\frac{d}{t}\right)_{mean} + \varepsilon_d StD\left(\frac{d}{t}\right) \tag{2.28}$$

$$Q = \sqrt{1+0.31\left(\frac{L}{\sqrt{Dt}}\right)^2} \tag{2.29}$$

In the allowable stress design approach, the failure pressure of the pipe is calculated and multiplied by safety factors. These factors may be based on design factor and can consider uncertainties such as presented above. The uncertainties caused by the presence of a corrosion defect, can be described by the additional 0.9 factor. This is a commonly used approach because of its simplicity as shown in Eq.(2.30).

$$P_f = 0.9FSMYS \frac{2t}{D-t}\left(\frac{1-\frac{d}{t}}{1-\frac{1}{Q}\frac{d}{t}}\right) \tag{2.30}$$

### 2.9.4 PCORRC Criterion

The PCORRC, defined as in Eq.(2.31):

$$P_b = \sigma_O \frac{2t}{D}\left(1-\frac{d}{t}\left(1-e^{-c\frac{L}{\sqrt{\frac{D}{2}(t-d)}}}\right)\right) \tag{2.31}$$

On comparison with experimental test result, estimation of PCORRC equation proved to be conservative and the closest when using 95% of UTS of tensile test, $\sigma_u$. The C value varies from 0.142 to 0.224 with the change of pit depth. However for conservative prediction of damaged pipe, we can choose maximum value of 0.224 as curve fit constant and the above equation is rewritten as in Eq.(2.32).

$$P_b = 0.95\sigma_{a,test}\frac{2t}{D}\left(1-\frac{d}{t}\left(1-e^{-0.224\frac{L}{\sqrt{\frac{D}{2}(t-d)}}}\right)\right) \tag{2.32}$$

## 2.10 COMPARISION AMONGEXPERIMENTAL METHOD, STRAIN AND STRESS BASEDMICROMECHNICAL MODEL.

These three methods are important to make comparisons so as to determine the accuracy and relationship between each other. The experimental results will not be assured until the validation from the design codes and the results analysis from the finite element analysis. Figure 2.22 below show the comparison between the three methods.

**Figure 2.22:** Comparison among experimental method, strain based and stress based micromechanical method

| **Methods** | **Strain based failure criteria (FE method)** | | **Stress based failure criteria (Design codes)** | **Experimental (Pipe burst test)** |
|---|---|---|---|---|
| | Coupled modeling | Uncoupled modeling | | |
| Advantages | 1. Transferability of model parameters to different actual geometries/ structures.<br><br>2. Ductile fracture parameters are contact to the micro-ductile fracture mechanism which involves void nucleation, growth and coalescence which are more details.<br><br>3. Easy to determine the variable loading conditions with sensitivity analysis in order to cope with possible failure occur.<br><br>4. One of the popular methods used in micromechanical model in literatures. | 1. Less parameter.<br><br>2. Ductile fracture parameters are contact to macroscopic fracture.<br><br>3. Easy to determine the variable loading conditions with sensitivity analysis in order to cope with possible failure occur.<br><br>4. Induce innovative and efficient geometry design and development of accurate design methods. | 1. The fastest way to determine load capacity of a structure. | 1. It is the most accurate method as it is based on the actual testing experiment.<br><br>. |

| | | | | |
|---|---|---|---|---|
| | 5. It is reliable on numerical tool which is the FEM where the models are easily refined or improve accuracy by varying element size and type. | | | |
| Limitations | 1. Relate to lots of parameters and determinations of these parameters are not easy, and often not robust. | 1. Robust parameter determination is a common problem in FE simulations. | 1. The failure assessments may be overly conservative and limited since they are dependent on material properties, pipelines geometry and defect geometry.<br><br>2. Any changes in either of these properties will require the development of a large test set in order to update the empirical solutions.<br><br>3. Analytical solutions to engineering problems are possible if the geometry, loading and boundary conditions are simple. | 1. Difficult to perform tests reflecting complex geometries and variation in dependent loading conditions.<br><br>2. Expensive and time-consuming |

# CHAPTER 3

# METHODOLOGY

## 3.1 INTRODUCTION

Methodology is a set of methods and steps to how on how to conduct research. Methodology is important as it is a guideline in obtaining the result based on the objective and it is usually represented in flow chartwhich helps the viewer to visualize what is going on the project and keep the research experiment on the right track. The terminology of work planning for this research was shown in the flow chart Figure 3.1.

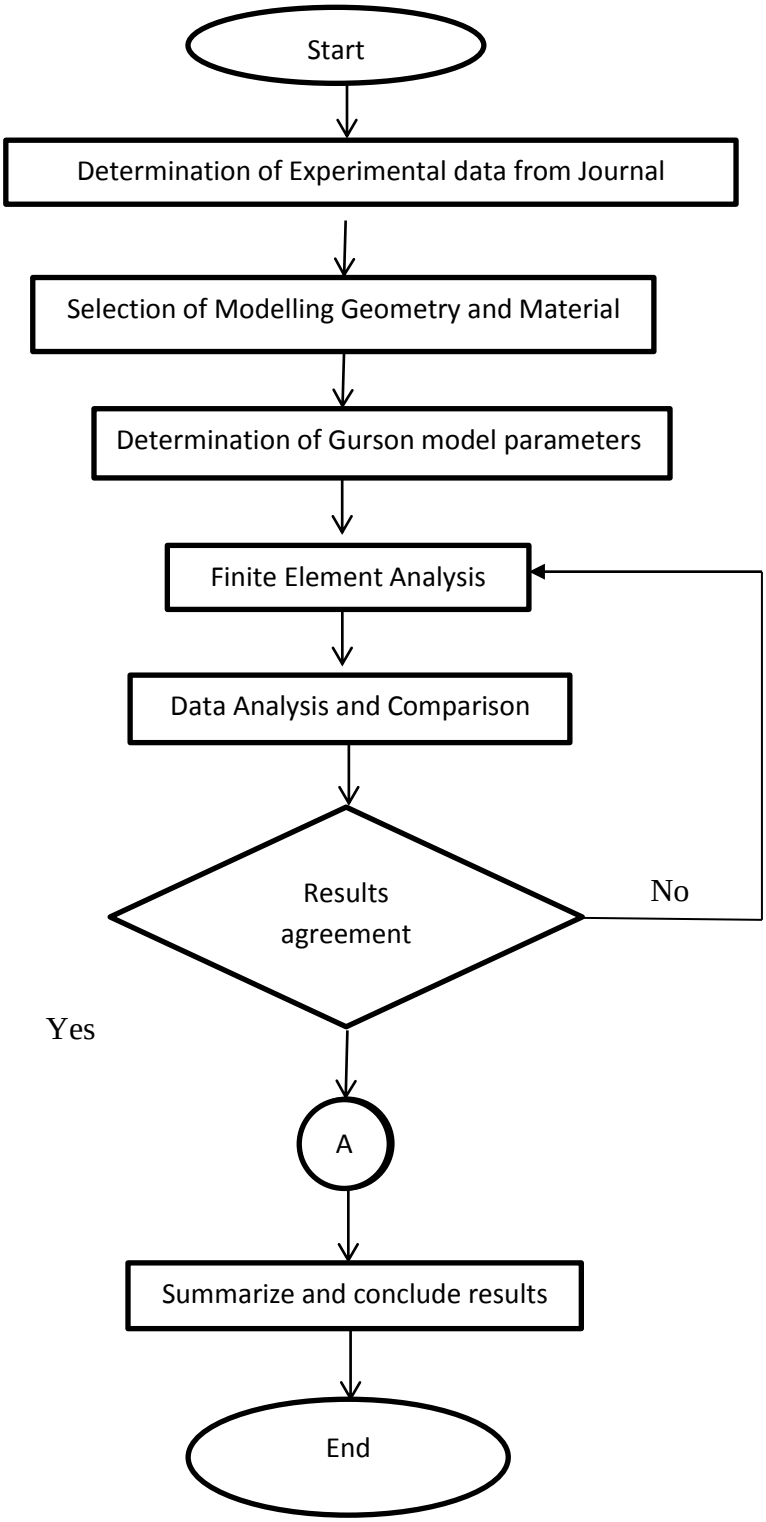


**Figure 3.1:** Overall Flowchart Research

The complete procedure to analyse the corrosion defect geometry in steel pipeline is shown in Figure 3.2 below. It consists of modelling design until analysis of the result.

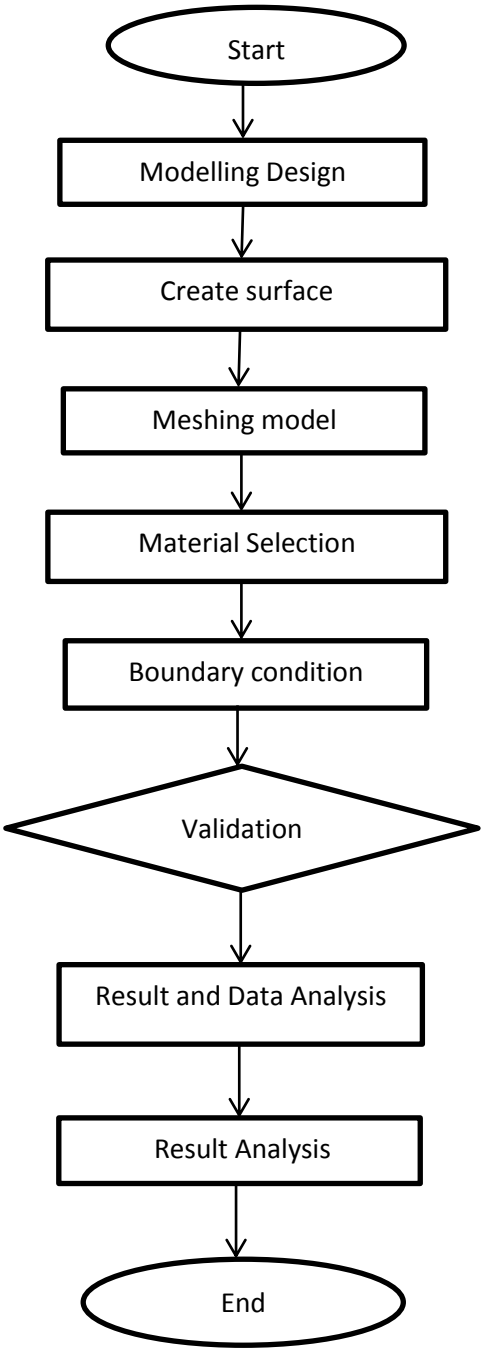


**Figure 3.2:** Procedure in Patran Analysis

## 3.2 DETERMINATION OF EXPERIMENTAL DATA AND MATERIAL

### 3.2.1 Determination of Material properties

To determine mechanical properties, tensile and Charpy tests were performed using specimens extracted from a pipe of outer diameter Do = 762 mm and wall thickness t = 17.5 mm (in the longitudinal direction), made of the American Petroleum Institute (API) 5L X65 steel . It is in smooth and notches test specimens. A schematic diagram for tensile specimen used in this present work is illustrated in Fig.1. The tensile properties of the present API X65 steel as summarized in Tables 3.1.

**Table 3.1:** Mechanical tensile properties at room temperature of the API X65 steel, used in the present work

| **Young's Modulus E (GPa)** | **Poisson's ratio, v** | **Yield strength $\sigma_y$ (MPa)** | **Tensile strength $\sigma_u$ (MPa)** |
|---|---|---|---|
| 210.7 | 0.3 | 464.5 | 563.8 |

Source: Chang-Kyun Oh et.al. (2007)

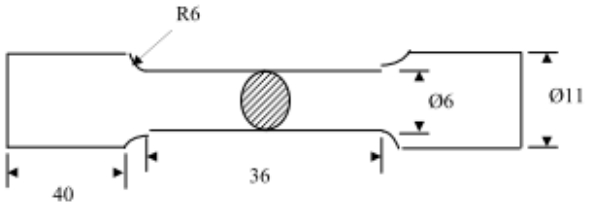


**Figure 3.3:** Tensile specimen

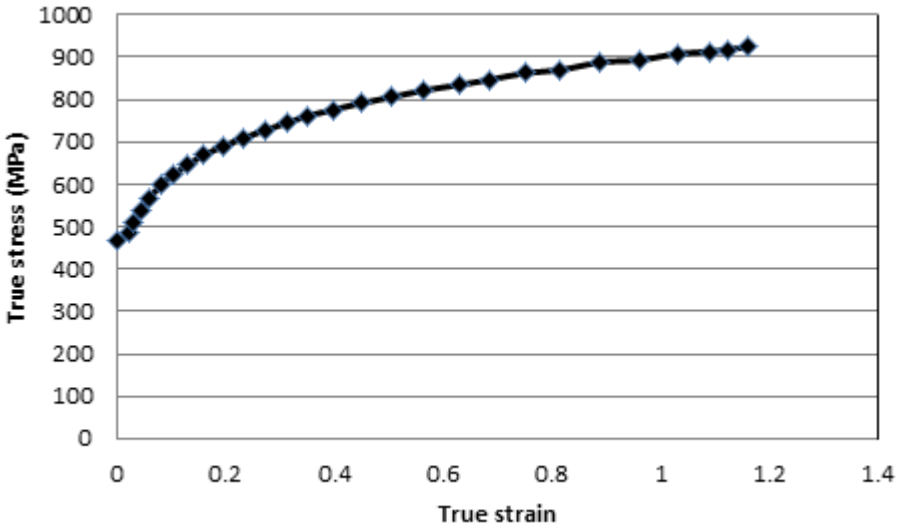


**Figure 3.4:** True stress-strain data for AP1 5L X65 steel at room temperature.

Source: Chang-Kyun Oh et.al. (2007)

Engineering stress strain data was then converted to true stress strain data as plotted in Fig.3.4 These true stress-strain data will be input into the materials properties in Marc. The data can be obtained from the scanned graphs into data by using Engauge software. This will give an accurate data for the analysis. Table 3.2 below show the dimensions for the pipe design.

**Table 3.2:** Dimensions for the pipe design.

| **Specifications** | **Dimensions (mm)** |
|---|---|
| Outer diameter, OD | 762 |
| Defect depth, d | 4.375, 8.75, 13.125 |
| Defect width, c | 50 |
| Defect length, l | 200 |
| Pipe thickness, t | 17.5 |
| Ratio of d/t | 0.25 |
| Pipe length | 2300 |
| A quarter of pipe length, L/2 | 1150 |
| Defect length, I/2 | 100 |
| Defect width, c/2 | 25 |

### 3.2.2 Determination of Experimental data

The experimental results are based on the journal Chang-Kyun Oh et.al. (2007). There are two part of failure analysis. First is the pipe defect with rectangular shape and the second is with gouge. Test pipes were prepared from API 5L X65 pipelines. A pipeline of total length 12m was cut into pieces with 2.3m length each. The geometrical configuration of the pipe tested for both parts shown in figure 3.5 and Figure respectively. The pipes were pressurized by water and burst pressures were experimentally determined at the point where ligament failed. The defect area show a significant amount of thickness reduction as it is due to the local necking prior to final failure. The experimental data for rectangular defect are shown in Table 3.3 and with gouges in Table 3.4. The criterion is in terms of true strain as a function of the stress triaxiality and equivalent strain, and has been determined from results of smooth and notched round bar tests.

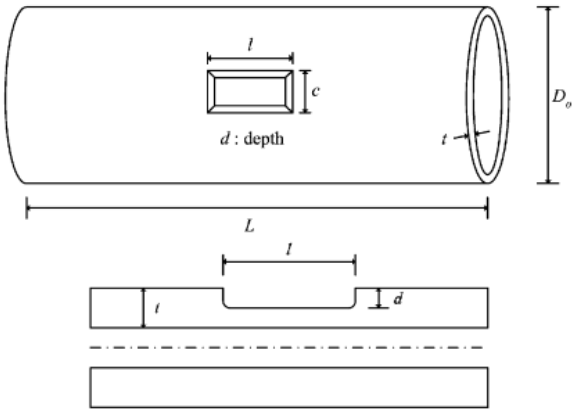


**Figure 3.5:** Pipe with simulated corrosion defect.

Source: Chang-Kyun Oh et.al. (2007)

**Table 3.3:**Defect design dimension and experiment data for rectangular defect.

| **Pipe no** | **OD mm** | **L mm** | **t mm** | **length l (mm)** | **width c (mm)** | **depth d (mm)** | **d/t** | $P_{exp}$ **(Mpa)** |
|---|---|---|---|---|---|---|---|---|
| **A1** | 762 | 2300 | 17.5 | 200 | 50 | 4.375 | 0.25 | 24.11 |
| **A2** | | | | 200 | 50 | 8.75 | 0.5 | 21.76 |
| **A3** | | | | 200 | 50 | 13.125 | 0.75 | 17.15 |

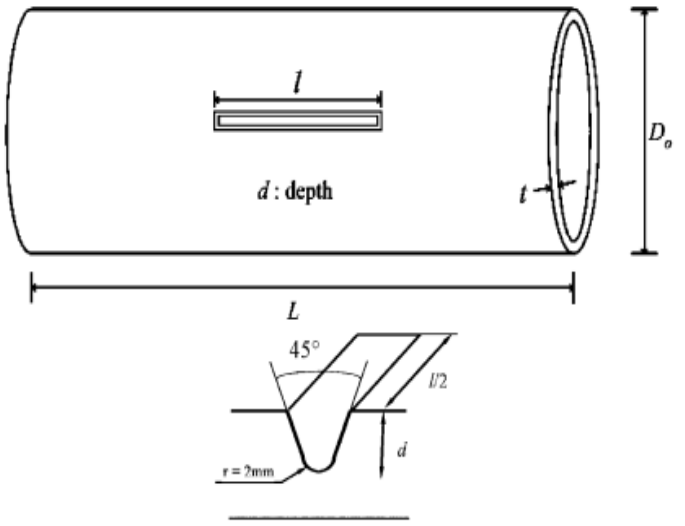


**Figure 3.6:** Pipe with gouge defect design.

Source: Chang-Kyun Oh et.al. (2007)

**Table 3.4:** Dimensions and experiment data for gouge defect.

| Pipe no | d/t | length l (mm) | P exp (MPa) |
|---|---|---|---|
| **MNA** | 0.5 | 100 | 24.68 |
| **MNB** | 0.5 | 200 | 22.48 |
| **MNC** | 0.5 | 300 | 17.7 |
| **MND** | 0.5 | 400 | 18.14 |
| **MNE** | 0.5 | 600 | 16.57 |

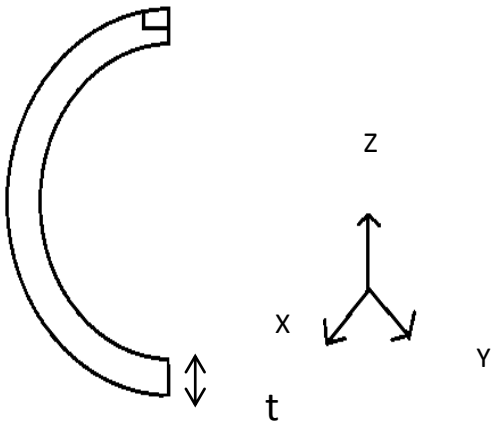


**Figure 3.7:** 2 Dimensional of the pipe

### 3.3 Finite Element Analysis

#### 3.3.1 FE Modelling

In the present study, the FE analysis is conducted using MSC.PATRAN 2008r1 as the pre- and post-processor while utilizing MSC.MARC 2008r1 as the solver. Three dimensional elastic-plastic damage analyses were performed to stimulate the pipe burst tests. A quarter of a full pipe was modeled due to simplify and reduce computation time. During designing of the model, defect with 4 edges is preferred compared to 3 edges and sharp edges should be avoided. The FE mesh is shown in Figure 3.8.

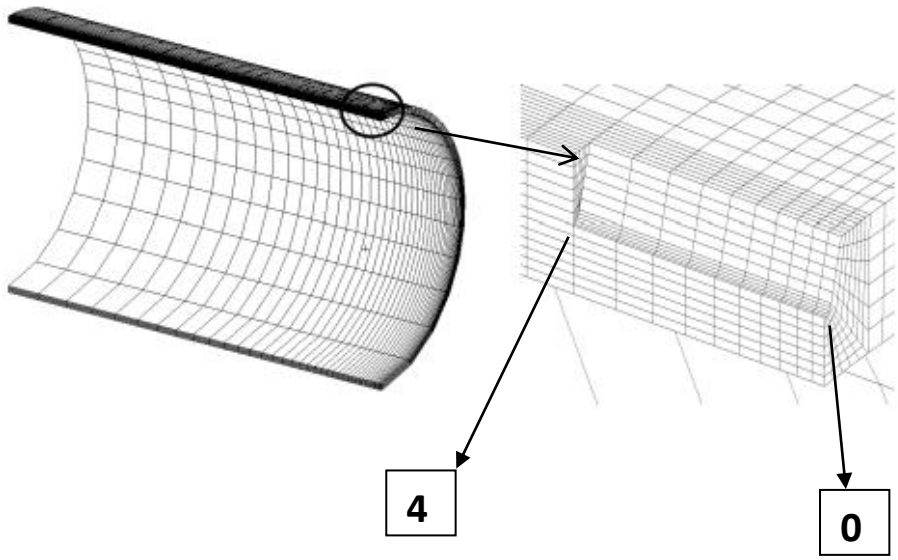


**Figure 3.8:** FE model of meshing for a quarter of pipe model using MSC.PATRAN. Number 0 denoted the tip of defect and number 4 is the end of defect for normalized distance analysis.

Then boundary conditions are applied to the each edges surface of the pipe model to define symmetrical deformations for the sides of the model. For the meshing, the mesh is created based on mesh seeds at the edge of each of the sides of the model. The numbers of mesh seeds used are given in Table 3.6.

**Table 3.6:** Number of elements for mesh seeds for FE model.

| Direction | Method | Number of elements |
|---|---|---|
| **Defect thickness** | uniform | 10 |
| **Defect length** | uniform | 30 |

| | | |
|---|---|---|
| **Circumferential** | One way bias | 50, 10 |
| **Pipe length** | One way bias | 50, 10 |

### 3.3.2 Load Case, Boundary Conditions and Loads

In the present FE model, the load case is set to be time-dependant. The boundary conditions are defined at every side of the pipe surface along x-axis and y-axis to define symmetrical deformation of the nodes as if it is a full model pipe. Then the pressure is applied to the inner surface of the pipe. The displacement boundary conditions applied are shown in Figure 3.9 and summarized in Table 3.7

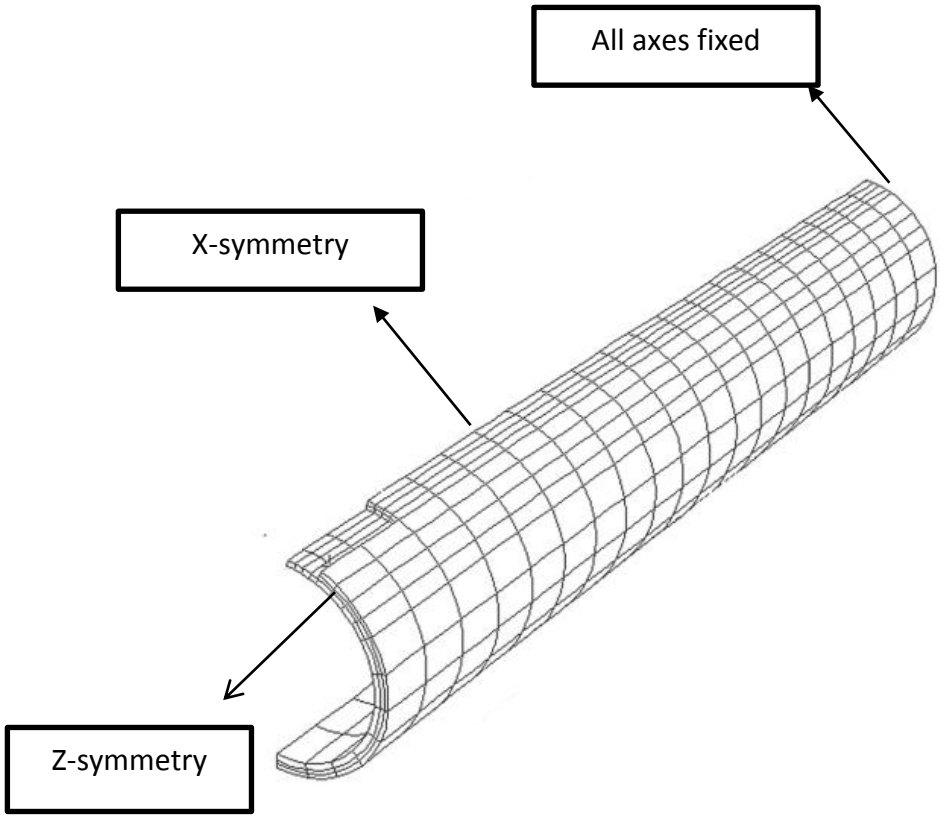


**Figure 3.9:** Boundary conditions applied on the pipe model.

**Table 3.7:** Boundary conditions applied on the pipe model.

| Applied surface | Boundary Condition | Description |
|---|---|---|
| **All surface along X-axis** | X-symmetry: constrain translational motion in X-direction and rotational motions about Y-axis and Z-axis. | To define symmetrical deformation of pipe in Y-direction on X-axis. |
| **All surface along Z-axis at defect side** | Z-symmetry: constrain translational motion in Z-direction and rotational motions about X-axis and Y-axis. | To define symmetrical deformation of pipe in X-direction on Z-axis. |
| **All surface along Z-axis at end of pipe** | Fixed at all translation and rotation motions | To fix the deformation at all directions. |

## 3.4 VALIDATION USING CLOSED CALCULATIONS AND SMCS

### 3.4.1 Closed form calculations

There are numerous design codes available in practice for prediction of failure pressure of defective pipe due to corrosion. Examples of the codes are American Society of Mechanical Engineer (ASME) B31G, modified ASME B31G and PCORRC. According to ASME B31G, the failure of corroded pipeline is controlled by the defect size as well as the flow stress of the material. The input parameter including outer diameter of the pipe, D, wall thickness, t, yield strength of the material, $\sigma_y$ or ultimate tensile strength, $\sigma_u$, the length of the defect, L and defect depth, d.

All three codes use the stress based failure criterion to predict the burst pressure. This leads to conservative results because stress based failure criterion rely on flow stress only. Another method is using strain based failure criteria which can be grouped into micro-mechanical models. In fact, micro-mechanical model for ductile fracture, incorporating void nucleation, growth and coalescence are the Gurson–Tvergaard–Needleman (GTN) model, void growth model (VGM), continuum damage model (CDM) model and SMCS model . However, a few issues need to be resolved in using these models. For example, GTN models consist of relatively high number of parameters compare to SMCS and VGM models.

These GTN parameters are difficult to identify and calibrate which requires a large number of FE and experimental work.

### 3.4.2 Stress Modified Critical Strain

SMCS is adopted in the validation as this model is a direct approach since the critical plastic strain as a function of stress triaxiality and equivalent strain can be directly calculated. There are two parameters used from SMCS in validating the present work, which are the stress triaxiality, T and equivalent strain, $\varepsilon_{eq}$. SMCS is evaluated by Eq.( ) and Eq ( ), where the stress triaxiality, T is defined by ratio of hydrostatic stress, $\sigma_m$ and equivalent stress, $\sigma_{eq}$ given by as in Eq.(3.1), Eq.(3.2) and Eq.(3.3):

$$T = \frac{\sigma_m}{\sigma_e} = \frac{\sigma_1 + \sigma_2 + \sigma_3}{3\sigma_e} \tag{3.1}$$

$$\sigma_e = \frac{1}{\sqrt{2}}[(\sigma_1 - \sigma_2)^2 + (\sigma_3 - \sigma_1)^2 + (\sigma_2 - \sigma_3)^2]^{\frac{1}{2}} \tag{3.2}$$

$$\varepsilon_{eq} = \frac{\sqrt{2}}{3}[(\varepsilon_1 - \varepsilon_2)^2 + (\varepsilon_3 - \varepsilon_1)^2 + (\varepsilon_2 - \varepsilon_3)^2]^{\frac{1}{2}} \tag{3.3}$$

Where the $\sigma_1, \sigma_2, \sigma_3$ and $\varepsilon_1, \varepsilon_2, \varepsilon_3$ are the principle stresses and principle strain respectively.

# CHAPTER 4

# RESULTS AND ANALYSIS

## 4.1 FINITE ELEMENT ANALYSIS RESULTS

The applicability of the ductile fracture depends on the use of suitable damage evolution rules. In this present study, the burst pressure is predicted with according to the critical void volume fraction $f_c$ where $f_c$=0.015 for the API X65 steel. From the finite element analysis results, the burst pressure is calculated with the increment of time step and predicted from the void volume fraction where $f > f_c$. Figure 4.1 and 4.2 show an example of pipe defect profile in FE analysis results with void volume fraction profile represented by contour makers. The node with the critical void volume fraction is being analyzed. The void volume fraction profiles for three different defect depths are plotted in Figure 4.3.

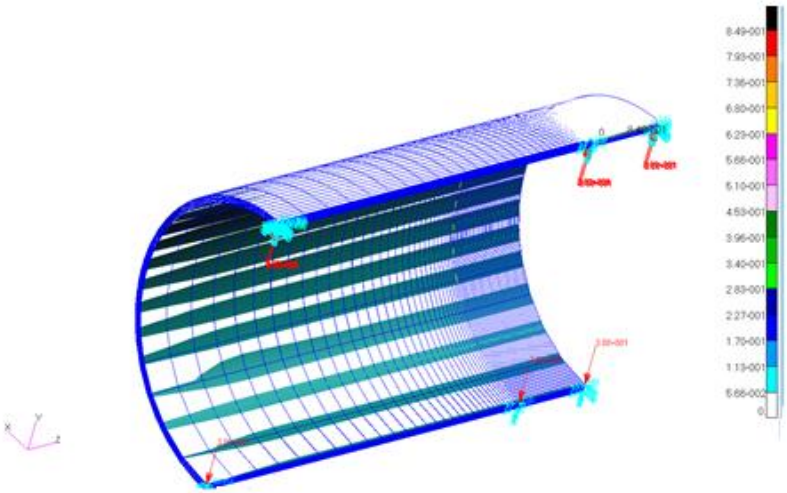

**Figure 4.1**: Void volume fraction contour profile for the pipe.

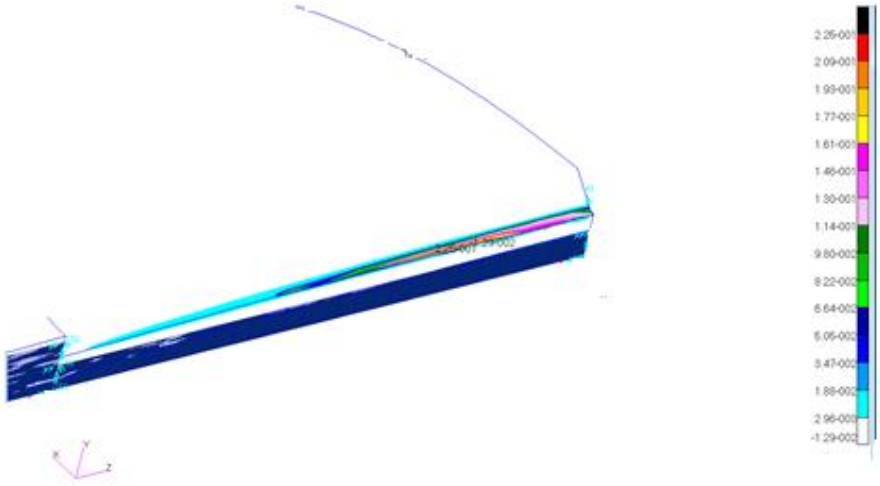

**Figure 4.2:** A typical finite element mesh for pipe with gouges and the contour markers showing void volume fraction profile at the final time step 1s. The critical void happens at the tip of the defect.

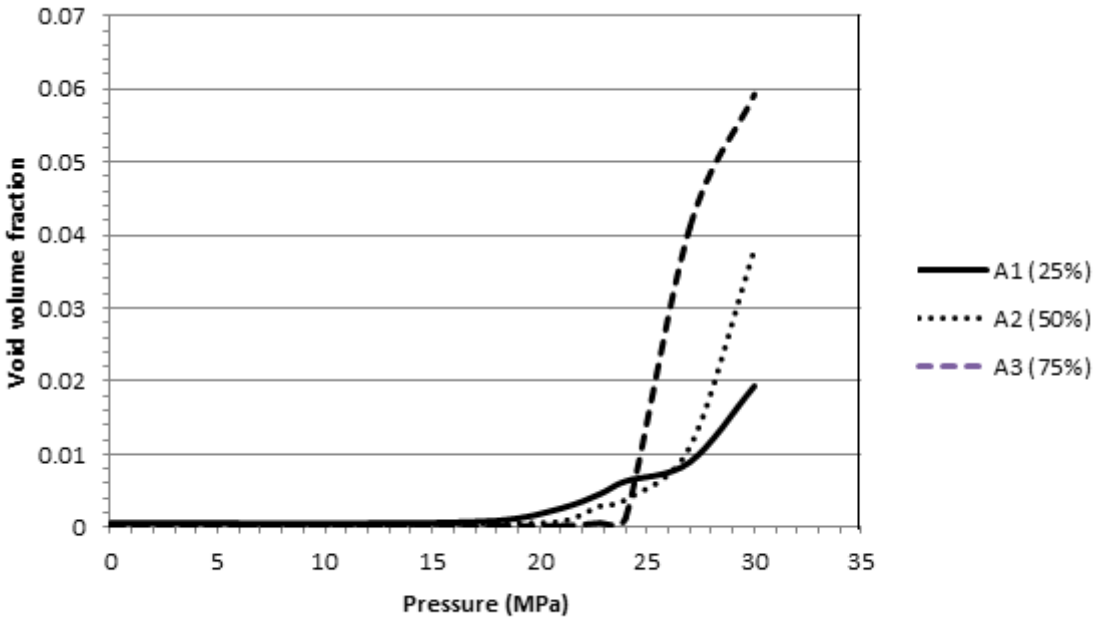


**Figure 4.3**: Comparison between the void volume fractions for different defect depth on the pressure increment.

Figure 4.3 showed the increment of void volume fraction for three different depths. The burst pressure is predicted at $f > f_c$ which is 0.016 > 0.015 for A1, for

defect depth 0.5%, the burst pressure is predicted at 27.6MPa, (0.02 > 0.015), whereas for depth 0.75%, it is at 26.4MPa (0.029 > 0.015). For all cases, the coalescence process started to occur at the pressure between 26 to 29MPa before it continue to reach fracture. Also, the value of void volume fraction increase with decreasing depth. This also showed in Table 4.1.

**Table 4.1:** Value of $f$ reached for different depths, d.

| **Pipe** | **Defect depth, d (%)** | **Value of $f$ ( $f > f_c$ ) with $f_c = 0.015$** |
|---|---|---|
| A1 | 0.25 | 0.016 |
| A2 | 0.5 | 0.02 |
| A3 | 0.75 | 0.029 |

## 4.2 RESULTS COMPARISION AND ANALYSIS

### 4.2.1 Application to failure predictions of corroded API X65 pipes

The predicted burst pressure from FEA is compared with the experimental results from the journal for API X65. Also, the available codes for pipeline defect assessment are used to compare and validate the results as shown in Table 4.2.

**Table 4.2:** Burst pressure predicted for FEA and design codes for different depths.

| **Pipe no** | **depth d (mm)** | **d/t** | $P_{\exp}$ **(Mpa)** | $P_{fem}$ **(Mpa)** | **Predicted failure pressure (Mpa)** | | |
|---|---|---|---|---|---|---|---|
| | | | | | ASME B31G | Modified ASME B31G | PCORRC |
| A1 | 4.375 | 0.25 | 24.11 | 28.8 | 19.55 | 22.08 | 21.72 |
| A2 | 8.75 | 0.5 | 21.76 | 27.6 | 17.36 | 18.84 | 17.96 |
| A3 | 13.125 | 0.75 | 17.15 | 26.4 | 14.64 | 14.28 | 12.31 |

#### 4.2.1.1 Comparisons

The burst pressure results from FE was initially compared to the SMCS, however, an issue occur where even the void volume fraction has reached the $f_c$, the strains equivalent did not reach the critical values. Thus, the present approach suggests that failure of the present API X65 pipes with simulated corrosion is governed by global plastic instability, possibly due to sufficiently high ductility of the material.

Although the present approach suggests that failure is governed by global plastic instability, thus these experimental data are not appropriate to validate with SMCS, but the maximum loads predicted by FE analysis could compare with experimental results. Overall the predicted values are in good agreement with the experimental one. For corroded pipes with sufficient ductility, one solution to estimate the burst pressure of pipes with local wall thinning is so-called PCORRC equation. Chang, K.O., (2007). This is shown in Eq.(4.1).

$$P_f = \frac{2t}{D_0}\sigma_U\left[1-\frac{d}{t}(1-\exp(-0.157\frac{l}{\sqrt{R_0(t-d)}}))\right] \tag{4.1}$$

This equation is based on limit load analysis for pipes with constant depth thinning under internal pressure. Table 4.3 lists ratios of maximum pressure ( $P_{PCORRC}$ ), predicted form equation 4.1, to experimental one.

**Table 4.3:** Comparison between burst pressure for experimental FE and $P_{PCORRC}$

| **Pipe no** | **length l (mm)** | **width c (mm)** | **depth d (mm)** | **d/t** | $P_{\exp}$ **(MPa)** | $P_{fem}$ **(MPa)** | $P_{PCORRC}$ **(MPa)** |
|---|---|---|---|---|---|---|---|
| A1 | 200 | 50 | 4.375 | 0.25 | 24.11 | 28.8 | 25.88 |
| A2 | 200 | 50 | 8.75 | 0.5 | 21.76 | 27.6 | 25.86 |
| A3 | 200 | 50 | 13.125 | 0.75 | 17.15 | 26.4 | 25.85 |

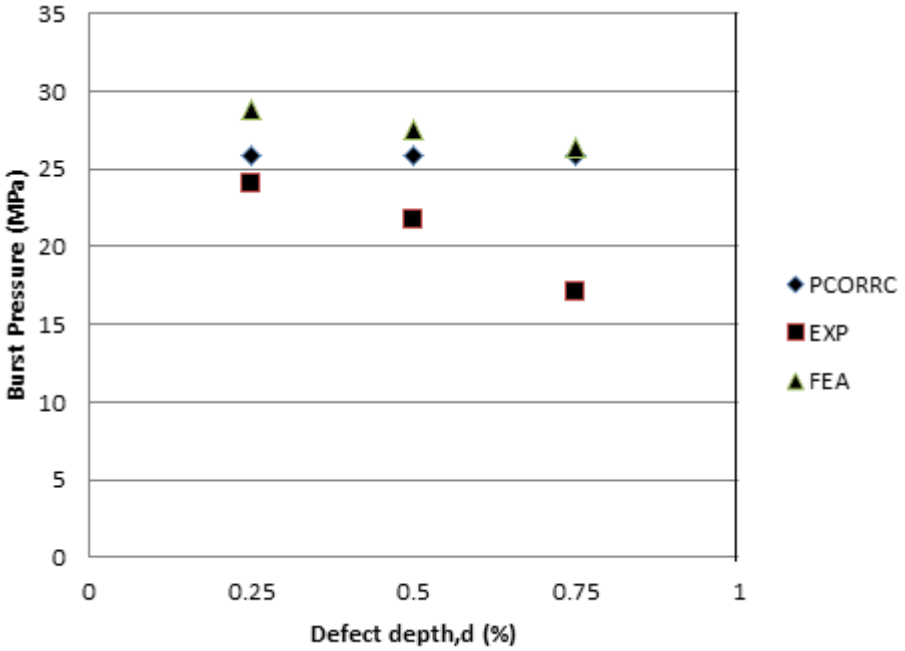


**Figure 4.4:** Comparison on the burst pressure for different defect depth for FEA, experimental and Equation 4.1.

This will be the comparison between FE results and available Codes for Pipeline Defect Assessments**.** For the purpose of comparison, the rectangular defect will be assumed to be as part of the corrosion defect. Figure 4.4 compares the results for burst pressure between $P_{PCORRC}$ , FE and experimental Chang, K.O., (2007). In contrast, FE results shows higher values as compare to experimental and design codes. In Figure 4.5, the most conservative code in predicting the burst pressure is the ASME B31G followed by Modified ASME and PCORRC. It is noted that for the design codes, all cases are with Modified ASME the highest, followed by ASME B31G and PCORRC the lowest except for the case of 75%. This might be due to limitation of design code only applicable for ratio of gouge depth to pipe thickness less or equal to 70%. It is to note that all three design codes predict failure based on stress criterion where the flow stress govern the predicted results whereas the burst pressure obtained from FE results is based on strain criterion.

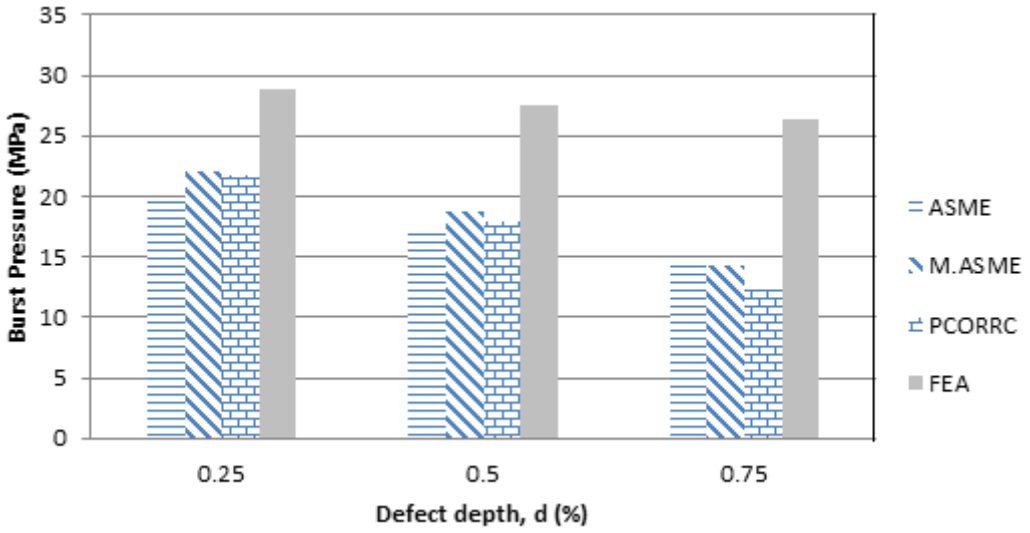


**Figure 4.5**: Relationship between burst pressure and defect depth for different design codes and FEA.

### 4.2.2 Application to failure predictions of API X65 pipes with gouges

The second type of defect considered is a gouge with the same geometry but different in defect length. There are two different depth cases considered, which are 50% and 75%.

#### 4.2.2.1 Comparisons

The burst pressure from FE is compared with the experimental results; also the pressure is normalized with respect to the theoretical pressure of a plain pipe.

$$P_O = \frac{t}{R_m}\sigma_f = \frac{t}{R_m}\left(\frac{\sigma_y + \sigma_u}{2}\right)$$

Where $\sigma_f$ , $\sigma_y$ and $\sigma_u$ denote the flow strength, yield strength and ultimate tensile strength, respectively.

Noting that an engineering assessment equation for gouge defects is not currently available, gouge defects could be assessed using an expression of failure pressure of axial surface cracked pipes under internal pressure, assuming that the gouge is idealized as an axial crack. One popular expression in Chang, K.O, (2007) is given by, as shown in Eq.(4.2) and Eq.(4.3).

$$P_f = P_O\left(\frac{1-\frac{a}{t}}{1-\left(\frac{a}{t}\right)\left(\frac{1}{M}\right)}\right);\quad M = \sqrt{1+1.61\frac{l^2}{4R_m t}} \qquad (4.2)$$

$$P_f = P_O\left(\frac{1-\frac{d}{t}}{1-\left(\frac{d}{t}\right)\left(\frac{1}{M_g}\right)}\right);\ M_g = \sqrt{1+0.64\frac{d}{t}\frac{l^2}{4R_m t}} \qquad (4.3)$$

Where a and l denote the crack depth and length, respectively. As the gouge is idealized as an axial crack, Eq. 4.2 can be used to estimate failure pressure, simply by replacing the crack depth a with the gouge depth d. Table shows the results of burst pressure of FE analysis, with the experimental and compared with Equation 4.2 and 4.3.

**Table 4.4** Burst pressure comparison for gouge defect of 50%.

| **Pipe no** | **d/t** | **length l (mm)** | $P_{\exp}$ **(MPa)** | $P_{fem}$ **(MPa)** | **Predicted failure pressure (Mpa)** | |
|---|---|---|---|---|---|---|
| | | | | | Eq4.2 | Eq4.3 |
| MNA | 0.5 | 100 | 24.68 | 28.62 | 19.51 | 22.38 |
| MNB | 0.5 | 200 | 22.48 | 22.5 | 16.19 | 20.05 |
| MNC | 0.5 | 300 | 17.7 | 21.3 | 14.7 | 18.07 |
| MND | 0.5 | 400 | 18.14 | 21.75 | 13.94 | 16.7 |
| MNE | 0.5 | 600 | 16.57 | 21 | 13.19 | 15.08 |

**Table 4.5** Burst pressure comparison for gouge defect of 75%.

| **Pipe no** | **d/t** | **length l (mm)** | $P_{fem}$ **(MPa)** | **Predicted failure pressure (Mpa)** | |
|---|---|---|---|---|---|
| | | | | Eq4.2 | Eq4.3 |
| MNA | 0.75 | 100 | 24.6 | 14.48 | 19.07 |
| MNB | 0.75 | 200 | 23.125 | 9.94 | 13.79 |
| MNC | 0.75 | 300 | 16.5 | 8.38 | 11 |
| MND | 0.75 | 400 | 18.75 | 7.66 | 9.53 |
| MNE | 0.75 | 600 | 16.25 | 7.00 | 8.13 |

As shown in the Table 4.4 and 4.5, the FE results show good agreement with the experimental results and also all with higher pressure. For the case MNC, it somewhat show lower burst both for the experiment and the FE results.

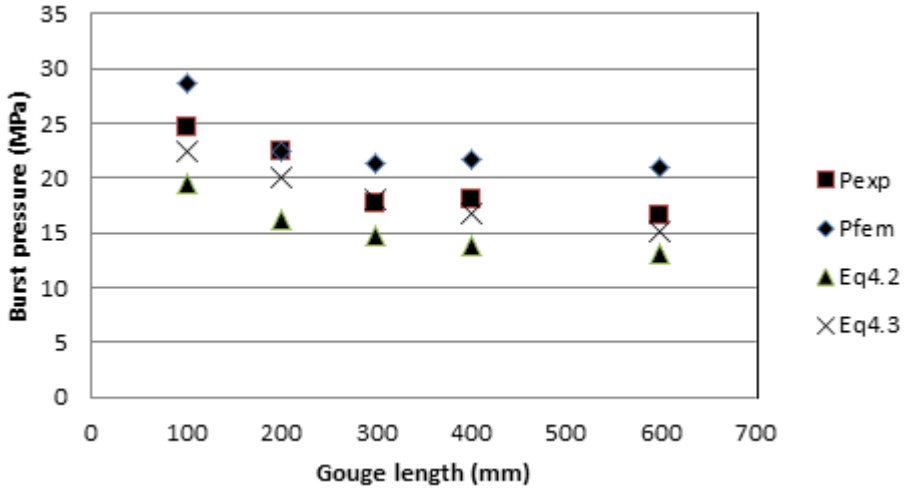


**Figure 4.6**: Comparison of burst pressure for the case of defect length 50%.

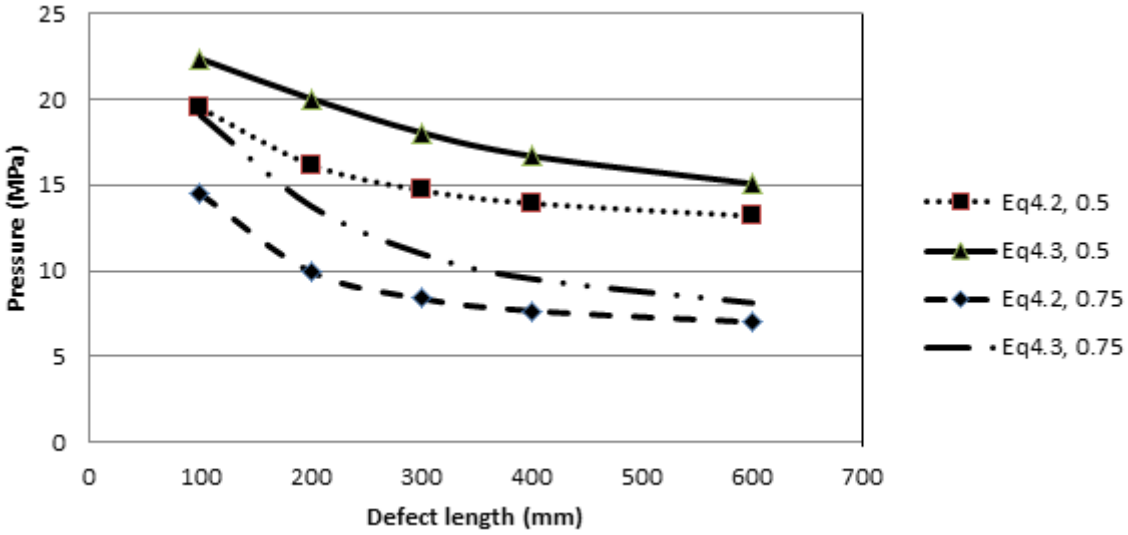


**Figure 4.7:** Comparison for Equation 4.2 and Equation 4.3 for gouge defect of different length.

In Figure 4.6, results of FE for MNA and MNB agree well with the experimental and the rest cases show much higher predicted pressure compare to experimental. Also, Equation 4.3 show more accurate results base on the experimental results and the

Equation 4.2 gives lower failure pressure as expected. Also, Figure 4.7 show Equation 4.2 and Equation 4.3 both give decreasing predicated pressure along with the increase of gouge length. For both defect cases, Equation 4.2 gives lower predicted pressure.

The following figures will compare the gouge defect of 50% results based on stress triaxiality and strain equivalent as this two are the key quantities that determine the void growth characteristics. (Agarwal et al., 2003)The stress triaxiality, T and strain equivalent, $\varepsilon_{eq}$ is calculated using SMCS. Where the stress triaxiality, T is define by the ratio of hydrostatic stress, $\sigma_m$ and equivalent stress, $\sigma_{eq}$ given by as in Eq. (4.5), Eq.(4.6) and Eq.(4.7):

$$T = \frac{\sigma_m}{\sigma_{eq}} = \frac{\sigma_1 + \sigma_2 + \sigma_3}{3\sigma_{eq}} \tag{4.5}$$

$$\sigma_{eq} = \frac{1}{\sqrt{2}}[(\sigma_1 - \sigma_2)^2 + (\sigma_3 - \sigma_1)^2 + (\sigma_2 - \sigma_3)^2]^{\frac{1}{2}} \tag{4.6}$$

On the other hand, the equivalent strain $\varepsilon_{eq}$ is given by:

$$\varepsilon_{eq} = \frac{\sqrt{2}}{3}[(\varepsilon_1 - \varepsilon_2)^2 + (\varepsilon_3 - \varepsilon_1)^2 + (\varepsilon_2 - \varepsilon_3)^2]^{\frac{1}{2}} \tag{4.7}$$

Where the $\sigma_1, \sigma_2, \sigma_3$ and $\varepsilon_1, \varepsilon_2, \varepsilon_3$ are the principle stresses and principle strain respectively.

(a)

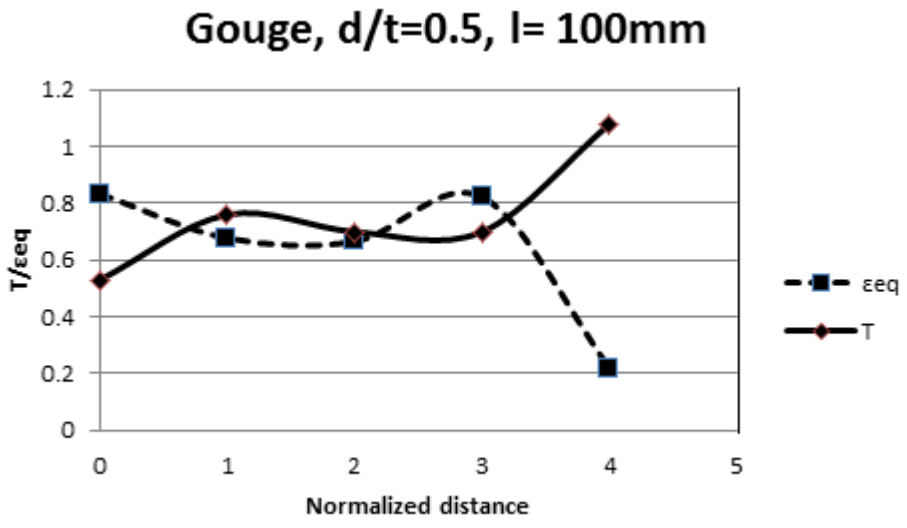

(b)

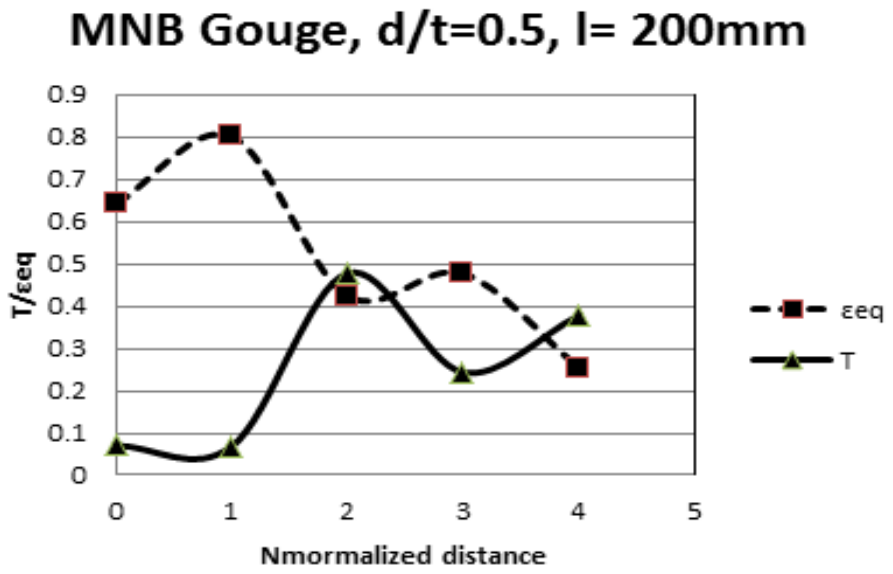
MNB Gouge, d/t=0.5, l= 200mm
T/εeq
0.9
0.8
0.7
0.6
0.5
0.4
0.3
0.2
0.1
0
0
1
2
3
4
5
Nmormalized distance
εeq
T

(c)

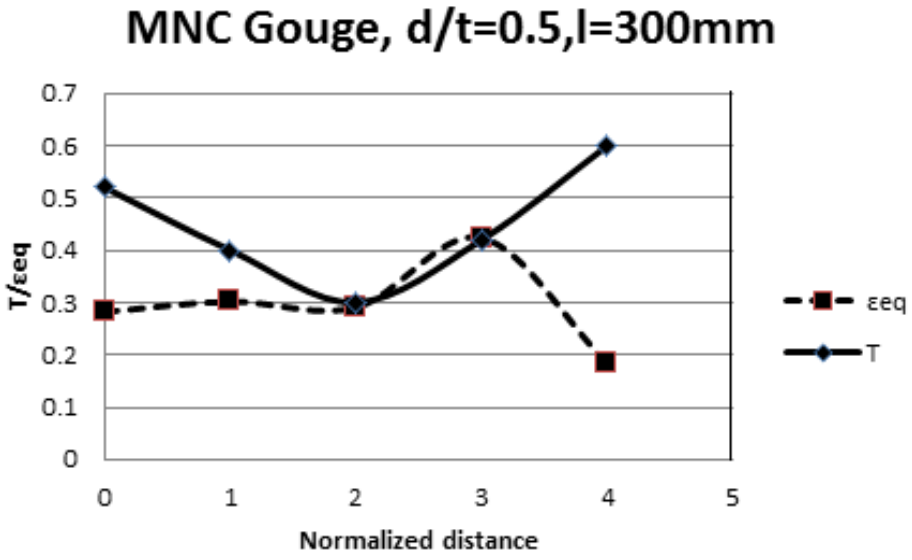
MNC Gouge, d/t=0.5,l=300mm
T/εeq
0.7
0.6
0.5
0.4
0.3
0.2
0.1
0
0
1
2
3
4
5
Normalized distance
εeq
T

(d)

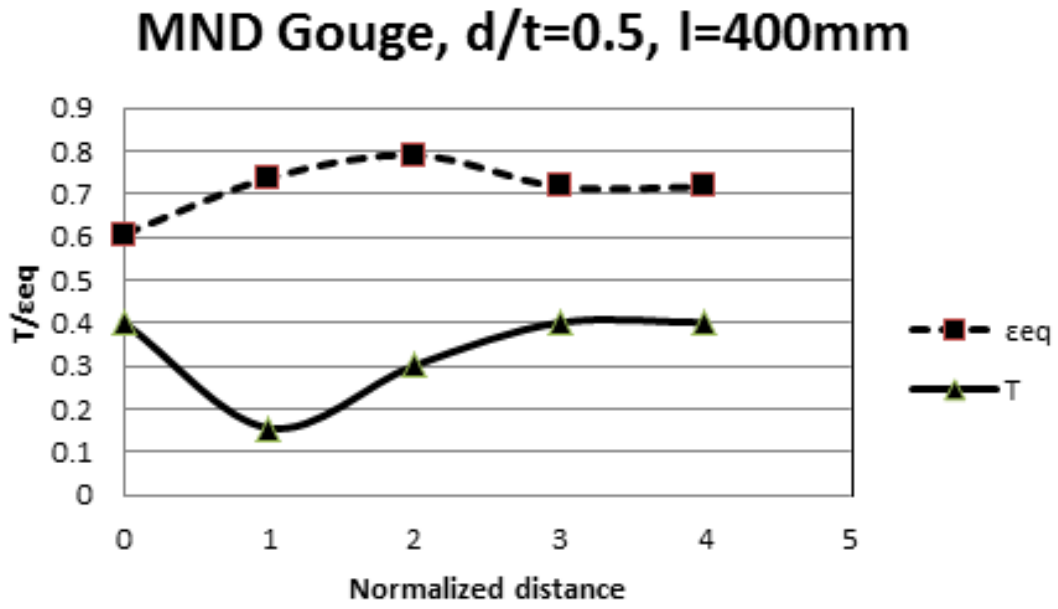


(e)

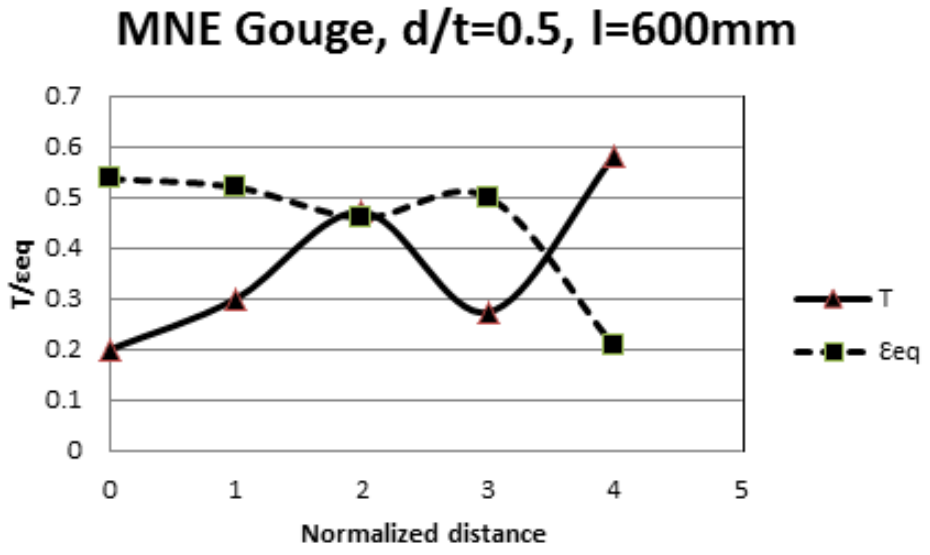


**Figure 4.8:** Distributions of stress triaxiality and equivalent strain for pipes with gouge along the defect length: (a) MNA pipe test and (b) MNB pipe test and (c) MNC pipe test and (d) MND pipe test and (e) MNE pipe test.

In Figure 4.8 shows tyipical radial variations of stress triaxiality and equivalent strain. The 0 denote the tip of the defect, while the number 4 denote the most inner part of the defect. Cases of MNA, MNB and MNE show that strain equivalent occur maximum at the tip with number denote 0 and minimum at the most inner defect end with number 4. Also, with stress triaxility, T maximum at the end, 4, and minimum at the tip, 0. But this is not the same with case MNC where $\varepsilon_{eq}$ maximum and T minimum in the middle of defect. MND, both strain equivalent and stress triaxiality decrease constantly towards the inner end of defect.

It is hard to determine the critical point along the defect length and depth is dependent either the strain equivalent or the stress triaxiality parameters. Hence, through the void volume fraction analysis as shown in the Figure 4.9 below, it can be seen that the void volume fraction agree well with the variations of strain equivalent.

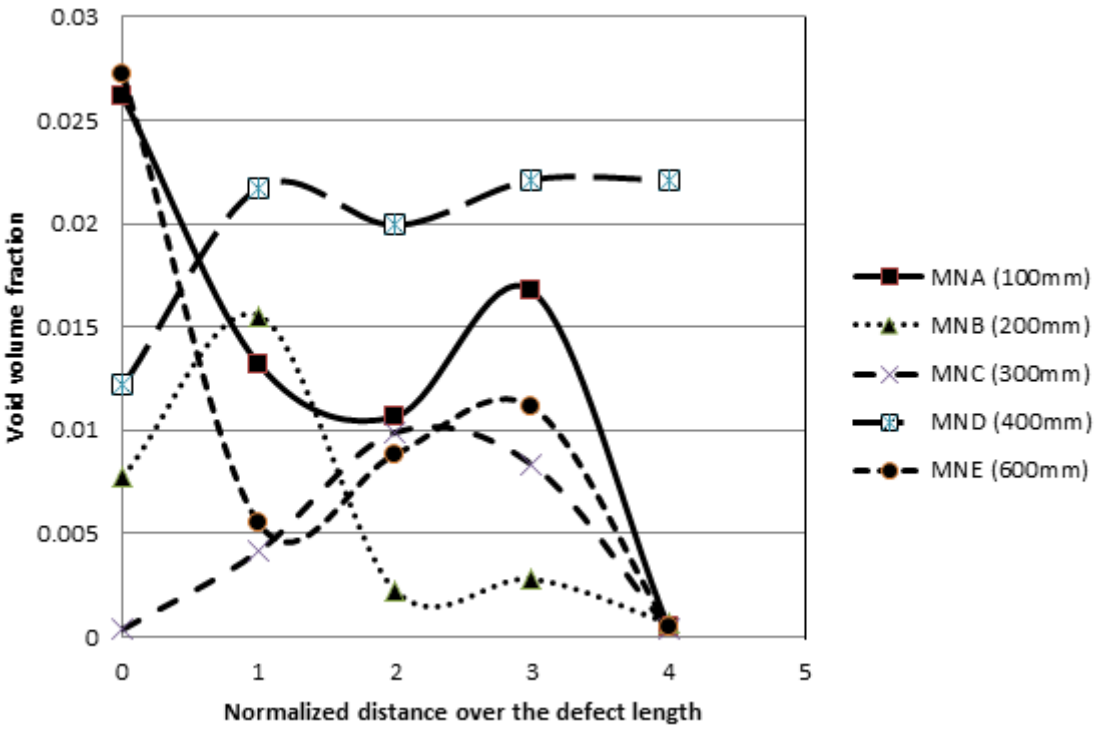


**Figure 4.9**: Distribution of void volume fraction over the normalized distance on the defect depth following the variation of defect length, MNA(100 mm), MNB(200 mm), MNC(300 mm), MND(400 mm), and MNE(600 mm) with case 50% depth.

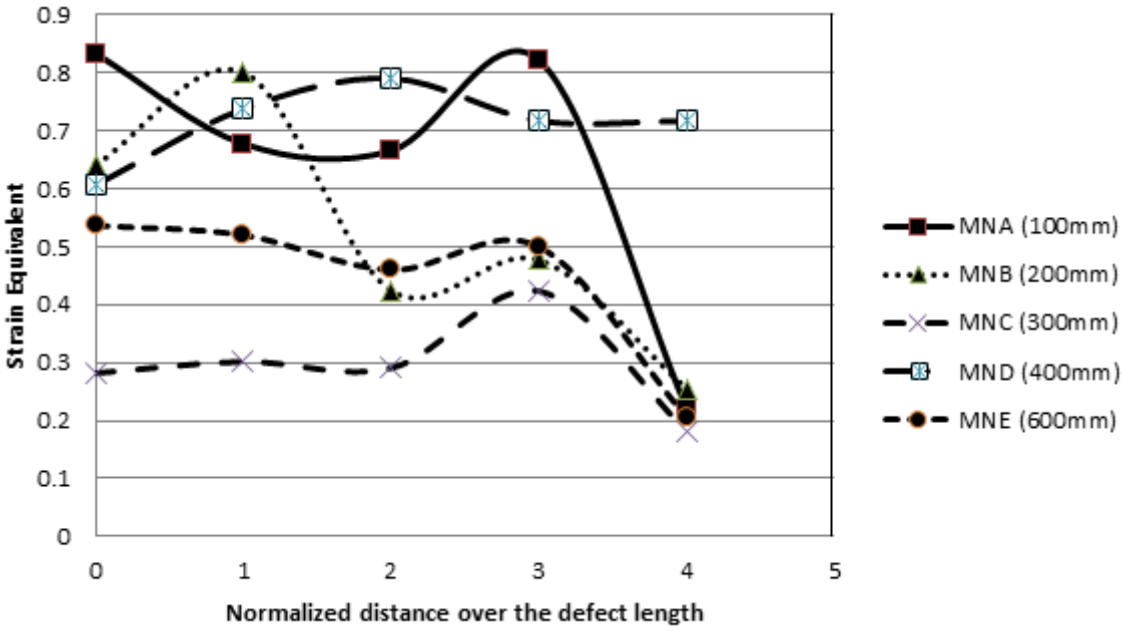


**Figure 4.10**: Distribution of strain equivalent over the normalized distance on the defect depth following the variation of defect length, MNA(100 mm), MNB(200 mm), MNC(300 mm), MND(400 mm), and MNE(600 mm) with case 50% depth.

For comparisons between the critical point for Figure 4.9 and 4.10, case MNA (100 mm) and MNE(600 mm) show the critical point at the tip of defect (denoted number 0). For case MNB (200 mm) and MND (400 mm), critical point occur at place in between the tip and the middle of the defect, ( with denote number 1). Only case MNC shows somehow critical at the middle of defect.

For Figure 4.10 on the strain equivalent, MNA (100 mm) and MNE (600 mm) also showing critical at the tip of defect (denote number 0) while case MNB (200 mm) and MND (400 mm) occur between the tip and middle of the defect with number denoted 1, except for the case MNC (300 mm) where it occur at the inner side of the defect.

However, overall, it can be seen that the void volume fraction distribution agree well with the strain equivalent distributions and from this the critical point of defect can be determined which it occurs at the tip of defect.

(a)

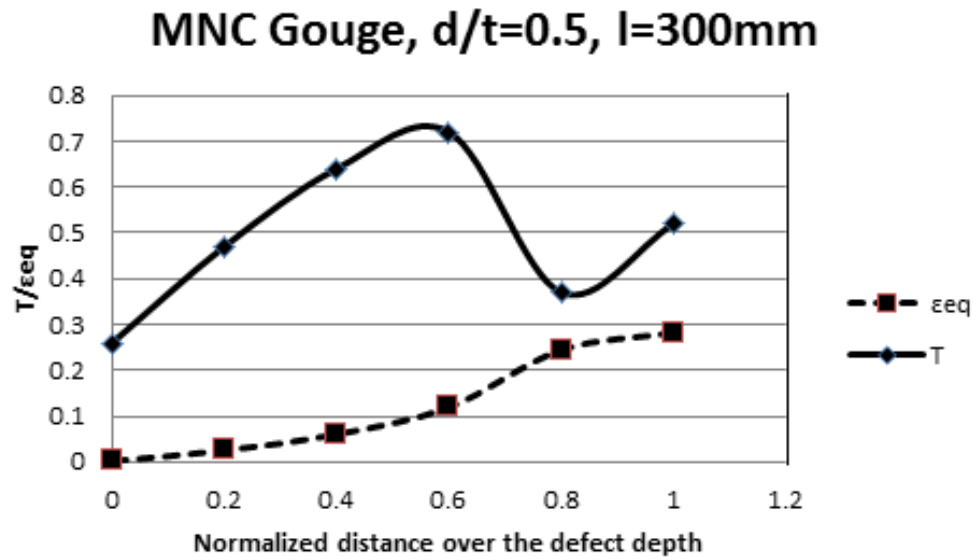
MNC Gouge, d/t=0.5, l=300mm
T/εeq
0.8
0.7
0.6
0.5
0.4
0.3
0.2
0.1
0
0
0.2
0.4
0.6
0.8
1
1.2
Normalized distance over the defect depth
εeq
T

(b)

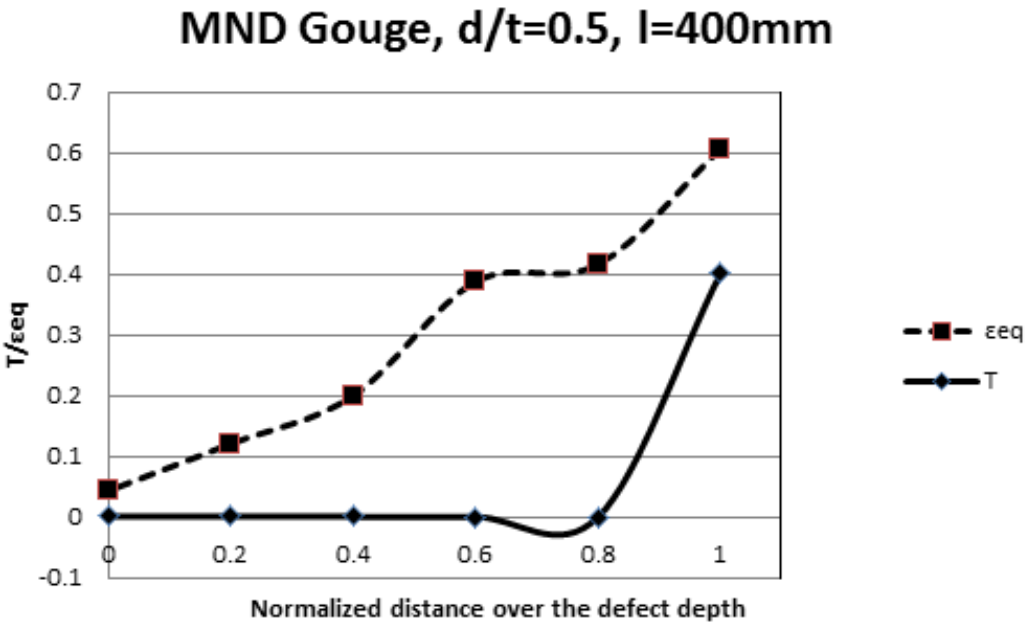
MND Gouge, d/t=0.5, l=400mm
T/εeq
0.7
0.6
0.5
0.4
0.3
0.2
0.1
0
-0.1
0
0.2
0.4
0.6
0.8
1
Normalized distance over the defect depth
εeq
T

(c)

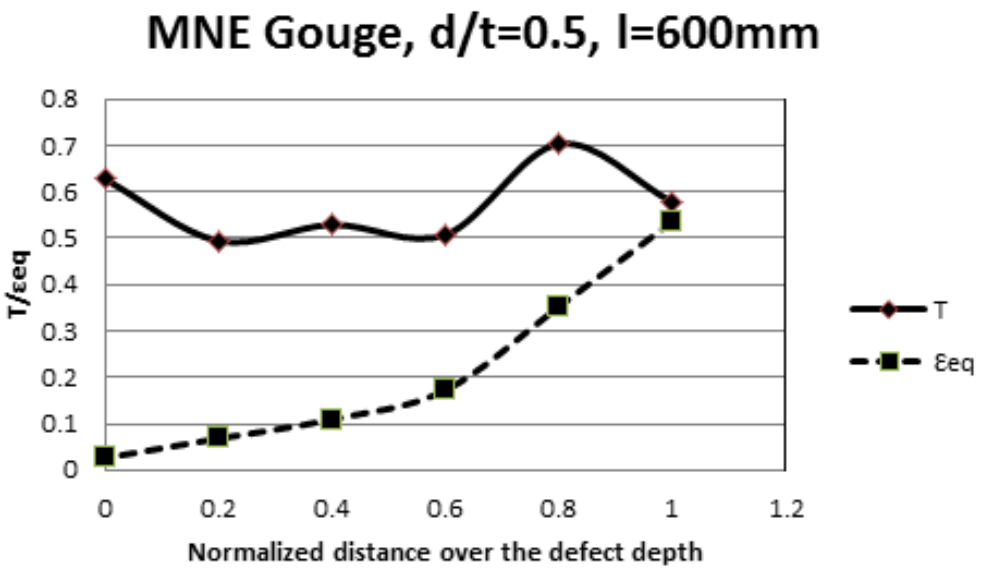


**Figure 4.11:** Distributions of stress triaxiality and equivalent strain for pipes with gouges along the defect depth from the inner surface to the notch tip of the defect.

For figure 4.11, only three cases considered. The radial distance is normalized with respect to the minimum ligament size, and the values of 0 and 1 denote the inner surface and the notch tip of the pipe, respectively. These show that the equivalent strain takes the maximum value at the notch tip, but the maximum value of stress triaxiality occurs somewhere in between the notch tip and the center except for case MND, T occur highest at the tip.

However, based on the void volume fraction, it can be seen that it follow well with the strain equivalent as shown in Figure 4.12 and 4.13 below.

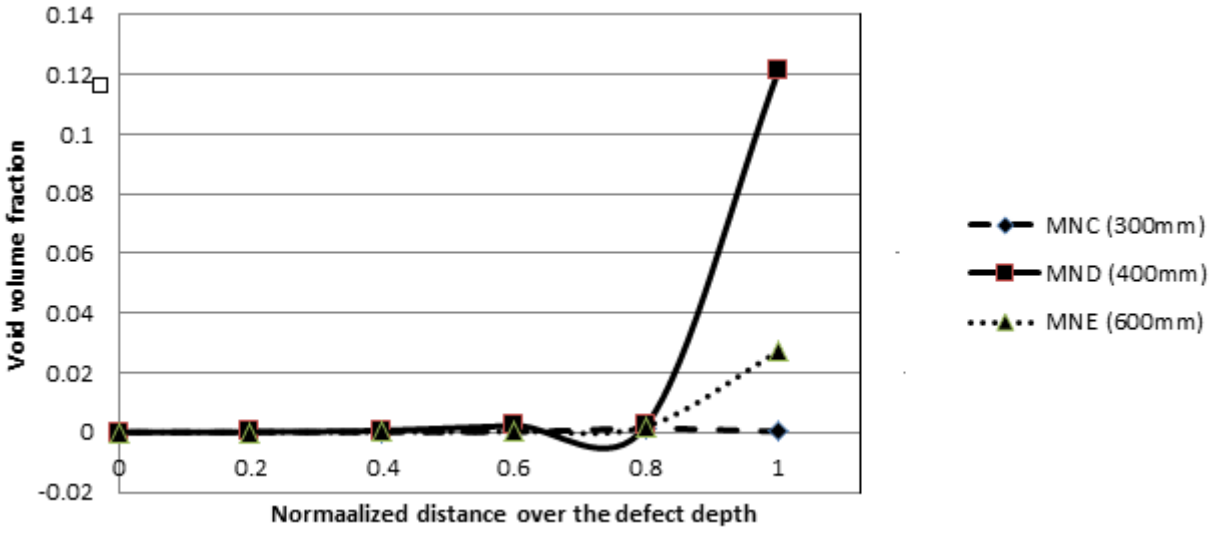


**Figure 4.12:** Distribution of Void volume fraction over the defect depth with varied with the defect length, MNC (300mm), MND (400mm) and MND (600mm) for the case 50% depth.

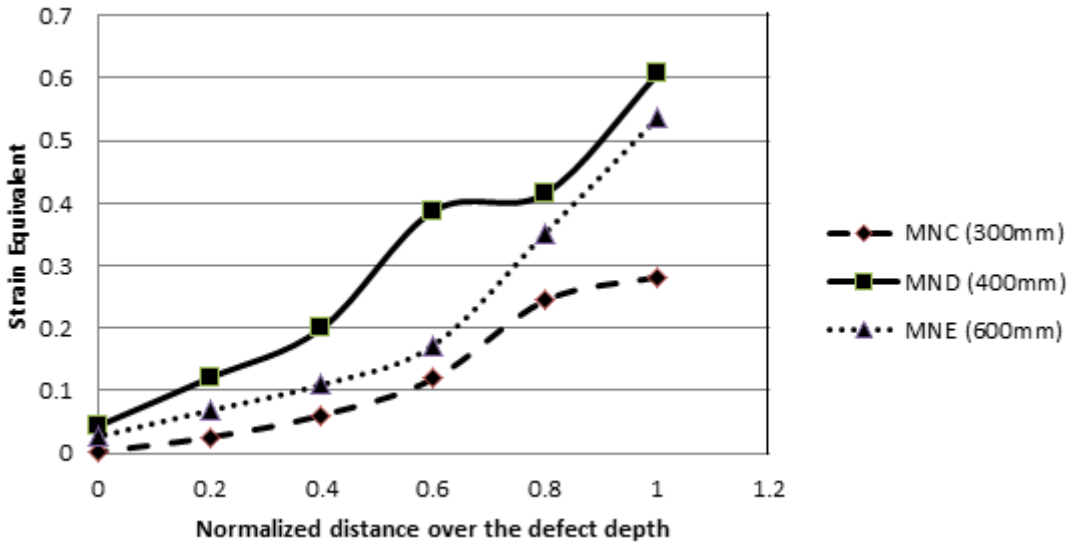


**Figure 4.13:** Distribution of strain equivalent over the defect depth with varied with the defect length, MNC (300mm), MND (400mm) and MND (600mm) for the case 50% depth.

## 4.3 DISCUSSIONS

### 4.3.1 Summary of Comparison

Analysis from Section 4.1 showed that for defect varies in depth, the prediction of burst pressure using damage model by Gurson model is in good agreement with the experiment results. An increase in defect depth requires lower burst pressure to reach failure. Besides, the void volume fraction value is higher for larger defect depth in order to reach critical status. Also, in prediction using design codes, PCORRC shows the most conservative towards the FE results.

In Section 4.2, gouge defect varies in length is being analyzed. The burst pressure predicted is decreasing with the increase in defect length. As engineering assessment for gouge defects is not currently available, gouge defects could be assessed using an expression of failure pressure of axial surface cracked pipes under internal pressure. In fact, Equation 4.3 is more suitable to asses particular for API X65 steel.

In order to predict more accurately the critical point location, the stress triaxiality and strain equivalent criteria are used for every case of defect length, which are the MNA, MNB, MNC, MND and MNE. Based on the comparisons, it is found that both criteria do not agree well to each other. As along the tip to the inner defect end, strain equivalent shows the maximum at the tip and minimum at the defect end, whereas the stress triaxiality is maximum at the inner end and minimum at the tip. This is hard to predict the critical point. However, through the void volume fraction distribution along the defect length and depth, it is found that it agree well with the strain equivalent as both the maximum value occur at the tip of defect, which shown that the critical point occur at the tip of defect.

### 4.3.2 Limitations of Present Study

The limitations observed in the present study are listed as below:

i. A quarter of pipe is analyzed in FE as to reduce the computation time and for simplicity.
ii. Careful design on the pipe geometry and the mesh size are critical to avoid error in analysis.
iii. Issue occurs where the void volume fraction may not reach the critical value even though the pressure applied is high. This is due to the determination of Gurson parameter for API X65 steel on the previous research was done on a specimen, but the present study is on a real pipe model.
iv. Due to the complexity of model, the time step may not complete even the analysis has finish.
v. Proper selection on Gurson model parameters is crucial for a particular material and the numerous parameters Gurson model involved leads to complexity in analysis.

# CHAPTER 5

# CONCLUSION

## 5.1 CONCLUSION

In the present study, Gurson model based on the critical void volume fraction is used to predict the burst pressure for pipe with defect. For increasing defect depth, the critical void volume fraction reached also increased and the burst pressure predicted decreasing. The characteristic of void is, it need more time for void growth for the beginning, once void coalescence occur during the end of middle half of the process, void critical will soon reached before it reach failure. In fact, as in most engineering alloys, ductile fracture often comes after the nucleation, growth and coalescence of micro voids. Hence, GursonTevaagard model which involve micro-ductile fracture mechanisms rather than to macroscopic fracture parameters makes it a more reasonable and suitable model in studying ductile fracture of material which causes burst pressure of steel pipe due to failure. The FE results based on Gurson model always predict higher value of burst pressure compared to ASME B31G, Modified ASME B31G and PCORRC design codes. Also, the PCORRC is the most conservative methods among other design codes.

Besides, the predicted burst pressure for defect varies with length show decreasing trend when the length increasing. As the Gurson model is based on the void volume fraction parameters, the void volume fraction distribution agreed well with the strain equivalent and the prediction of critical point along the defect based on strain equivalent found that critical point occurs at the defect tip.

## 5.2 RECOMMENDATIONS

From the present study, there are several recommendations which can contribute for the improvements of the results for similar studies in the future. The recommendations are as below:

i. The data for stress triaxiality and equivalent strain curve in FEA can be averaged to improve accuracy in the determination of critical node and thus to determine the burst pressure prediction.
ii. The prediction of burst pressure following the time step linearly can be made more accurately by determine the slope equation after plotting the graph and burst pressure can be determined from the equation.
iii. Sensitivity analysis on the mesh size and the parameters values can be done to make the comparisons and validation

**REFERENCES**


Antaki, G.A.2003. *Piping and Pipeline Engineering: Design Construction, Maintenance, Integrity and Repair*.CRC Press.

Amit, Kanvinde. And Geogor, Delerlein.2004. Prediction of Ductile fracture in steel moment connections during earthquakes using micromechanical fracture models.*13th World Conference on Earthquake Engineering.* Voncouver, B.C,.Canada.Paper No.294.

Agarwal, H., Gokhale, A.M., Graham, S., Horstemeyer, M.F., 2003. Void growth in 6061-Al-alloy under triaxial stress state. *Mater.Sci. Eng.***A 341**, 35–42.

Bauvineau, L., Burlet, H., Eripret, C., Pineau, A. Modelling ductile stable crack growth in a C–Mn steel with local approaches.*First European mechanics of materials conference on local approach to fracture*, Fontainebleau, September 1996.

Banora, N., Gentile, D., Pirondi, A., Nawaz, G., 2005. Ductile fracture evolution under triaxial state of stress: theory and experiments. Int. J. Plats. 21, 981–1007.

Bauvineau, L., Besson, J., Pineau, A. 1997. Size and geometry effects on ductile rupture of notched bars in a C–Mn steel. Experiments and modelling.Int J Fract**88**:1–18.

Beremin, F.M. 1981. Cavity formation from inclusions in ductile fracture of A508 steel. Metal Trans A.**12**: 723–31.

Cheng, LY. XU, Y.F.2012.Reliability and Failure Pressure Prediction of Various Grades pf Pipelines Steel in the Presence of Corrosion Defects and Pre Strain, *International Journal of Pressure Vessels and Piping.***89**

Chen CR, Kolednik O, Scheider I, Siegmund T, Tatschl A, Fischer FD.2003. On the determination of the cohesive zone parameters for the modelling of micro-ductile crack growth in thick specimens.Int J Fract.**120**:517–36

Chang, K.O., Kim, Y.J., Baek, J.H., Kim, Y.P., Kim, W.S.2007. Ductile failure analysis of API X65 pipes with notch-type defects using a local fracture criterion. *International Journal of Pressure vessels and piping*.**84**:512-525

Chang, S.O., Nak, H.K., Yun, J.K., Jong, H.B., Young, P.K., Woo, S.K.2011.A finite element ductile failure simulation method using stress-modified fracture strain model. Engineering Fracture Mechnics.**78**:124-137

Cheng, J., He, S., Zhou, G.T., Fu, C. Experimental and numerical investigations of void damage in aluminum alloy welds under thermal cycling condition

Chang, K.O., Kim, Y.J., Baek, J.H., Kim, Y.P., Kim, W. 2007.A phenomenological model of ductile fracture for API X65 steel. *International Journal of Mechanics Sciences.* **49**:1399-1412.

Cosham, A., Hopkins, P., Macdonald, K.A.2007.Best practice for the assessment of defects in pipelines-Corrosion. *Engineering Failure Analysis.***14**: 1245-1265.

Gurson, AL.1975. Plastic flow and fracture behaviour of ductile materials incorporating void nucleation, growth and coalescence, PhD Diss, Brown University.

Hansen, B., Lee, D. and Demartini, C. The cracking of stormwater pipe and the s ignificance of construction loads.

Hancock, J. W., and Brown, D. K.1983.On the role of strain and stress state in ductile failure. *J. Mech. Phys. Solids*. **31**(1) 1–24.

He, R., Steglich, D., Heerens, J., Wang G.X., Brocks, W., Dahms, M. 1998.Influence of particle size and volume fraction on damage and fracture in Al-A13Ti composites and micromechanical modelling using the GTN model. Fatigue FractEng Mater Struct .**21**(10): 1189–201.

Koplik J, Needleman A. 1988. Void growth and coalescence in porous plastic solids. Int J Solids Struct .**24**(8):835–53.

Kanvinde, A.M. and Deierlein, G.G.2005. The Void Growth Model and The Stress Modified Critical Strain Model To Predict Ductile Fracture In Structural Steels.

Kanvinde, A.M. and Delerlein, G.G.2007. Finite element simulation of ductile fracture in in reduced section pull-plates using micromechanics-based fracture models. *Journal of Structural Engineering.*

Kiefner, J.F.,Vieth, P,H., Roytman I.1995. Continued Validation of RSTRENG, Updated Draft Final Report on Contract No. PR 218-9304 to Line Pipe Research Supervisory Committee, Pipeline Research Committee of the American Gas Association, Kiefner and Associates, Inc.

Lassance, D., Scheyvaerts, F., Pardoen, T.2006.Growth and coalescence of penny-shaped voids in metallic alloys.*Engineering Fracture Mechanics*.**73**:1009-1034.

Liu, P.F., Zheng, J.Y. Finite element analysis of tensile behavior of ductile steel with defects Fail.Anal.andPreven**10**:212-217

McClintock, FA.1968. A criterion for ductile fracture by the growth of holes.*JApplMech* **1;35**:363–71.

Mackenzie, A.C., Hancock, J.W., and Brown, D.K. 1997. On The Influence of State of Stress on Ductile Failure Initiation In High Strength Steels, *Int J FractMech*

Majid, Anvari., Liu, J., Christian, T.2007. Dynamic ductile fracture in aluminum round bars: experiments and simulations.**143**:317–332

Needleman, A., Tvergaard, V., 1987. An analysis of ductile rupture modes at a crack tip.*Journal of the Mechanics and Physics of Solids*.**35**: 151±183.

N, Benseddiq., A. Imad. 2008. A ductile fracture analysis using a local damage model. *International Journal of Pressure Vessels and Piping*.**85:** 219-227.

Pardoen, T. and Hutchinson, J.W.,2000. An extend model for void growth and coalescence. *Journal of the Mechnics and Physics of Solids*.**48**:2467-2512.

Rakina, M., Cvijovic, Z., Grabulov, V., Putic, S., Sedmak A., 2004.Prediction of ductile fracture initiation using micromechanical analysis. *Engineering Fracture Mechanics*.**71**:813-827.

Roylance, D.2001.*Stress strain curve.* Department of Materials Science and Engineering Massachusetts Institute of Technology Cambridge.

Rice, J.R. and Tracey, Ai.1969. On the ductile enlargement of voids in triaxial stress fields, *J.Mech. Phys. Solids*. **17** :201- 217.

Steglich, D., Brocks, W. 1998. Micromechanical modelling of damage and fracture of ductile materials. *Fatigue FractEng Mater Struct* .**21**(10):1175–88.

Thomason, PF. 1990. Ductile fracture of metals.*Oxford:*Pergamon.

Toshiyuki, M. 2010.Fracture Behavior Prediction for Wall-thinned Pipe- Internal Burst Pressure Equation Applicable to Planar/non-planar Flaw in Wall Thinned Pipe. *International Symposium on the Ageing Management & Maintainance of Nuclear Power Plants*.72-82

Vadillo, G., Fernández-Sáez, J., 2009.An analysis of Gurson model with parameters dependent on triaxiality based on unitary cells. *European Journal of Mechanics A/Solids*.28: 417-427.

Vieth PH. Kiefner JF.1994.Database of Corroded Pipe Tests, Final Report on Contract No.PR 218-9206 to Line Pipe Research Supervisory Committee of the American Gas Association, Kiefner and Associates, Inc.

Zhang,Z.L., Thaulow, C., Odegard, J.2000. A complete Gurson model approach for ductile fracture.*Engineering fracture mechanics*.**67**: 155-168.

Zhang, Z.L., Niemi, E. 1995. A new failure criterion for the Gurson–Tver-gaard dilatation constitutive model.Int J Fract .**70**:321–34.

Zhang ZL, Thaulow C, Phidegard J. 2000. A complete Gurson model approach for ductile fracture. EngFractMech .**67**:155–68

# APPENDICES A1

## TRUE STRESS-STRAIN DATA AT ROOM TEMPERATURE FOR API X65 STEEL

| True strain | True stress |
|---|---|
| 0 | 465.5 |
| 0.02081 | 486.01 |
| 0.030518 | 511.45 |
| 0.04343 | 536.89 |
| 0.05957 | 567.43 |
| 0.08214 | 600.51 |
| 0.10467 | 623.41 |
| 0.13042 | 646.31 |
| 0.15937 | 669.21 |
| 0.1947 | 689.57 |
| 0.2333 | 709.92 |
| 0.27185 | 727.74 |
| 0.31362 | 745.55 |
| 0.34897 | 760.81 |
| 0.39714 | 776.08 |
| 0.4485 | 791.35 |
| 0.50633 | 806.62 |
| 0.56413 | 821.88 |
| 0.62835 | 834.61 |
| 0.68614 | 847.33 |
| 0.75036 | 862.6 |
| 0.8146 | 870.23 |
| 0.88841 | 888.04 |
| 0.95902 | 893.13 |
| 1.0297 | 908.4 |
| 1.09063 | 913.49 |
| 1.12273 | 918.58 |
| 1.15824 | 923.664 |

Source: Chang-Kyun Oh et.al. (2007)

## APPENDICES A2

## DATA COLLECTED AND CALCULATED FOR GOUGE DEFECT, 50%, l= 100mm

## NORMALIZED DISTANCE ON DEFECT LENGTH

**(a) From the tip of the notch, with number denote (0)**

| Time step | Pressure (MPa) | Void volume fraction, f | σ1(MPa) | σ2 (MPa) | σ3 (MPa) | σeq (MPa) | εeq | T |
|---|---|---|---|---|---|---|---|---|
| **0** | 0 | 0.000125 | 0 | 0 | 0 | 0 | 0 | 0 |
| **0.0125** | 0.46153846 | 0.000125 | 81.379143 | 18.773224 | 0.66630763 | 73.35433489 | 0 | 0.4581355 |
| **0.025** | 0.92307692 | 0.000125 | 162.71759 | 37.538727 | 1.3276068 | 146.6746303 | 0 | 0.458120406 |
| **0.0375** | 1.38461538 | 0.000125 | 243.92224 | 56.277931 | 1.985641 | 219.8743992 | 0 | 0.458118837 |
| **0.05** | 1.84615384 | 0.000125 | 325.02283 | 74.995819 | 2.6376083 | 292.9830671 | 0 | 0.458110954 |
| **0.0625** | 2.30769230 | 0.000125 | 406.01993 | 93.692528 | 3.2835407 | 366.0011281 | 0 | 0.45810059 |
| **0.075** | 2.76923076 | 0.000125 | 486.91434 | 112.36823 | 3.9234779 | 438.9292854 | 0 | 0.458089012 |
| **0.0875** | 3.23076923 | 0.000125004 | 565.71393 | 131.73387 | 5.696281 | 508.8388749 | 1.45E-05 | 0.460619996 |
| **0.1** | 3.69230769 | 0.000125162 | 576.81079 | 179.07162 | 40.89534 | 481.9157563 | 0.000601532 | 0.551118281 |
| **0.1125** | 4.15384615 | 0.000125368 | 588.69739 | 226.04659 | 50.352509 | 475.4947689 | 0.00127415 | 0.606453562 |
| **0.125** | 4.61538461 | 0.000125614 | 593.73328 | 259.43301 | 51.191422 | 474.0592138 | 0.001999487 | 0.635896449 |
| **0.1375** | 5.07692307 | 0.000125882 | 596.37598 | 281.05316 | 53.172405 | 472.4508867 | 0.002749218 | 0.656577273 |
| **0.15** | 5.53846153 | 0.000126187 | 598.46527 | 297.31546 | 54.636421 | 471.8715925 | 0.003566463 | 0.671381202 |
| **0.1625** | 6 | 0.000126532 | 600.1073 | 308.15976 | 55.925167 | 471.6891535 | 0.004464273 | 0.68137545 |
| **0.175** | 6.46153846 | 0.000126899 | 601.36151 | 312.87976 | 56.538368 | 472.0997435 | 0.005402342 | 0.685433994 |
| **0.1875** | 6.92307692 | 0.000127294 | 602.22314 | 315.2951 | 56.497868 | 472.8166686 | 0.006400175 | 0.686676375 |
| **0.2** | 7.38461538 | 0.00012771 | 603.06653 | 316.39719 | 56.350021 | 473.6529192 | 0.00744537 | 0.686729109 |
| **0.2125** | 7.84615384 | 0.000128153 | 603.95123 | 317.34256 | 56.05125 | 474.6595747 | 0.008551848 | 0.686348064 |
| **0.225** | 8.30769230 | 0.000128612 | 605.55182 | 317.77011 | 56.257973 | 475.8791619 | 0.00969375 | 0.686154512 |

| | | | | | | | | |
|---|---|---|---|---|---|---|---|---|
| **0.2375** | 8.76923076 | 0.000129118 | 606.82086 | 319.47528 | 56.108608 | 477.0769014 | 0.010941453 | 0.686405584 |
| **0.25** | 9.23076923 | 0.000129659 | 608.2088 | 321.15271 | 55.990856 | 478.3554575 | 0.012265635 | 0.686624943 |
| **0.2625** | 9.69230769 | 0.000130254 | 609.72943 | 323.0499 | 55.843166 | 479.7737775 | 0.013710495 | 0.686867118 |
| **0.275** | 10.1538461 | 0.000130914 | 611.50281 | 325.00668 | 55.730682 | 481.3851704 | 0.01529344 | 0.687072939 |
| **0.2875** | 10.6153846 | 0.00013165 | 613.44623 | 326.98798 | 55.609516 | 483.154967 | 0.017038986 | 0.6871803 |
| **0.3** | 11.0769230 | 0.000132489 | 615.42682 | 329.40039 | 55.344566 | 485.0777351 | 0.019004887 | 0.687293124 |
| **0.3125** | 11.5384615 | 0.000133442 | 617.80347 | 331.4314 | 55.183079 | 487.265171 | 0.021201078 | 0.687112486 |
| **0.325** | 12 | 0.000134747 | 622.96857 | 333.14383 | 53.479641 | 493.2133145 | 0.023596445 | 0.682322781 |
| **0.3375** | 12.4615384 | 0.000135837 | 630.40802 | 334.9166 | 52.609921 | 500.4264566 | 0.026179764 | 0.678044714 |
| **0.35** | 12.9230769 | 0.000137095 | 638.40289 | 338.39679 | 52.302605 | 507.6205286 | 0.028997349 | 0.67576876 |
| **0.3625** | 13.3846153 | 0.000138494 | 647.10938 | 342.93204 | 51.958744 | 515.4529079 | 0.032078464 | 0.673841165 |
| **0.375** | 13.8461538 | 0.000139972 | 654.85675 | 347.95273 | 52.647751 | 521.5555348 | 0.035445035 | 0.674557269 |
| **0.3875** | 14.3076923 | 0.000141764 | 662.68774 | 353.46472 | 52.420929 | 528.5173155 | 0.039158292 | 0.673944106 |
| **0.4** | 14.7692307 | 0.000143842 | 671.52502 | 358.47186 | 51.920826 | 536.5976748 | 0.043340966 | 0.672084976 |
| **0.4125** | 15.2307692 | 0.000146329 | 681.42078 | 363.96188 | 51.154423 | 545.8263966 | 0.048187472 | 0.669649477 |
| **0.425** | 15.6923076 | 0.000149334 | 692.07922 | 370.39908 | 50.121185 | 555.947077 | 0.053744912 | 0.667089567 |
| **0.4375** | 16.1538461 | 0.000152852 | 703.96906 | 377.11752 | 48.84866 | 567.3459106 | 0.059928034 | 0.663872028 |
| **0.45** | 16.6153846 | 0.000156837 | 716.01532 | 383.63263 | 48.02879 | 578.4899986 | 0.066758156 | 0.661306011 |
| **0.4625** | 17.0769230 | 0.000161798 | 726.99268 | 390.37646 | 47.15115 | 588.7636629 | 0.074249394 | 0.659302628 |
| **0.475** | 17.5384615 | 0.000167659 | 738.61096 | 395.71875 | 45.675842 | 600.104311 | 0.082456321 | 0.65544469 |
| **0.4875** | 18 | 0.000174359 | 750.33752 | 401.82886 | 43.347153 | 612.2860517 | 0.091388583 | 0.650846953 |
| **0.5** | 18.4615384 | 0.000182965 | 759.95593 | 404.74207 | 44.066879 | 619.9781723 | 0.10109711 | 0.649896471 |
| **0.5125** | 18.9230769 | 0.000193454 | 768.5506 | 415.97852 | 36.487793 | 634.1217595 | 0.11168935 | 0.641841463 |
| **0.525** | 19.3846153 | 0.000205604 | 789.12738 | 396.82114 | 43.38044 | 646.1218919 | 0.12320805 | 0.634209002 |
| **0.5375** | 19.8461538 | 0.000222107 | 836.24286 | 476.37082 | -54.683666 | 776.2904449 | 0.13570124 | 0.540145776 |
| **0.55** | 20.3076923 | 0.000238528 | 1218.7516 | 243.80409 | -107.67377 | 1190.254017 | 0.1468035 | 0.37943775 |
| **0.5625** | 20.7692307 | 0.000248396 | 1780.6541 | 528.07062 | -544.22943 | 2015.405714 | 0.15264843 | 0.291834588 |
| **0.575** | 21.2307692 | 0.000267321 | 1638.8435 | 538.36694 | -152.79547 | 1565.028814 | 0.16290842 | 0.431177358 |
| **0.5875** | 21.6923076 | 0.000286639 | 2024.9425 | 756.60553 | -262.27798 | 1984.695027 | 0.17422645 | 0.423116233 |
| **0.6** | 22.1538461 | 0.000315849 | 2165.2656 | 890.31616 | -6.6617107 | 1890.396325 | 0.1837831 | 0.537615668 |
| **0.6125** | 22.6153846 | 0.000358854 | 2513.8413 | 1181.58 | -77.629326 | 2244.555083 | 0.19856964 | 0.537269353 |

| | | | | | | | | |
|---|---|---|---|---|---|---|---|---|
| **0.625** | 23.0769230 | 0.00040876 | 2989.3875 | 1268.6174 | 280.01114 | 2374.752198 | 0.2099026 | 0.636980993 |
| **0.6375** | 23.5384615 | 0.000483665 | 3408.2605 | 1808.6395 | 181.0524 | 2794.852374 | 0.22585292 | 0.643796962 |
| **0.65** | 24 | 0.000580635 | 4080.438 | 1923.7891 | 544.05286 | 3087.107128 | 0.24017428 | 0.707056767 |
| **0.6625** | 24.4615384 | 0.000704864 | 4688.3618 | 2411.4663 | 541.53851 | 3596.979993 | 0.25746682 | 0.708127988 |
| **0.675** | 24.9230769 | 0.000873226 | 5270.7695 | 2878.5354 | 938.08795 | 3758.969784 | 0.27506793 | 0.805840729 |
| **0.6875** | 25.3846153 | 0.001109185 | 4244.8872 | 2110.3152 | -1115.6984 | 4674.323544 | 0.29691344 | 0.373637237 |
| **0.7** | 25.8461538 | 0.001274443 | 4889.2314 | 1170.5496 | -1088.7242 | 5228.184056 | 0.31931624 | 0.316939671 |
| **0.7125** | 26.3076923 | 0.001397784 | 4501.9121 | 1869.351 | -1163.5391 | 4910.45887 | 0.34518254 | 0.35351238 |
| **0.725** | 26.7692307 | 0.00154101 | 4935.5811 | 1503.2836 | -1249.6368 | 5367.264305 | 0.36982957 | 0.322276403 |
| **0.7375** | 27.2307692 | 0.001660894 | 5440.5327 | 1790.9551 | -1339.9543 | 5877.741446 | 0.39686006 | 0.334115496 |
| **0.75** | 27.6923076 | 0.001772901 | 4432.3428 | 1872.8757 | -1111.8557 | 4806.076586 | 0.42190537 | 0.360194205 |
| **0.7625** | 28.1538461 | 0.014582006 | 1682.3345 | 785.37128 | 250.92511 | 1252.806521 | 0.73964137 | 0.723344173 |
| **0.775** | 28.6153846 | 0.026138689 | 2162.9902 | 1630.2262 | -277.55045 | 2222.554656 | 0.83337289 | 0.527271015 |
| **0.7875** | 29.0769230 | 0.080776952 | 1176.9725 | -191.11349 | -350.39621 | 1454.270317 | 0.88001871 | 0.145654443 |
| **0.8** | 29.5384615 | 0.091807403 | 2158.4888 | 403.54852 | 184.42853 | 1874.114214 | 0.91319531 | 0.488491368 |
| **0.8125** | 30 | 0.12161639 | 2008.9424 | 626.09814 | 212.23537 | 1629.661761 | 0.95083117 | 0.582385862 |

**(b) Second node from the tip, denote number 1**

| Time step | Void volume fraction, f | σ1 (MPa) | σ2 (MPa) | σ3 (MPa) | σeq (MPa) | εeq | T |
|---|---|---|---|---|---|---|---|
| **0** | 0.000125 | 0 | 0 | 0 | 0 | 0 | 0 |
| **0.0125** | 0.000125 | 57.675636 | 19.584412 | 7.9747028 | 45.03238647 | 0 | 0.630914456 |
| **0.025** | 0.000125 | 115.33286 | 39.161392 | 15.943199 | 90.05323605 | 0 | 0.630876648 |
| **0.0375** | 0.000125 | 172.9099 | 58.706291 | 23.886936 | 135.0222134 | 0 | 0.630768129 |
| **0.05** | 0.000125 | 230.42648 | 78.226746 | 31.811518 | 179.9524844 | 0 | 0.630656744 |
| **0.0625** | 0.000125 | 287.88297 | 97.722916 | 39.717037 | 224.8443007 | 0 | 0.630544369 |
| **0.075** | 0.000125 | 345.27988 | 117.19497 | 47.603615 | 269.6980268 | 0 | 0.630431587 |
| **0.0875** | 0.000125 | 402.62122 | 136.64699 | 55.471947 | 314.5158992 | 0 | 0.630323362 |
| **0.1** | 0.000124991 | 466.89471 | 153.09656 | 56.583729 | 371.5735528 | -3.36E-05 | 0.60694578 |

| | | | | | | | |
|---|---|---|---|---|---|---|---|
| **0.1125** | 0.000124998 | 525.91449 | 169.79999 | 57.016319 | 423.9081828 | -1.40E-05 | 0.591897671 |
| **0.125** | 0.000125044 | 572.86719 | 190.17841 | 59.584961 | 462.0366916 | 0.000126645 | 0.59348141 |
| **0.1375** | 0.00012515 | 601.22601 | 216.68666 | 67.949738 | 476.6382543 | 0.000441398 | 0.619521129 |
| **0.15** | 0.000125316 | 613.7381 | 247.27759 | 80.125862 | 472.7401258 | 0.000913299 | 0.66360741 |
| **0.1625** | 0.000125538 | 621.07501 | 277.76419 | 85.231804 | 470.1332266 | 0.00150665 | 0.69772492 |
| **0.175** | 0.0001258 | 628.16077 | 305.20389 | 87.909477 | 470.8401871 | 0.002171183 | 0.723015413 |
| **0.1875** | 0.000126108 | 633.9538 | 329.08838 | 90.485039 | 471.817885 | 0.00291673 | 0.744303577 |
| **0.2** | 0.000126469 | 638.11353 | 348.8439 | 92.760147 | 472.5767412 | 0.003751409 | 0.761581829 |
| **0.2125** | 0.000126867 | 641.32153 | 362.98068 | 94.956268 | 473.189774 | 0.004639857 | 0.774360548 |
| **0.225** | 0.000127281 | 642.93457 | 371.44852 | 96.07724 | 473.5917824 | 0.005538879 | 0.781587555 |
| **0.2375** | 0.000127737 | 644.59827 | 377.36746 | 96.946747 | 474.3214323 | 0.006511251 | 0.786325054 |
| **0.25** | 0.000128228 | 646.2016 | 381.05255 | 97.717079 | 475.0840028 | 0.007543568 | 0.789313905 |
| **0.2625** | 0.00012876 | 647.70911 | 383.13257 | 98.195618 | 475.996953 | 0.008650102 | 0.790647427 |
| **0.275** | 0.000129335 | 649.17511 | 384.26282 | 98.404358 | 477.0918525 | 0.00983508 | 0.790792718 |
| **0.2875** | 0.000129959 | 650.64124 | 384.814 | 98.412598 | 478.3500705 | 0.011114096 | 0.790124156 |
| **0.3** | 0.000130656 | 652.14307 | 385.28076 | 98.278633 | 479.761763 | 0.012532841 | 0.789073905 |
| **0.3125** | 0.00013143 | 653.73035 | 385.7959 | 98.024048 | 481.3533599 | 0.01409519 | 0.787744439 |
| **0.325** | 0.000132278 | 655.44214 | 386.50671 | 97.851242 | 482.9839054 | 0.015804671 | 0.786637732 |
| **0.3375** | 0.000133214 | 657.53961 | 387.80298 | 98.209007 | 484.4916087 | 0.017661881 | 0.786770831 |
| **0.35** | 0.000134244 | 660.89783 | 389.46484 | 98.494232 | 487.1490872 | 0.019678384 | 0.786109039 |
| **0.3625** | 0.000135444 | 665.21106 | 391.64572 | 98.397171 | 490.9691664 | 0.02187481 | 0.784335711 |
| **0.375** | 0.000136746 | 670.98352 | 394.10513 | 98.041412 | 496.2703797 | 0.024236202 | 0.781247555 |
| **0.3875** | 0.000138121 | 677.70929 | 396.81583 | 97.334465 | 502.7004413 | 0.026790485 | 0.777043005 |
| **0.4** | 0.000139611 | 685.07721 | 399.64471 | 96.267334 | 509.9983514 | 0.029598847 | 0.771890897 |
| **0.4125** | 0.000141297 | 692.79724 | 402.43927 | 95.275352 | 517.5323929 | 0.032753017 | 0.766787341 |
| **0.425** | 0.000143236 | 700.44092 | 405.33569 | 94.408646 | 524.8939282 | 0.036271453 | 0.762176376 |
| **0.4375** | 0.000145387 | 708.1637 | 408.68188 | 93.505905 | 532.3619957 | 0.040095523 | 0.757849918 |
| **0.45** | 0.000147802 | 716.1734 | 411.97162 | 92.54097 | 540.1300211 | 0.044229411 | 0.753328484 |
| **0.4625** | 0.000150473 | 724.63123 | 415.33633 | 91.194092 | 548.6176207 | 0.048670735 | 0.74803871 |
| **0.475** | 0.00015339 | 733.28766 | 418.77451 | 89.71904 | 557.3888564 | 0.053453628 | 0.74261813 |
| **0.4875** | 0.000156711 | 742.3205 | 422.54718 | 88.215485 | 566.5128938 | 0.058595415 | 0.737307823 |

| | | | | | | | |
|---|---|---|---|---|---|---|---|
| **0.5** | 0.000160409 | 751.5777 | 426.08704 | 86.569763 | 575.9509451 | 0.064120255 | 0.731679503 |
| **0.5125** | 0.000164609 | 760.87317 | 429.46304 | 84.948975 | 585.3985765 | 0.070094407 | 0.72616347 |
| **0.525** | 0.000169497 | 768.81744 | 433.35538 | 83.22802 | 593.7774372 | 0.076586939 | 0.721595197 |
| **0.5375** | 0.000175302 | 780.87329 | 434.71417 | 82.955948 | 604.414835 | 0.083747745 | 0.716143578 |
| **0.55** | 0.000181585 | 784.5719 | 453.25131 | 80.910881 | 609.7275198 | 0.091469459 | 0.720941759 |
| **0.5625** | 0.000189449 | 834.34357 | 466.67795 | 108.88908 | 628.2754008 | 0.099600099 | 0.748032152 |
| **0.575** | 0.000199084 | 893.52161 | 512.19397 | 156.19116 | 638.6663116 | 0.10819943 | 0.815191862 |
| **0.5875** | 0.000210864 | 1003.4406 | 599.0625 | 118.89715 | 766.9664141 | 0.11716215 | 0.748142386 |
| **0.6** | 0.000222716 | 1278.131 | 542.77429 | 215.58195 | 942.5446203 | 0.12477934 | 0.720208959 |
| **0.6125** | 0.000235185 | 1438.6146 | 843.94379 | 183.7047 | 1087.2678 | 0.13190259 | 0.756104151 |
| **0.625** | 0.000252703 | 1762.5024 | 906.4519 | 401.71524 | 1191.484115 | 0.14116967 | 0.859060142 |
| **0.6375** | 0.0002775 | 2095.8911 | 1251.6277 | 300.90176 | 1555.402589 | 0.1500902 | 0.781881293 |
| **0.65** | 0.000310393 | 2572.2026 | 1384.2314 | 609.7868 | 1712.016844 | 0.16087186 | 0.889052935 |
| **0.6625** | 0.000362067 | 2996.8093 | 1897.9497 | 526.72089 | 2143.469311 | 0.17244612 | 0.84310046 |
| **0.675** | 0.000432347 | 3612.5137 | 2034.2396 | 1024.1697 | 2259.482148 | 0.18582809 | 0.98413745 |
| **0.6875** | 0.000554554 | 3016.3633 | 1738.0529 | -568.67468 | 3146.997539 | 0.20105982 | 0.443358203 |
| **0.7** | 0.000639296 | 3281.6455 | 1028.699 | -189.58835 | 3050.336007 | 0.21811296 | 0.450306255 |
| **0.7125** | 0.000751547 | 3359.3782 | 1849.9044 | -645.03345 | 3502.71809 | 0.2377291 | 0.434353078 |
| **0.725** | 0.000868731 | 3668.7439 | 1173.6575 | -254.10858 | 3438.916257 | 0.25640795 | 0.44474213 |
| **0.7375** | 0.001019719 | 4055.8789 | 2136.9475 | -930.37427 | 4356.188316 | 0.27958831 | 0.402680183 |
| **0.75** | 0.001154897 | 3589.3362 | 1296.4755 | -170.85191 | 3282.442781 | 0.29866397 | 0.478805989 |
| **0.7625** | 0.008330838 | 1565.5621 | 817.63788 | 176.02789 | 1204.533869 | 0.58487201 | 0.708220814 |
| **0.775** | 0.013179453 | 1705.2163 | 1290.509 | 154.80336 | 1390.236596 | 0.67739314 | 0.755393882 |
| **0.7875** | 0.036896184 | 1783.7881 | 986.03784 | 228.77579 | 1346.8194 | 0.71660393 | 0.74214398 |
| **0.8** | 0.04274641 | 2368.8823 | 1111.3728 | 291.08249 | 1812.640663 | 0.74771053 | 0.693525504 |
| **0.8125** | 0.056225304 | 2132.1687 | 1143.9086 | 391.26666 | 1512.24669 | 0.78227055 | 0.808365457 |

### (c) Third node from the tip, denote number 2

| Time step | Void volume | σ1 (MPa) | σ2 (MPa) | σ3 (MPa) | σeq (MPa) | εeq | T |
|---|---|---|---|---|---|---|---|

| | fraction, f | | | | | | |
|---|---|---|---|---|---|---|---|
| **0** | 0.000125 | 0 | 0 | 0 | 0 | 0 | 0 |
| **0.0125** | 0.000125 | 56.48959 | 19.180954 | 7.7995305 | 44.11416078 | 0 | 0.630712625 |
| **0.025** | 0.000125 | 112.96149 | 38.35487 | 15.593218 | 88.21712535 | 0 | 0.630677159 |
| **0.0375** | 0.000125 | 169.35626 | 57.497746 | 23.363075 | 132.2702571 | 0 | 0.630570284 |
| **0.05** | 0.000125 | 225.69295 | 76.617096 | 31.114588 | 176.2861811 | 0 | 0.630460901 |
| **0.0625** | 0.000125 | 281.97189 | 95.713066 | 38.847839 | 220.2651205 | 0 | 0.630350664 |
| **0.075** | 0.000125 | 338.19357 | 114.78584 | 46.562946 | 264.2074187 | 0 | 0.630240133 |
| **0.0875** | 0.000125 | 394.35968 | 133.83611 | 54.260185 | 308.114332 | 0 | 0.6301297 |
| **0.1** | 0.000124993 | 456.04211 | 150.55415 | 56.684898 | 361.6735372 | -2.69E-05 | 0.611307427 |
| **0.1125** | 0.000124993 | 516.32654 | 166.66856 | 56.807281 | 415.620937 | -2.87E-05 | 0.593331018 |
| **0.125** | 0.00012503 | 564.91028 | 185.40944 | 58.236046 | 456.5658456 | 8.25E-05 | 0.590317018 |
| **0.1375** | 0.000125121 | 596.21948 | 210.40247 | 65.722733 | 474.9763867 | 0.000357097 | 0.612202141 |
| **0.15** | 0.00012527 | 611.41187 | 239.72905 | 78.021889 | 473.7053876 | 0.00078221 | 0.653826079 |
| **0.1625** | 0.000125478 | 619.05554 | 269.85129 | 84.051712 | 470.4708793 | 0.001346493 | 0.689350879 |
| **0.175** | 0.000125721 | 626.28479 | 297.68317 | 87.169777 | 470.6014317 | 0.001973718 | 0.71620248 |
| **0.1875** | 0.000126008 | 632.25085 | 321.79553 | 89.737625 | 471.4580839 | 0.002676255 | 0.737982895 |
| **0.2** | 0.00012635 | 636.74426 | 343.017 | 91.894508 | 472.3298124 | 0.00347896 | 0.756290583 |
| **0.2125** | 0.000126727 | 640.25543 | 358.43854 | 94.202278 | 472.9730569 | 0.004328614 | 0.770231505 |
| **0.225** | 0.000127126 | 642.31665 | 368.60721 | 95.669266 | 473.4061386 | 0.005203496 | 0.779171086 |
| **0.2375** | 0.000127559 | 643.92078 | 375.17352 | 96.581596 | 474.030649 | 0.006132715 | 0.784531477 |
| **0.25** | 0.000128027 | 645.53284 | 379.65411 | 97.383301 | 474.777621 | 0.007121804 | 0.788137577 |
| **0.2625** | 0.000128532 | 647.03882 | 382.35559 | 97.958572 | 475.615032 | 0.008175865 | 0.790101872 |
| **0.275** | 0.00012908 | 648.49426 | 383.83145 | 98.266533 | 476.6212134 | 0.009311902 | 0.790699345 |
| **0.2875** | 0.000129674 | 649.9469 | 384.58688 | 98.359421 | 477.7981206 | 0.010532177 | 0.790356954 |
| **0.3** | 0.000130336 | 651.42926 | 385.15527 | 98.289658 | 479.1389828 | 0.011883713 | 0.789523311 |
| **0.3125** | 0.000131074 | 652.96326 | 385.6268 | 98.078743 | 480.6457287 | 0.013378563 | 0.78829287 |
| **0.325** | 0.000131884 | 654.5907 | 386.23984 | 97.807053 | 482.2886913 | 0.01500772 | 0.786968202 |
| **0.3375** | 0.000132768 | 656.43958 | 387.21149 | 97.926674 | 483.7856742 | 0.016785689 | 0.786558873 |
| **0.35** | 0.000133801 | 659.25317 | 388.76086 | 98.274895 | 485.9196194 | 0.01871665 | 0.78633645 |
| **0.3625** | 0.000134909 | 662.9671 | 390.6438 | 98.397293 | 489.0285746 | 0.020828061 | 0.785235773 |

| | | | | | | | |
|---|---|---|---|---|---|---|---|
| **0.375** | 0.000136108 | 668.02765 | 392.98587 | 98.156654 | 493.617186 | 0.023105325 | 0.782772701 |
| **0.3875** | 0.000137392 | 674.276 | 395.5506 | 97.642426 | 499.4666344 | 0.025565835 | 0.779143821 |
| **0.4** | 0.000138898 | 681.46985 | 398.2955 | 96.611809 | 506.5816053 | 0.028269414 | 0.774062294 |
| **0.4125** | 0.000140516 | 689.13336 | 401.27463 | 95.462166 | 514.207767 | 0.031306606 | 0.768736058 |
| **0.425** | 0.000142365 | 696.82983 | 404.13754 | 94.541809 | 521.6601932 | 0.034700532 | 0.763913108 |
| **0.4375** | 0.000144432 | 704.62506 | 407.02689 | 93.590378 | 529.2257346 | 0.038406961 | 0.759123029 |
| **0.45** | 0.000146745 | 712.41394 | 410.50354 | 92.654984 | 536.7810097 | 0.042424995 | 0.754853123 |
| **0.4625** | 0.00014932 | 720.69147 | 413.62936 | 91.495995 | 544.9461433 | 0.046753787 | 0.749809157 |
| **0.475** | 0.00015217 | 729.35797 | 417.18417 | 89.832214 | 553.8922315 | 0.051422551 | 0.744052293 |
| **0.4875** | 0.000155366 | 738.05493 | 420.6181 | 88.367714 | 562.6889873 | 0.056454644 | 0.738738908 |
| **0.5** | 0.000158978 | 747.70929 | 424.25317 | 86.739792 | 572.4540367 | 0.061875511 | 0.732927695 |
| **0.5125** | 0.000162947 | 756.12482 | 428.45172 | 84.694969 | 581.5253376 | 0.067745134 | 0.727552998 |
| **0.525** | 0.00016741 | 767.28003 | 429.40695 | 84.395813 | 591.4001775 | 0.074150436 | 0.722062005 |
| **0.5375** | 0.000172873 | 770.81091 | 443.18237 | 79.577728 | 598.8899519 | 0.081197456 | 0.719982585 |
| **0.55** | 0.000179313 | 807.69934 | 432.6673 | 102.40033 | 611.2109559 | 0.088930048 | 0.732298703 |
| **0.5625** | 0.000186472 | 854.88098 | 508.89679 | 114.04326 | 642.0432556 | 0.096425556 | 0.767248944 |
| **0.575** | 0.000196453 | 935.05774 | 540.52979 | 153.68863 | 676.6899241 | 0.10504694 | 0.802571509 |
| **0.5875** | 0.000207013 | 1143.347 | 502.81223 | 160.02536 | 864.4884062 | 0.11314311 | 0.696436789 |
| **0.6** | 0.000217014 | 1267.4427 | 725.95795 | 148.18381 | 969.4671475 | 0.11985243 | 0.736344175 |
| **0.6125** | 0.000230739 | 1591.2366 | 699.4538 | 269.72217 | 1167.53885 | 0.12835354 | 0.730999963 |
| **0.625** | 0.000247513 | 1781.2479 | 1052.4313 | 238.67915 | 1336.565752 | 0.13637024 | 0.766232001 |
| **0.6375** | 0.000271133 | 2165.0063 | 1139.0647 | 447.65323 | 1496.63316 | 0.14605753 | 0.835592032 |
| **0.65** | 0.000305391 | 2523.0571 | 1554.5526 | 366.2951 | 1871.021765 | 0.15622979 | 0.791707306 |
| **0.6625** | 0.000349645 | 3029.6677 | 1669.6549 | 790.23743 | 1954.214847 | 0.167778 | 0.93636242 |
| **0.675** | 0.000423994 | 3449.5154 | 2292.9067 | 658.3551 | 2428.976339 | 0.18122639 | 0.878391595 |
| **0.6875** | 0.000526141 | 3053.8259 | 1319.3519 | -75.711143 | 2715.540478 | 0.19595537 | 0.527515203 |
| **0.7** | 0.000619805 | 3113.8794 | 1424.2529 | -652.21082 | 3267.228592 | 0.21411335 | 0.396454403 |
| **0.7125** | 0.000718098 | 3579.2078 | 1348.6494 | -128.01952 | 3232.574471 | 0.23198852 | 0.49494479 |
| **0.725** | 0.000848257 | 3462.1096 | 1601.0959 | -681.54102 | 3594.659099 | 0.25223857 | 0.406312473 |
| **0.7375** | 0.000992612 | 4549.5259 | 1536.0161 | -397.23721 | 4317.896463 | 0.27414131 | 0.43912623 |
| **0.75** | 0.001132614 | 3308.3818 | 1638.626 | -429.31076 | 3243.022441 | 0.29390252 | 0.464350476 |

| | | | | | | | |
|---|---|---|---|---|---|---|---|
| **0.7625** | 0.007449346 | 1574.5442 | 784.89288 | 164.58212 | 1223.983301 | 0.57817233 | 0.687378441 |
| **0.775** | 0.010669881 | 1904.7955 | 1217.8131 | 124.38151 | 1555.20395 | 0.66564947 | 0.6959409 |
| **0.7875** | 0.021751735 | 2353.1221 | 1124.4347 | 449.59766 | 1671.582463 | 0.7048161 | 0.783121094 |
| **0.8** | 0.025870139 | 2540.229 | 1086.1072 | 427.02249 | 1872.747992 | 0.74314249 | 0.72146363 |
| **0.8125** | 0.035722069 | 2536.8394 | 1454.4487 | 794.34839 | 1523.726994 | 0.79208088 | 1.046914683 |

**(d) Fourth node from the tip, denote number 3**

| Time step | Void volume fraction, f | σ1 (MPa) | σ2 (MPa) | σ3 (MPa) | σeq (MPa) | εeq | T |
|---|---|---|---|---|---|---|---|
| **0** | 0.000125 | 0 | 0 | 0 | 0 | 0 | 0 |
| **0.0125** | 0.000125 | 76.090485 | 17.573528 | 0.61942375 | 68.58344026 | 0 | 0.458241991 |
| **0.025** | 0.000125 | 152.14528 | 35.140587 | 1.2348408 | 137.1366782 | 0 | 0.458230699 |
| **0.0375** | 0.000125 | 228.08188 | 52.683899 | 1.8470376 | 205.5838282 | 0 | 0.458228028 |
| **0.05** | 0.000125 | 303.92691 | 70.208328 | 2.4539506 | 273.9508145 | 0 | 0.458219954 |
| **0.0625** | 0.000125 | 379.68088 | 87.714012 | 3.055604 | 342.2380776 | 0 | 0.458209773 |
| **0.075** | 0.000125 | 455.34451 | 105.20111 | 3.6520281 | 410.4462525 | 0 | 0.458198562 |
| **0.0875** | 0.000125 | 530.91956 | 122.67003 | 4.243259 | 478.5769107 | 0 | 0.458186786 |
| **0.1** | 0.000125074 | 571.62354 | 153.59277 | 23.830389 | 495.8104004 | 0.000279086 | 0.503584097 |
| **0.1125** | 0.000125236 | 583.25732 | 197.37245 | 52.349907 | 475.2855387 | 0.000844212 | 0.584195962 |
| **0.125** | 0.000125462 | 590.79956 | 240.59793 | 49.268452 | 475.6550287 | 0.00154354 | 0.617160119 |
| **0.1375** | 0.000125692 | 594.51196 | 265.57037 | 52.213943 | 473.1818281 | 0.002209538 | 0.64266787 |
| **0.15** | 0.000125958 | 596.58826 | 285.63373 | 53.156895 | 472.2537939 | 0.002939929 | 0.660223307 |
| **0.1625** | 0.000126253 | 598.70221 | 299.60632 | 54.909943 | 471.718222 | 0.00372623 | 0.673579006 |
| **0.175** | 0.000126578 | 600.08771 | 308.77747 | 55.830257 | 471.7263971 | 0.004568864 | 0.681677234 |
| **0.1875** | 0.000126924 | 601.3197 | 312.80121 | 56.460857 | 472.1312866 | 0.00545147 | 0.685248499 |
| **0.2** | 0.000127294 | 602.16528 | 315.16965 | 56.451965 | 472.8085124 | 0.006389 | 0.686526624 |
| **0.2125** | 0.000127683 | 602.9502 | 316.33533 | 56.310246 | 473.5861926 | 0.007366605 | 0.686672452 |

| | | | | | | | |
|---|---|---|---|---|---|---|---|
| **0.225** | 0.000128097 | 603.77258 | 317.24835 | 56.041237 | 474.5135809 | 0.008400086 | 0.686360522 |
| **0.2375** | 0.000128526 | 605.21594 | 318.03912 | 56.190247 | 475.6342563 | 0.009468051 | 0.686413488 |
| **0.25** | 0.000128994 | 606.45715 | 319.28949 | 56.109238 | 476.7615834 | 0.010624817 | 0.686475807 |
| **0.2625** | 0.000129496 | 607.73749 | 320.91754 | 55.992649 | 477.945859 | 0.011857309 | 0.68672191 |
| **0.275** | 0.000130048 | 609.14075 | 322.77026 | 55.844784 | 479.2623927 | 0.013200578 | 0.68699722 |
| **0.2875** | 0.000130661 | 610.73468 | 324.72339 | 55.689983 | 480.7531496 | 0.014678689 | 0.68721897 |
| **0.3** | 0.000131358 | 612.60913 | 326.59729 | 55.585365 | 482.4504027 | 0.016338244 | 0.687318862 |
| **0.3125** | 0.000132157 | 614.50671 | 328.92279 | 55.327293 | 484.2960327 | 0.018219143 | 0.687428574 |
| **0.325** | 0.000133052 | 616.72461 | 331.03653 | 55.14727 | 486.3602562 | 0.020293556 | 0.687356335 |
| **0.3375** | 0.000134143 | 620.07489 | 332.95758 | 54.283241 | 490.0034268 | 0.022569897 | 0.685243991 |
| **0.35** | 0.000135173 | 626.96765 | 334.1875 | 52.699104 | 497.3584256 | 0.025041135 | 0.679492697 |
| **0.3625** | 0.000136331 | 634.71704 | 337.34082 | 52.297489 | 504.422982 | 0.027738245 | 0.676915595 |
| **0.375** | 0.000137657 | 643.01392 | 341.26959 | 51.95731 | 511.9028717 | 0.030682912 | 0.674763956 |
| **0.3875** | 0.000139097 | 651.2525 | 346.17438 | 52.167381 | 518.8474861 | 0.033910573 | 0.674311359 |
| **0.4** | 0.000140833 | 658.94885 | 351.90396 | 52.259361 | 525.4164997 | 0.037533212 | 0.674456786 |
| **0.4125** | 0.000142895 | 667.61664 | 357.27042 | 51.624954 | 533.4645103 | 0.04172495 | 0.672654565 |
| **0.425** | 0.000145368 | 677.73871 | 363.2323 | 50.813049 | 542.9293449 | 0.046589099 | 0.670304567 |
| **0.4375** | 0.000148282 | 688.44275 | 369.32672 | 49.972504 | 552.9261628 | 0.052084386 | 0.667805847 |
| **0.45** | 0.000151727 | 700.20227 | 376.17523 | 48.651459 | 564.2568515 | 0.058237709 | 0.664608063 |
| **0.4625** | 0.000155739 | 713.0072 | 382.32745 | 47.507217 | 576.3380825 | 0.065058134 | 0.66097886 |
| **0.475** | 0.000160641 | 723.91003 | 389.97986 | 46.613705 | 586.5691725 | 0.072608948 | 0.659486638 |
| **0.4875** | 0.000166476 | 736.0351 | 394.30469 | 45.58321 | 597.9533595 | 0.080934405 | 0.655526601 |
| **0.5** | 0.000173419 | 747.48755 | 403.15991 | 41.584091 | 611.3852922 | 0.090078227 | 0.650016482 |
| **0.5125** | 0.000182223 | 760.18152 | 399.55829 | 44.951591 | 619.4086529 | 0.10013007 | 0.64830189 |
| **0.525** | 0.000193135 | 762.8598 | 430.32056 | 26.543324 | 638.6566795 | 0.11124742 | 0.636608955 |
| **0.5375** | 0.000206146 | 826.23767 | 354.84674 | 41.25983 | 684.367738 | 0.12346657 | 0.595364243 |
| **0.55** | 0.000222222 | 962.67139 | 640.76324 | -284.27521 | 1121.193246 | 0.13565417 | 0.392189132 |
| **0.5625** | 0.000233916 | 1627.6042 | 261.3288 | -331.19629 | 1739.910584 | 0.14333525 | 0.29843233 |
| **0.575** | 0.000245837 | 1778.0802 | 730.97852 | -564.47211 | 2032.487038 | 0.15153623 | 0.318917427 |
| **0.5875** | 0.000264977 | 1947.2844 | 527.69354 | -78.836029 | 1801.132404 | 0.160788 | 0.443451003 |
| **0.6** | 0.000288054 | 2037.7711 | 1191.4258 | -184.08649 | 1942.271977 | 0.17358957 | 0.522602815 |

| | | | | | | | |
|---|---|---|---|---|---|---|---|
| **0.6125** | 0.000325439 | 2677.0103 | 965.19922 | 123.05686 | 2254.105609 | 0.18402234 | 0.556801238 |
| **0.625** | 0.000377198 | 2823.6992 | 1768.156 | -46.223988 | 2514.195976 | 0.19905485 | 0.602662012 |
| **0.6375** | 0.000441478 | 3579.1138 | 1456.0157 | 462.6825 | 2757.363666 | 0.21198665 | 0.664621799 |
| **0.65** | 0.000537748 | 3876.353 | 2507.8931 | 90.056381 | 3320.710464 | 0.2290218 | 0.649891296 |
| **0.6625** | 0.000655331 | 4650.2822 | 2081.3354 | 949.86218 | 3284.236126 | 0.24526277 | 0.779631294 |
| **0.675** | 0.000843333 | 4925.541 | 3413.7715 | 495.00848 | 3900.875496 | 0.26514384 | 0.754900704 |
| **0.6875** | 0.001105991 | 4346.5063 | 1498.4274 | -621.28943 | 4317.582204 | 0.28533733 | 0.40328468 |
| **0.7** | 0.001288272 | 4367.9717 | 1799.538 | -1723.5562 | 5296.917985 | 0.30958501 | 0.279656555 |
| **0.7125** | 0.0014336 | 4924.8765 | 1480.0569 | -935.9223 | 5101.553772 | 0.33336365 | 0.357342837 |
| **0.725** | 0.001602606 | 4468.4629 | 2103.0815 | -1802.917 | 5485.476507 | 0.36034757 | 0.289772906 |
| **0.7375** | 0.001741528 | 6121.4023 | 1419.7355 | -1308.3998 | 6509.55938 | 0.38715261 | 0.319158212 |
| **0.75** | 0.001865439 | 4005.6914 | 2267.2107 | -1433.7686 | 4811.77721 | 0.41320321 | 0.335228426 |
| **0.7625** | 0.011492938 | 1858.8383 | 936.74731 | 242.9471 | 1404.036907 | 0.72999883 | 0.721380066 |
| **0.775** | 0.016735323 | 2109.4438 | 1418.2144 | 113.55764 | 1755.472969 | 0.82168621 | 0.691402622 |
| **0.7875** | 0.026041016 | 3281.4983 | 1881.4014 | 1841.8271 | 1420.283992 | 0.85628939 | 1.64397328 |
| **0.8** | 0.059472758 | 1825.4015 | 272.13565 | 182.60187 | 1599.897424 | 0.88330191 | 0.475059419 |
| **0.8125** | 0.076775499 | 2325.1094 | 838.72797 | 818.75787 | 1496.452069 | 0.92330176 | 0.887119457 |

**(e) Fifth node from the tip, denote by number 4**

| **Time step** | **Void volume fraction, f** | **σ1 (MPa)** | **σ2 (MPa)** | **σ3 (MPa)** | **σeq (MPa)** | **εeq** | **T** |
|---|---|---|---|---|---|---|---|
| **0** | 0.000125 | 0 | 0 | 0 | 0 | 0 | 0 |
| **0.0125** | 0.000125 | 15.714476 | 6.1405969 | -0.97419238 | 9.820792081 | 0 | 0.70873036 |
| **0.025** | 0.000125 | 31.427748 | 12.281219 | -1.9471279 | 19.64009275 | 0 | 0.708785504 |
| **0.0375** | 0.000125 | 47.132103 | 18.413208 | -2.9174223 | 29.45108856 | 0 | 0.708835018 |
| **0.05** | 0.000125 | 62.830349 | 24.539812 | -3.8852017 | 39.25601174 | 0 | 0.7088932 |
| **0.0625** | 0.000125 | 78.522514 | 30.66107 | -4.8504786 | 49.05489618 | 0 | 0.708954753 |
| **0.075** | 0.000125 | 94.208664 | 36.777031 | -5.8132629 | 58.84779474 | 0 | 0.709017971 |
| **0.0875** | 0.000125 | 109.88893 | 42.887814 | -6.7735868 | 68.6348246 | 0 | 0.709082005 |

| | | | | | | | |
|---|---|---|---|---|---|---|---|
| **0.1** | 0.000125 | 125.6018 | 49.021011 | -7.7401457 | 78.44755889 | 0 | 0.709104985 |
| **0.1125** | 0.000125 | 141.39326 | 55.210407 | -8.7229309 | 88.32363298 | 0 | 0.709061776 |
| **0.125** | 0.000125 | 157.3214 | 61.502296 | -9.7321529 | 98.30977409 | 0 | 0.708954747 |
| **0.1375** | 0.000125 | 173.39169 | 67.911232 | -10.758465 | 108.4055318 | 0 | 0.708895118 |
| **0.15** | 0.000125 | 189.65016 | 74.443306 | -11.795715 | 118.6305543 | 0 | 0.708917284 |
| **0.1625** | 0.000125 | 206.1429 | 81.083679 | -12.849939 | 129.0081771 | 0 | 0.708938628 |
| **0.175** | 0.000125 | 222.86681 | 87.787811 | -13.922701 | 139.5271401 | 0 | 0.708898927 |
| **0.1875** | 0.000125 | 239.8119 | 94.542946 | -15.057896 | 150.2113388 | 0 | 0.708550483 |
| **0.2** | 0.000125 | 257.01361 | 101.43489 | -16.217978 | 161.0716263 | 0 | 0.708236722 |
| **0.2125** | 0.000125 | 274.51987 | 108.49569 | -17.417675 | 172.1499963 | 0 | 0.707905688 |
| **0.225** | 0.000125 | 292.36505 | 115.77697 | -18.614965 | 183.4454189 | 0 | 0.707798278 |
| **0.2375** | 0.000125 | 310.58725 | 123.18105 | -19.970581 | 195.069735 | 0 | 0.707093661 |
| **0.25** | 0.000125 | 329.15939 | 130.74985 | -21.500402 | 207.0325817 | 0 | 0.705861262 |
| **0.2625** | 0.000125 | 348.11908 | 138.44136 | -23.254293 | 219.3785182 | 0 | 0.703967661 |
| **0.275** | 0.000125 | 367.56622 | 146.36134 | -25.31842 | 232.2470773 | 0 | 0.701277774 |
| **0.2875** | 0.000125 | 387.86069 | 154.65341 | -27.665745 | 245.8290725 | -4.35E-07 | 0.698111564 |
| **0.3** | 0.000125 | 411.27164 | 163.4498 | -28.508869 | 259.9128067 | -2.06E-06 | 0.700507448 |
| **0.3125** | 0.000124998 | 440.85162 | 172.00185 | -28.497066 | 276.2941377 | -6.45E-06 | 0.704993127 |
| **0.325** | 0.000124999 | 471.11655 | 181.18777 | -27.906725 | 292.8279561 | -2.02E-06 | 0.710767286 |
| **0.3375** | 0.000125007 | 499.38892 | 191.52446 | -24.949425 | 307.0006482 | 2.49E-05 | 0.723086372 |
| **0.35** | 0.00012503 | 523.2511 | 202.89696 | -16.14521 | 315.1046736 | 9.79E-05 | 0.751076187 |
| **0.3625** | 0.000125055 | 547.6319 | 215.19026 | -5.1710978 | 322.2046846 | 0.00017873 | 0.783819622 |
| **0.375** | 0.000125108 | 565.7453 | 230.3813 | 15.129688 | 320.2589506 | 0.000359574 | 0.844375347 |
| **0.3875** | 0.000125228 | 583.20728 | 247.88506 | 38.810162 | 316.1184776 | 0.000741406 | 0.91727476 |
| **0.4** | 0.000125364 | 598.71936 | 265.48611 | 59.662678 | 312.86356 | 0.001140554 | 0.984314215 |
| **0.4125** | 0.000125534 | 615.97729 | 284.5647 | 76.334396 | 313.4886393 | 0.001594049 | 1.038715351 |
| **0.425** | 0.00012575 | 630.8147 | 304.10605 | 89.670822 | 315.1980844 | 0.00213398 | 1.083542511 |
| **0.4375** | 0.000126021 | 642.3833 | 325.19629 | 99.252769 | 318.3588076 | 0.00276581 | 1.117012559 |
| **0.45** | 0.000126337 | 654.19189 | 339.34909 | 110.59085 | 319.2042801 | 0.003466273 | 1.153004412 |
| **0.4625** | 0.000126747 | 662.70392 | 352.30728 | 117.90676 | 321.1147195 | 0.004331987 | 1.17602619 |
| **0.475** | 0.000127257 | 666.78595 | 363.04065 | 120.47429 | 323.9861561 | 0.005369384 | 1.183487698 |

| | | | | | | | |
|---|---|---|---|---|---|---|---|
| **0.4875** | 0.000127861 | 667.59656 | 369.07852 | 119.88217 | 326.5781458 | 0.006573185 | 1.180480348 |
| **0.5** | 0.000128578 | 665.56049 | 373.72421 | 115.99025 | 330.1649746 | 0.00798649 | 1.166361303 |
| **0.5125** | 0.000129402 | 664.04297 | 373.73187 | 112.9366 | 331.8920419 | 0.00960491 | 1.155708579 |
| **0.525** | 0.000130337 | 663.05603 | 371.43674 | 110.01721 | 332.9548761 | 0.011442889 | 1.145810901 |
| **0.5375** | 0.000131379 | 665.20081 | 366.30737 | 110.0965 | 332.1303033 | 0.013489792 | 1.145739758 |
| **0.55** | 0.000132549 | 666.97406 | 363.27826 | 109.44352 | 332.4838709 | 0.015775399 | 1.142607647 |
| **0.5625** | 0.000133832 | 668.80872 | 363.63571 | 108.69274 | 334.0045826 | 0.018274788 | 1.138843826 |
| **0.575** | 0.000135396 | 670.81573 | 362.06256 | 106.9809 | 335.7510254 | 0.021140473 | 1.131651237 |
| **0.5875** | 0.000137179 | 676.43164 | 363.67365 | 104.50686 | 340.6963147 | 0.024386954 | 1.119875287 |
| **0.6** | 0.000139136 | 685.04102 | 363.57797 | 101.30593 | 347.0641999 | 0.028092502 | 1.104430554 |
| **0.6125** | 0.000141311 | 689.36127 | 363.51874 | 93.507355 | 354.9512765 | 0.032261845 | 1.076567819 |
| **0.625** | 0.00014382 | 699.07556 | 363.79221 | 93.437119 | 359.5787225 | 0.036954824 | 1.071907037 |
| **0.6375** | 0.000146848 | 703.0368 | 360.84912 | 86.584862 | 365.7383241 | 0.042324953 | 1.048537261 |
| **0.65** | 0.000150219 | 711.98413 | 363.073 | 83.242699 | 373.0573901 | 0.048178397 | 1.034961251 |
| **0.6625** | 0.000154345 | 727.6637 | 364.09241 | 80.430786 | 382.8226057 | 0.055016026 | 1.020652802 |
| **0.675** | 0.000158679 | 754.29083 | 368.20822 | 73.18396 | 401.9528654 | 0.061900571 | 0.991561543 |
| **0.6875** | 0.000162903 | 777.43597 | 394.7439 | 40.25811 | 445.9629703 | 0.068346068 | 0.906232177 |
| **0.7** | 0.00016783 | 815.6178 | 338.29205 | 15.484644 | 467.0335893 | 0.075341165 | 0.834625546 |
| **0.7125** | 0.000171926 | 826.65662 | 482.77094 | 16.209854 | 526.1203458 | 0.081533089 | 0.839882247 |
| **0.725** | 0.000177463 | 944.79175 | 404.79507 | 66.439285 | 510.1743351 | 0.087935627 | 0.925190997 |
| **0.7375** | 0.000184156 | 992.27954 | 657.45007 | -69.644447 | 764.6637226 | 0.095645718 | 0.688793046 |
| **0.75** | 0.000190126 | 1091.9321 | 534.81281 | 20.762522 | 647.6346234 | 0.10152292 | 0.847961372 |
| **0.7625** | 0.000373446 | 936.82721 | 519.92706 | 134.96407 | 484.8658186 | 0.19452222 | 1.094267238 |
| **0.775** | 0.000465219 | 952.20776 | 528.62189 | 132.00792 | 497.0014065 | 0.22015394 | 1.081712277 |

| TIME | SEMESTER 1 | | | | | | | | | | | | | |
|---|---|---|---|---|---|---|---|---|---|---|---|---|---|---|
| **PROJECT ACTIVITIES** | **Week 1** | **Week 2** | **Week 3** | **Week 4** | **Week 5** | **Week 6** | **Week 7** | **Week 8** | **Week 9** | **Week 10** | **Week 11** | **Week 12** | **Week 13** | **Week 14** |
| **Discuss on the title** | | | | | | | | | | | | | | |
| **Discuss on the objectives and scopes** | | | | | | | | | | | | | | |
| **Literature study** | | | | | | | | | | | | | | |
| **Discuss on methodology & simulation** | | | | | | | | | | | | | | |
| **Finalize chapter 1,2 and 3** | | | | | | | | | | | | | | |
| **Report submission and presentation** | | | | | | | | | | | | | | |

| | |
|---|---|
| Planning schedule | |
| Actual schedule | |

| TIME | SEMESTER 2 | | | | | | | | | | | | | | |
|---|---|---|---|---|---|---|---|---|---|---|---|---|---|---|---|
| **PROJECT ACTIVITIES** | **Week 1** | **Week 2** | **Week 3** | **Week 4** | **Week 5** | **Week 6** | **Week 7** | **Week 8** | **Week 9** | **Week 10** | **Week 11** | **Week 12** | **Week 13** | **Week 14** | **Week 15** |
| **Detail study on GTN model** | | | | | | | | | | | | | | | |
| **Analysis in Marc** | | | | | | | | | | | | | | | |
| **Analysis with different defect** | | | | | | | | | | | | | | | |
| **Comparison between methods** | | | | | | | | | | | | | | | |
| **Result analysis** | | | | | | | | | | | | | | | |
| **Report writing** | | | | | | | | | | | | | | | |
| **Report submission and presentation** | | | | | | | | | | | | | | | |